

Annual Report 2022

MLZ is a cooperation between:

Bavarian State Ministry of
Science and the Arts



SPONSORED BY THE



Federal Ministry
of Education
and Research

The Heinz Maier-Leibnitz Zentrum (MLZ):

The Heinz Maier-Leibnitz Zentrum is a leading centre for cutting-edge research with neutrons and positrons. Operating as a user facility, the MLZ offers a unique suite of high-performance neutron scattering instruments. This cooperation involves the Technische Universität München, the Forschungszentrum Jülich GmbH and the Helmholtz-Zentrum hereon GmbH. The MLZ is funded by the German Federal Ministry of Education and Research, together with the Bavarian State Ministry of Science and the Arts and the partners of the cooperation.

The Forschungs-Neutronenquelle Heinz-Maier-Leibnitz (FRM II):

The Forschungs-Neutronenquelle Heinz-Maier-Leibnitz provides neutron beams for the scientific experiments at the MLZ. The FRM II is operated by the Technische Universität München and is funded by the Bavarian State Ministry of Science and the Arts.

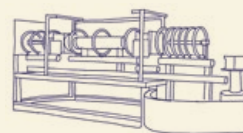
Joint Annual Report 2022
of the MLZ and FRM II



245
articles

3
years

14
projects



7.9
million
euros

New ErUM-Pro instrument and
method development funding by the
German Federal Ministry of
Education and Research (BMBF)

349
media
articles



1425
followers on
social media

48
news
articles
on the
web pages



3
calls
(2022–2024)

24
months each

45
fellow-
ships



Post-doctoral research programme*
funded by the European Union

* This project has received funding from the European Union's Horizon 2020 Research and Innovation Programme under the Marie Skłodowska-Curie Grant Agreement N°101034266.

PUBLICATIONS AND COMMUNICATION

FUNDING

2022 IN NUMBERS

SCIENTIFIC EVENTS

EVENTS FOR THE PUBLIC



225
in-person-
participants
at the MLZ
User Meeting

Around
50
participants
at the 8th TUM
Expert Forum,
a platform for industrial
applications



Around
50
participants
at MLZ Conference
“Neutrons for Mobility”

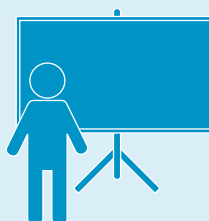


64 children
and around **800**
participants in total at
the “Open-Door-Day
with the Mouse”

2142
visitors



despite challenges due to
COVID 19 pandemic



80
in-person participants
at the “Science for
Everyone” lecture
(by Deutsches Museum)

Tackling challenges, reaching milestones 7

Scientific Highlights

Elusive carbonic acid: it really exists!	10
Levitate high-speed trains	11
Solid-state battery: New lithium conductor with high conductivity	12
Neutrons as a probe of electrolytes in batteries	13
It is in the sugar	14
Cleaner air thanks to polymer nanocomposites	15
Super spin for super computers	16
Waves on circular paths	17
Neutrons help track down mammalian ancestors	18
Exploring the early solar system	19

Industry & Medicine

Making CO ₂ more usable.....	22
Understanding the structure of fuel cell membranes.....	23
Neutrons explore more efficient hydrogen storage systems	24
Patent for a versatile valve	25
Super methods for superalloys.....	26
Less waste from lower enriched Uranium targets	27
How prefilled syringes become clogged.....	28
Better vaccines against multi-resistant germs	29

Scientific Reports

Materials Science	32
Quantum Phenomena	40
Soft Matter	47
Structure Research.....	56
Neutron Methods.....	64

News from the instruments

News from the instruments.....	72
--------------------------------	----

Reactor & Development

Drought – a neutron deficit relative to the average availability at a given location and season	78
A LEU solution for the conversion of FRM II.....	80

Facts & Figures

The year in pictures	84
Workshops, Conferences and Schools	94
No neutrons, no research results? Far from it!	96
Back to reality!	100
Organization, Staff and Budget	102
Publications & Theses	106
Cover pages	108
Committees	109
Partner institutions.....	114
Imprint.....	118



Tackling challenges, reaching milestones

No doubt about it – 2022 was a challenging year at the FRM II/MLZ. Looking back, perhaps the German figure of speech *Licht und Schatten* (light and shadow) best describes what we went through, but also what we have achieved, in the last twelve months.

On the one hand, we had another year without neutrons at MLZ. In addition to the removal of the defective cold source, we were facing a tiny leak on the light water side of the central channel that prevents us from restarting FRM II. It cannot be repaired and so we need to replace this component, which turned out to be difficult due to unexpected supply problems for the new central channel.

Still, we are shortening the time until the return of neutrons by as much as possible: The replacement of the central channel was routinely scheduled for 2024 but will now take place in 2023. We have also anticipated mandatory inspections and several refurbishments of the reactor systems, which would have been due in the coming years, such as the ten-year periodic inspection (WKP). In so doing, we are actively tackling the current challenges. We are confident that we will return to user operation in Q1/2024.

On the other hand, we can proudly say that we reached crucial milestones in 2022.

We assured the long-term availability of the FRM II for the user community: By the end of November, we announced that scientifically speaking it is possible to convert the FRM II to fuel using Low Enriched Uranium (LEU). This conclusion is the result of TUM researchers' calculations, which have been independently confirmed by experts in the US. It establishes the theoretical background to discontinue the use of Highly Enriched Uranium (HEU) as fuel for the FRM II in the future and lays the foundation for a continued reliable operation of our neutron source in the coming decades.

Moreover, the long-lasting cooperation with our university groups led to magnificent new projects funded by the German Federal Ministry of Education and Research (BMBF). In total, 14 instrument and method development projects at the FRM II/MLZ were awarded ErUM-Pro funding, with a total volume of grants of 7.9M €. Projects started on October 1st, 2022, with a duration of three years. The topics of the sponsored projects span the entire range from sample environment developments for dedicated applications, the design and construction of add-ons to existing instruments to enhance performance, to the commissioning and finalization of instrument construction projects.

The BMBF also funds the transfer of instruments from the Helmholtz-Zentrum Berlin and its re-installation at MLZ. Several key components of the instruments LaDiff and FIREPOD arrived at our site in Garching in November. Both instruments will significantly strengthen our instrument suite. Moreover, after almost 20 years of providing neutrons to our user community, we are now planning for a renewal of the instrument suite with our envisaged upgrade program MORIS. We will include our users in this process during a workshop in spring 2023.

Finally, we enjoyed returning to in-person meetings after the cessation of most COVID-19 restrictions. This is of major importance to a scientific institution such as ours. For years, we have organized annual conferences dedicated to specific applications of neutron science. This year's MLZ conference "Neutrons for Mobility" in Lenggries, Bavaria, dealt with the highly up-to-date topic of electric mobility. After two years of virtual conferences, the MLZ was happy to welcome 225 participants in person to the over-booked User Meeting. There was a clear focus on the future of neutron science at MLZ with a strong commitment on the part of the three MLZ partners to refurbish the instrument suite.

Overall, these positive developments provide us with some tailwinds on our path to regular operation. We will continue to put all our efforts into this. Meanwhile, we hope you will enjoy reading this year's annual report. It proves that the MLZ is a place of extraordinary scientific performance and lively exchange.

Together with you, we want to keep it exactly this way.



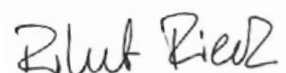
Peter Müller-Buschbaum



Martin Müller



Axel Pichlmaier



Robert Rieck



N

260kg

Scientific Highlights





ELUSIVE CARBONIC ACID: IT REALLY EXISTS!

The existence of carbonic acid has long been disputed: it is theoretically present, but practically extremely hard to detect, simply because the compound decays at the Earth's surface, under so-called "standard conditions". A German-Chinese team of researchers has now made the crystalline structure of carbonic acid molecules visible for the first time.

Everyone believes that they know it, but it has remained one of the biggest secrets in chemistry: carbonic acid. Until now, nobody had ever seen the molecular structure of the compound made up of hydrogen, oxygen and carbon with the chemical formula H_2CO_3 . The compound breaks down rapidly – at least at the Earth's surface – into water and carbon dioxide or reacts to form hydrogen carbonate, a substance that also breaks down. It is what gives the fizz to mineral water and champagne.

Seeing better with neutrons

The crystals contain hydrogen, but where are those atoms located in the molecule? When the monochromatic neutron beam hits a crystal, it interacts with the atoms, thereby creating a diffraction pattern from which the crystal structure can then be deduced – at least theoretically.

The structure puzzle

The researchers succeeded in producing (deuterated) crystalline carbonic acid by pressing it to about 20,000 atmospheres and analyzing its structure for the first time. It actually consists of H_2CO_3 molecules connected by hydrogen bonds, forming a low-symmetry "monoclinic" structure.

Fundamental research for practical applications

When cosmologists detect traces of carbonic acid on distant planets or moons, for example, they can draw conclusions about conditions there. The results could also be interesting for geoengineering: For example, it is now possible to calculate when carbonic acid crystals form when carbon dioxide is stored under high pressure and humid conditions underground.

*S. Benz, D. Chen, A. Möller, M. Hofmann, D. Schnieders, R. Dronskowski, The Crystal Structure of Carbonic Acid, Inorganics 10, 132 (2022)
DOI: 10.3390/inorganics10090132*

The experiments were carried out at STRESS-SPEC.

LEVITATE HIGH-SPEED TRAINS

Any material can become a superconductor if it offers the right conditions to bind together the negatively charged electrons into so-called “Cooper-pairs”. This can happen in different ways: In classical superconductors, such as tin and lead, the electrons are bound together by interactions with crystal lattice vibrations, called phonons. Unfortunately, these materials require extremely low temperatures (-200°C and below) to become superconducting. Unconventional superconductors, on the other hand, show transition temperatures up to -140°C, making them more attractive for applications such as levitation of high-speed trains.

A question of symmetry

A group of scientists from the University of Dresden has recently made a breakthrough in understanding the pairing mechanisms in the noncentrosymmetric compound Ru_7B_3 using small angle neutron scattering (SANS). So far, it was assumed that the pairing mechanism would be either singlet, or triplet. This means that the electron spins in a Cooper pair are either parallel (triplet) or antiparallel (singlet). However, the SANS study of the authors has shown that the lack of inversion symmetry in compounds, such as Ru_7B_3 , can lead to a mixing of both pairing mechanisms.

It's all in the mix

The nature of the pairing mechanism is reflected in the symmetry of the gap that opens up in the energy spectrum of a material when entering the superconducting state. A well-established method of determining this gap structure is by measuring the intensity distribution of the superconducting vortex lattice, using small angle neutron scattering. By analyzing the intensity distribution of this pattern, which arises from magnetic scattering off the flux lattice that emerges when type-II superconductors are exposed to a magnetic field, the researchers were able to determine that the pairing mechanism is a mixture of both singlet and triplet states.

A. S. Cameron, Y. S. Yerin, Y. V. Tymoshenko, P. Y. Portnichenko, A. S. Sukhanov, M. Ciomaga Hatnean, D. McK. Paul, G. Balakrishnan, R. Cubitt, A. Heinemann, D. S. Inosov, Singlet-triplet mixing in the order parameter of the noncentrosymmetric superconductor Ru_7B_3 , Phys. Rev. B 105, 094519 (2022)

DOI: 10.1103/PhysRevB.105.094519

Experiments were carried out at SANS-1.



BASIC RESEARCH



SOLID-STATE BATTERY: NEW LITHIUM CONDUCTOR WITH HIGH CONDUCTIVITY

A research team has discovered a new material class of Li-ion superionic conductors with above-average ionic conductivity. Lithium conductors are the key elements of ionic separator membranes and ionic conductors, crucial for the development of high-performance all-solid-state batteries.

All-solid-state lithium batteries promise to be lightweight and perform better, as well as being safer and more stable than their “liquid-based” siblings. The fact that they contain no liquid electrolyte, which is volatile, moisture and air sensitive, irritant, flammable, easily oxidized, automatically defines the advantages of the solid electrolyte in all-solid-state batteries.

However, the lithium ion diffusion process through solid matter proceeds in a more complex and remarkably slower way. That is why, in practice, the research on solid-state electrolytes becomes of increasing relevance. A team of researchers at the Technical University of Munich is looking for new solid-state Li electrolytes that are more efficient, stable and robust. Details of the ionic transport was defined as the major aim in the current contribution, which is a key to increasing conductivity.

A new material that shows promise

The result of their efforts is a successful synthesis of a Li_9AlP_4 crystalline powder that exhibits excellent ionic trans-

port properties and offers promising capabilities in terms of stability and further structure-performance tuning.

Greater detail with neutron beams

The researcher successfully applied neutron diffraction to visualize how the ions diffuse in the crystal lattice through the stable lithium framework. Structural motifs and high symmetry of synthesized compounds create a complex 3D percolation network through the crystal lattice.

The family of compounds investigated is highly promising for application as electrolytes in a new generation all-solid-state batteries. Thus, this basic research has the potential to accelerate the development of higher-performance electrochemical energy storage solutions.

*T. M. F. Restle, S. Strangmüller, V. Baran, A. Senyshyn, H. Kirchhain, W. Klein, S. Merk, D. Müller, T. Kutsch, L. van Wüllen, T.F. Fässler. Super-Ionic Conductivity in $\omega\text{-Li}_9\text{TrP}_4$ (Tr = Al, Ga, In) and Lithium Diffusion Pathways in Li_9AlP_4 Polymorphs, *Adv. Funct. Mater.*, 32, 2112377 (2022)
DOI: 10.1002/adfm.202112377*

The experiments were carried out at SPODI.

NEUTRONS AS A PROBE OF ELECTROLYTES IN BATTERIES

Using neutron scattering, a team of scientists managed to create a non-destructive look into the interior of running lithium-ion batteries. The independent quantification of the lithium concentration in the electrodes and the electrolyte, together with thermal imaging and calorimetry, facilitated a link towards longer-lasting batteries.

Lithium-ion batteries play an increasing role in our daily life. It is projected that in order to store renewable energy, the usage of rechargeable batteries will become even more important in the future. To a large extent, the Li-ion energy storage technology suffers from cell aging, where the storage capacity of even the best lithium-ion batteries decreases over their lifetime.

Lithium-ion batteries with 1000 charge cycles

Even low-energetic thermal neutrons penetrate the interior of cm-sized batteries non-destructively and interact with the components inside the cell in the form of scattering and absorption. Using neutron diffraction, one can non-destructively and unambiguously quantify the amount of lithium stored in the cell electrodes. The team looked inside a series of conventional cylindrical 18650 lithium-ion batteries at various states of fatigue. Some cells had undergone over 1000 charge cycles, which would correspond to a ride of half a million kilometers when embedded into a car. Pronounced losses of mobile lithium were observed, which

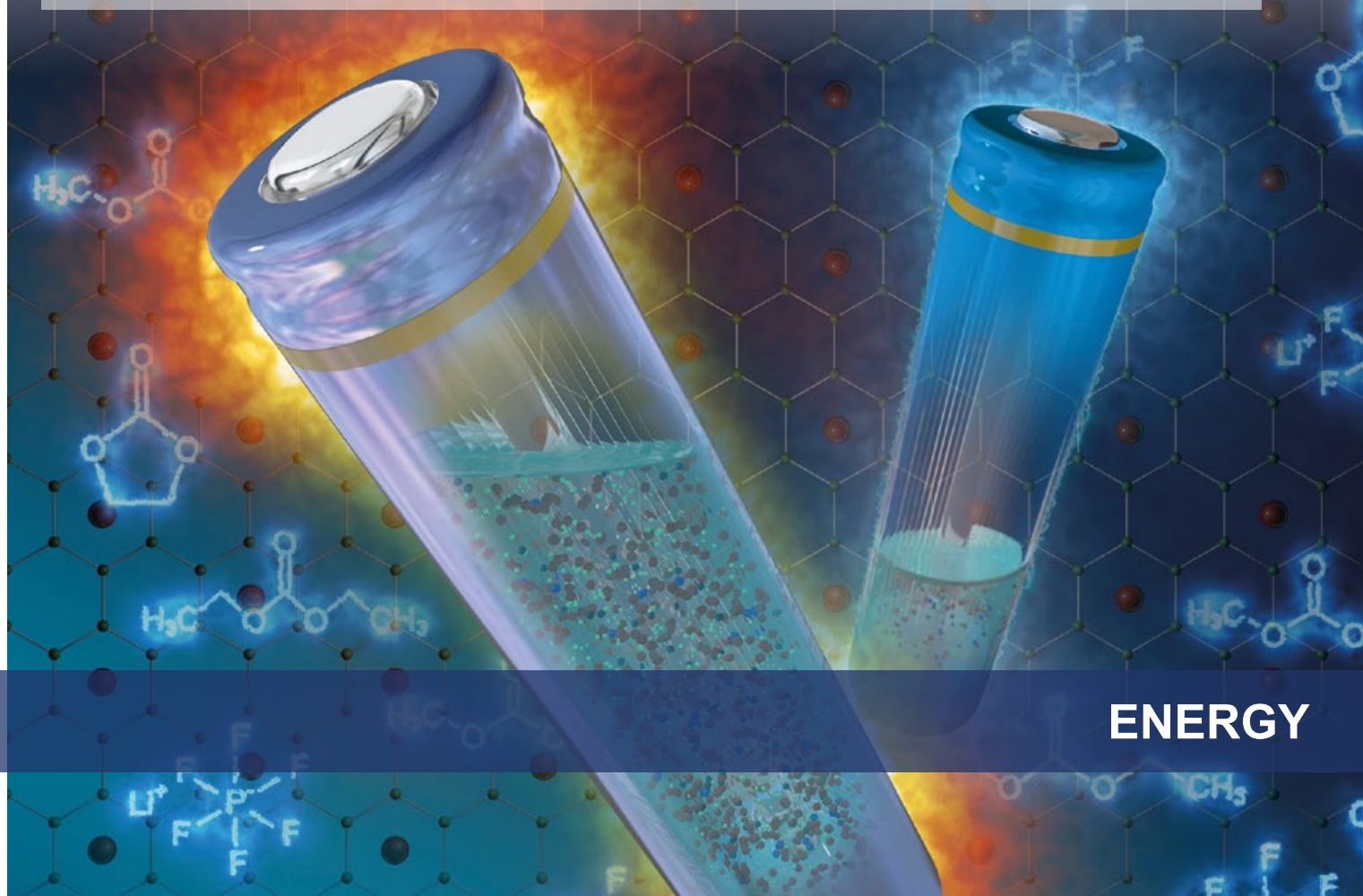
was attributed to the reactions with the electrolyte in which lithium ions are moving. If the battery loses movable lithium, it also loses capacity.

The older the warmer

The researchers found that the loss of lithium salt in the electrolyte and the available lithium in the electrodes are directly related. This leads them to the assumption that artificially adding fresh lithium could maintain the concentration constant for longer and thus increase the cell's lifetime. This approach could pave the way towards more stable batteries. Besides this, a direct correlation between the surface temperature of the cells and their state of fatigue was found: "old" batteries displayed a significantly greater temperature increase due to Joule heating as a consequence of an increased internal resistance at the same dis-/charging current.

D. Petz, V. Baran, C. Peschel, M. Winter, S. Nowak, M. Hofmann, R. Kostecky, R. Niewa, M. Bauer, P. Müller-Buschbaum, A. Senyshyn. Aging-Driven Composition and Distribution Changes of Electrolyte and Graphite Anode in 18650-Type Li-Ion Batteries, Adv. Energy Mat., 12, 2201652 (2022) DOI: 10.1002/aenm.202201652

The experiments were carried out at STRESS-SPEC and SPODI.



ENERGY



IT IS IN THE SUGAR

International researchers collaborated and utilized vastly different experimental techniques to understand how to augment cell membranes for specific tasks. They could be utilized in detergents.

Rhamnolipids (RLs) are among the most important lipids integrated into microorganisms' cell membranes, performing important tasks such as surface augmentation or signaling. Apart from their physical ability to reduce the surface tension of water, they show functionalities regarding cellular immunosuppression when integrated into human and animal cell membranes and trigger a better resistance to fungal pathogens in plants. This represents huge potential for cosmetic and pharmaceutical applications or in detergents. RLs' biological functionalities possibly come from the changes they make to the cell membranes during integration. However, this process's molecular mechanism is still unknown, although RLs have been shown to affect membrane stability, thickness and permeability, among other things.

Sugars are the driving forces

For their work, the researchers used small-angle X-ray scattering, neutron reflectometry and molecular dynamics simulations to investigate how the most abundant RL variant (diRL) integrates into planar or curved cell membranes. The presence of a specific type of membrane molecule

(GM1) in the standard phospholipid layer is necessary to facilitate the insertion of diRL. The scientists found the interactions between the sugar side-chains of diRL and GM1 to be the driving force of this process. diRL also induces modifications like increasing local membrane curvature upon integration. Additionally, neutron reflectometry proved to be a new tool to investigate these problems.

The science is not yet done

Although this work focused on the mechanics of diRL, other RLs might have different specific effects on their host membranes. Further research might reveal RLs' role for specific applications, like in diRL-based drug delivery by utilizing the lock-and-key related sugar-sugar interaction.

*V. Rondelli, L. Mollica, A. Koutsioubas, N. Nasir, M. Trapp, E. Deboever, P. Brocca, M. Deleu, Carbohydrate-carbohydrate interaction drives the preferential insertion of dirhamnolipid into glycosphingolipid enriched membranes, J. Colloid Interface Sci, 616, 739 (2022)
DOI: 10.1016/j.jcis.2022.02.120*

The experiments were carried out at MARIA.

CLEANER AIR THANKS TO POLYMER NANOCOMPOSITES

Advancements in technology have created space for sustainable engineering solutions in energy storage, food packaging and gas separation. Polymer nanocomposites have left a spectacular mark on these industrial applications. An analysis predicts a production of about one million tons and a market value of ~25 billion Euros by 2028.

Nine times higher gas permeation

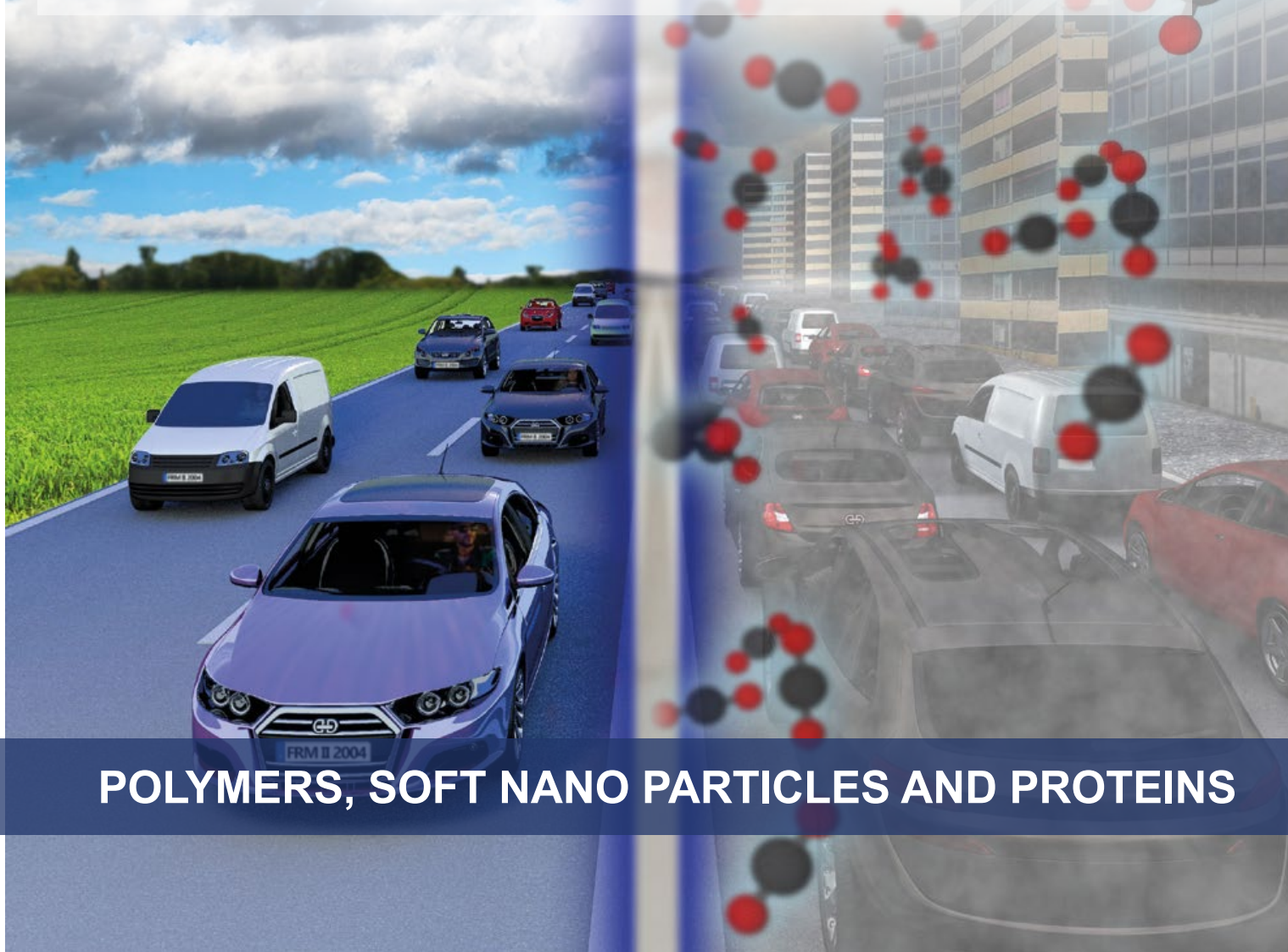
Introducing one-component nanocomposites (OCNC) with a polymer grafted onto nanometre-sized particle surfaces may prove to be a game-changing addition. OCNC have shown 200% higher energy storage in electrostatic capacitors as compared to more conventional composites. OCNC membranes could exhibit up to nine times higher gas permeation in gas separation applications than pure polymer membranes, providing a sustainable alternative to traditional, energy-intensive methods. Polymers being connected as chain-like objects offer a plethora of parameters to tune. Scientists explore these parameters to construct specifically optimized engineering solutions. Some applications require control of the flow of gas or ions through the composites at atomic levels. At this scale, the mobility of polymer chain segments plays a decisive role in regulating the flow.

Small polymers, big difference

Fortunately, the quasi-elastic neutron scattering technique is fully capable of detecting the motion of polymer segments. In order to address contradictions in previous results from the literature, the researchers investigated the mobility of grafted polymer chains in OCNC. They detected that there are slow- and fast-moving segments in both short and long polymer chains and learnt that these contribute differently to overall chain mobility. Since polymer mobility is a central parameter for governing OCNC properties, these results represent an important factor when it comes to eventually synthesizing specialized nanocomposites for particular applications like filtering gases.

*A. Sharma, M. Kruteva, M. Zamponi, S. Ehlert, D. Richter, S. Förster, Influence of Molecular Weight on the Distribution of Segmental Relaxation in Polymer Grafted Nanoparticles. Phys. Rev. Mater. 6 (1), L012601 (2022)
DOI: 10.1103/PhysRevMaterials.6.L012601*

The experiments were carried out at SPHERES.



POLYMERS, SOFT NANO PARTICLES AND PROTEINS

MAGNETIC MATERIALS



SUPER SPIN FOR SUPER COMPUTERS

The introduction of spintronic to electronic devices has greatly affected modern applications that make use of the spin. Newly discovered magnetic states in simple materials might soon extend our ability to store and handle information even further.

Applications like hard disk drives already manipulate magnetic spin states to store and read data. Controlling spin realizes fast response speeds and low-energy loss. Conventional spintronic devices however require costly integration of several complex materials to create these magnetic states.

Small rotating spheres?

Spins are often analogized as a spinning motion of particles; a better explanation is that spins indicate an orientation in space and a symmetry that these particles exhibit upon manipulation. Importantly though, spins influence the behavior of particles in magnetic fields.

Magnetic fields in stacks

Lanthanum strontium manganite (LSMO) is an oxide material. While ferromagnetic for low strontium content, LSMO displays antiferromagnetic properties when this is increased. Researchers have now discovered periodic spin structures emerging in stacks of these alternating thin LSMO layers when subjected to weak magnetic fields

over a wide range of temperatures. The reflection of polarized neutrons gave insight into this effect.

The atomic limit of computers

Conventional electronics utilize the distribution of negatively charged electrons in transistors to define the state of single bits, the 1s and 0s that make the modern world in the information age turn. However, smaller devices approaching the size of only dozens of silicon atoms physically limit this technology. Here, spin as another attribute of sub-atomic particles expands on classical capabilities.

Looking forward, these LSMO devices' chemical and structural simplicity and high-energy efficiency might lower the barriers to their adoption in spintronic devices, thus increasing the capabilities of, for example, superconducting spin valves and non-collinear spintronics.

*L. Guasco, Y. Khaydukov, G. Kim, T. Keller, A. Vorbiev, A. Devishvili, P. Wochner, G. Christiani, G. Logvenov, B. Keimer, Emergent Magnetic Fan Structures in Manganite Homojunction Arrays, Adv. Mater., 34, 2202971 (2022)
DOI: 10.1002/adma.202202971*

The experiments were carried out at NREX.

WAVES ON CIRCULAR PATHS

Just as electrons flow through an electrical conductor, magnetic excitations can travel through certain materials. Such excitations could transport information much more easily than electrical conductors. An international research team has now made an important discovery on the road to such components, which could be highly energy-efficient and considerably smaller.

At present the transport and control of electrical charges forms the basis for most electronic components. A major disadvantage of this technology is that the flow of electric currents generates heat due to the electrical resistance.

Propagation like waves in water

When throwing a stone into water, you bring the water molecules out of their equilibrium position. They start to oscillate, and a circular wave spreads out. In a very similar way, the magnetic moments in some materials can be made to oscillate. In this process, the magnetic moment performs a gyroscopic motion with respect to its rest position. The precession of one moment affects the vibration of its neighbor, and so the wave propagates.

Only neutrons capable to detect waves

Since neutrons are sensitive to magnetic fields like a compass needle, they are particularly well suited for the study of magnetic materials. Neutron scattering proved to be the only technique capable of detecting spin waves on circular

orbits since it provides the requisite resolution over very large length and time scales.

For applications utilizing these magnetic waves, controlling properties such as wavelength or direction is important. The team has now proven that the propagation of magnetic waves perpendicular to skyrmions does not occur in a straight line as it does in conventional magnets, but rather on a circular path.

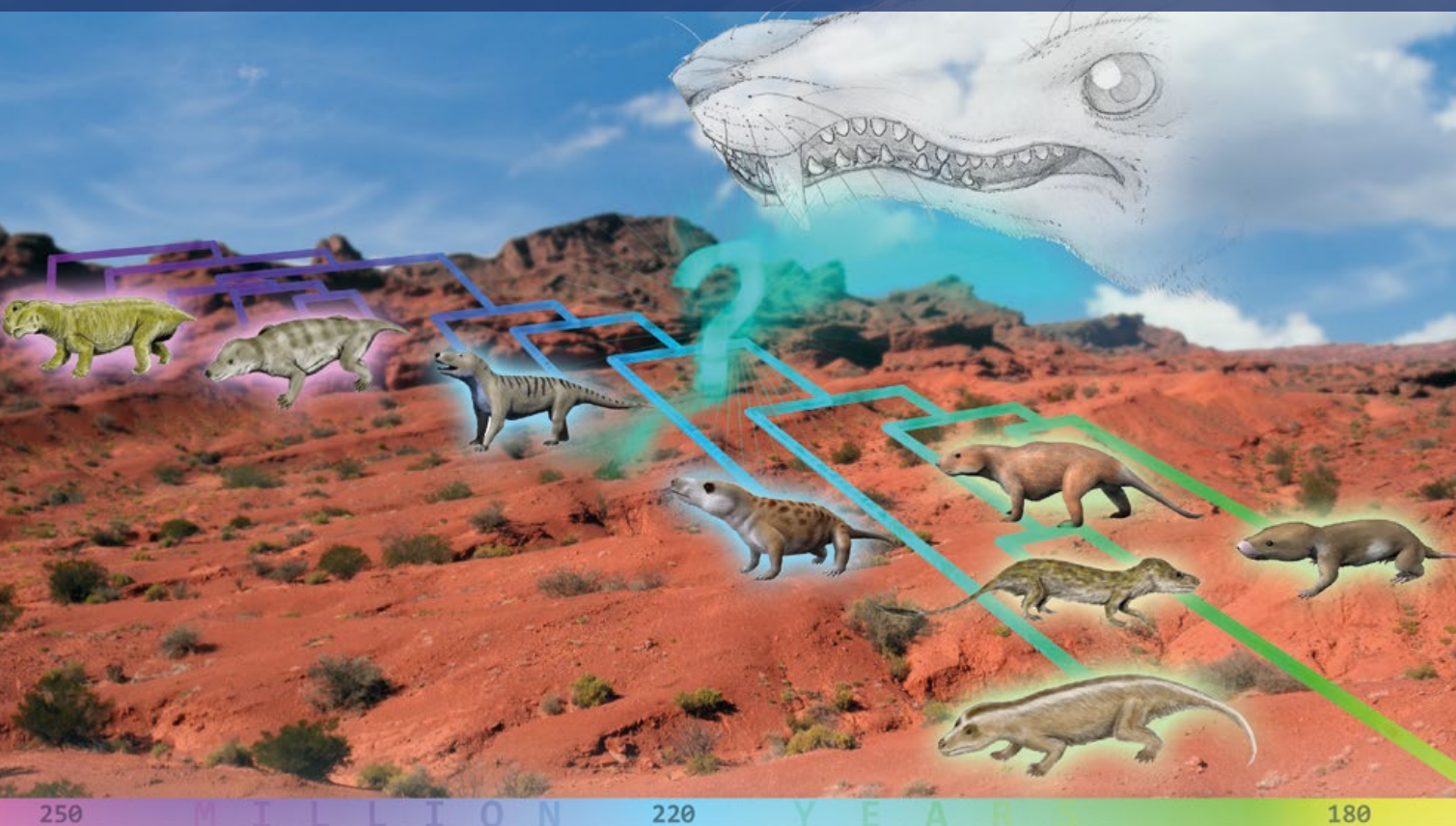
Coupling in quantum computers

The spontaneous motion of spin waves on circular orbits opens up a new perspective for realizing functional devices for information processing in quantum technologies, such as simple couplers between qubits in quantum computers.

T. Weber, D. M. Fobes, J. Waizner, P. Steffens, G. S. Tucker, M. Böhm, L. Beddrich, C. Franz, H. Gabold, R. Bewley, D. Voneshen, M. Skoulatos, R. Georgii, G. Ehlers, A. Bauer, C. Pfleiderer, P. Böni, M. Janoschek, M. Garst. Topological magnon band structure of emergent Landau levels in a skyrmion lattice, Science, 375, 1025 (2022)

DOI: 10.1126/science.abe4441

The experiments were carried out at RESEDA and MIRA.



NEUTRONS HELP TRACK DOWN MAMMALIAN ANCESTORS

A German-Argentine research team has used neutrons to identify a species of animal that has been extinct for 220 million years. The new species provides surprising insights into the evolution of mammals.

Argentinian researchers found the bones of the roughly mouse-sized cynodont species in the desert-like Talamapaya National Park in the west of Argentina.

Clear images thanks to neutrons

The researchers first performed X-ray imaging to take a look at the bones. However, due to the high iron content of the petrified soil, the fossilized bones could hardly be distinguished from the surrounding earth in the X-ray images. For neutrons, in contrast, iron is no problem at all. Therefore, the researchers used neutron tomography at the RA-6 facility of the Comisión Nacional de Energía Atómica in Argentina.

RA-6's thermal neutrons produced promising images, but with low spatial resolution. Therefore, the researchers continued their analysis at ANTARES, an instrument in Garching which uses cold neutrons with a longer wavelength. Moreover, ANTARES offers higher spatial resolution and much better contrast.

One step closer to unravelling the mystery of the origins of mammals

The new species adds new information to the evolutionary tree of cynodonts. With this new knowledge, researchers can better understand the evolution of mammals by reconstructing evolutionary steps – like the development of whiskers – in the evolutionary tree through comparison with closely-related species as well as with others belonging to more distant branches. The results also confirm the theory that the closest ancestors of mammals originated in what is now the south of Brazil. The finding thus takes researchers one step closer to unravelling the mystery of the origins of mammals.

L. C. Gaetano, F. Abdala, F.D. Seoane, A. Tartaglione, M. Schulz, A. Otero, J. M. Leardi, C. Apaldetti, V. Krapovickas, E. Steimbach, A new cynodont from the Upper Triassic Los Colorados Formation (Argentina, South America) reveals a novel paleobiogeographic context for mammalian ancestors. Sci Rep 12, 6451 (2022)

DOI: 10.1038/s41598-022-10486-4

The experiments were carried out at ANTARES.

EXPLORING THE EARLY SOLAR SYSTEM

What is the origin of the Earth? Why do planets look the way they do? How did the solar system form? These big questions have been forever driving mankind forward – and the answer is made up of an infinite number of small details.

Pallasites belong to the class of stony-iron meteorites. Characteristic for these beautiful rocks from space are centimeter-sized embedded olivine crystals, which shimmer greenish between iron and nickel. That is why they are also very popular among scientists and collectors.

The origin of everything

Pallasites were formed in the early days of the solar system by cosmic collisions and are one of the few sources that provide information about the rocky interior of asteroids. Understanding their formation and the processes before and after this event allows us to decipher the dynamics of the early solar system.

A common family on the way to earth

All Pallasites studied originated from the same parent body, even though they were found in different locations on Earth. This makes it possible to compare the development of different areas inside their parent body.

Metal veins reveal origin of meteorites

By comparing the metal veins running through the crystals in the pallasites with deformation experiments on the SAPHiR instrument, it is also possible to determine how quickly or slowly the pallasites cooled after they were formed. The differences in cooling times infer the origin of the meteorites, i.e., from which depth in the mantle of the mother body they originated.

The researchers can thus get a more precise picture of the structure of the mantle and its evolution. Among other things, it allows them to constrain the size of the asteroid and better understand its evolution 4.5 billion years ago.

N. Walte, G. Golabek, Olivine aggregates of Main Group Pallasites reveal the early evolution of their Parent Body, Meteorit, Planet. Sci., 57, 1098 (2022)

DOI: 10.1111/maps.13810

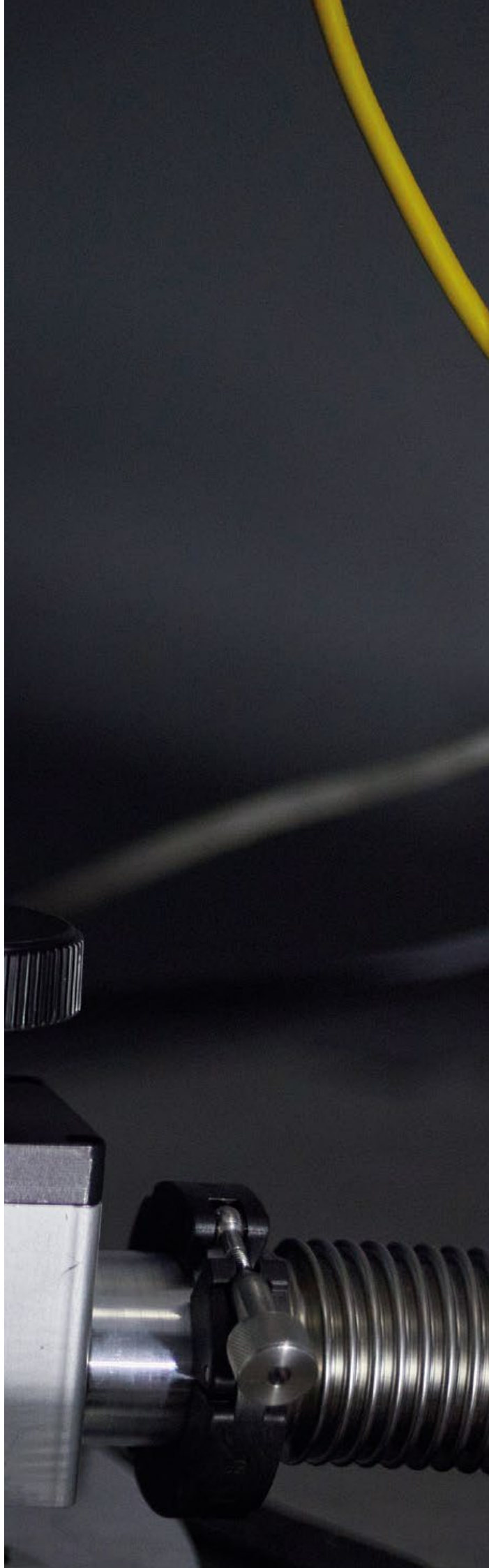
The experiments were carried out at SAPHiR.



EARTH, ENVIRONMENT AND CULTURAL HERITAGE



Industry & Medicine



Making CO₂ more usable

A team at the Albert Ludwigs University of Freiburg used high-resolution neutron microscopy to detect undesired salt formation in electrodes of CO₂-electrolysis for the first time, thus shedding light on the cause of a central problem area.

CO₂-electrolysis promises to convert harmful CO₂ into usable chemicals such as carbon monoxide (CO) or ethylene with the help of renewable energy. These, in turn, can serve as feedstock chemicals for alcohols, synthetic fuels or plastics and are thus key to “de-fossilising” the chemical industry.

Precipitates reduce efficiency

In CO₂-electrolysis, analogous to water electrolysis, i.e. hydrogen production, electrochemical reactions are carried out at two electrodes separated by a membrane. This continuously converts CO₂ into CO. The development can therefore be based on previous experience with water electrolysis and with the fuel cell – i.e. the conversion of hydrogen back into electricity, e.g. to power a truck. This is because the cathode electrode is designed as a so-called gas diffusion electrode, similar to the fuel cell. Unlike in the fuel cell, however, in CO₂-electrolysis gas diffusion can be impeded by the formation of salts. These salts are formed as an unwanted by-product and prevent the CO₂ from reaching

the catalyst and being converted into CO. This salt formation was already known, but it has not yet been detected in operation in the cell.

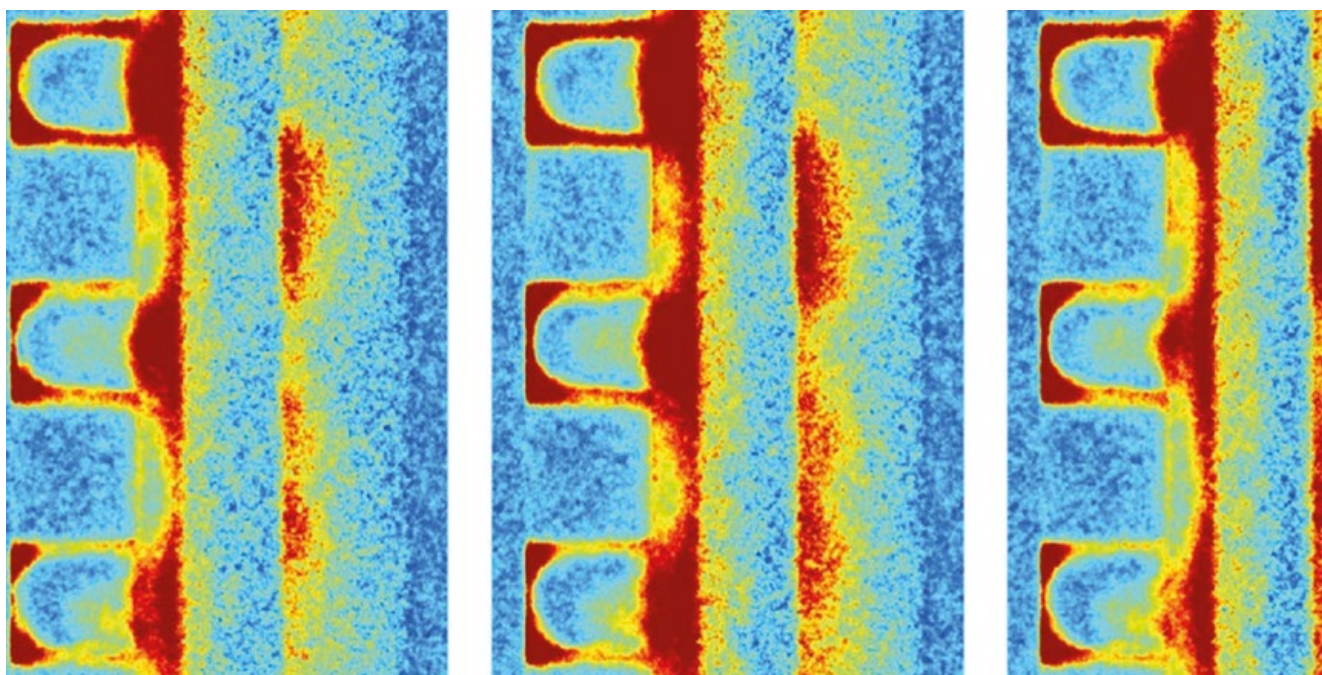
Neutrons make salts visible for the first time

In a cooperation with the French Centre national de la recherche scientifique and the Institut Laue-Langevin in Grenoble, the research group “Electrochemical Energy Systems” at the University of Freiburg has now been able to show for the first time in high resolution how salt formation takes place in the electrode. This means that further steps can now be taken to prevent salt formation and thus achieve consistently high efficiency.

International cooperation

While the electrochemical experiments were developed at the University of Freiburg, scientists from TUM contributed a neutron detector with record resolution. Finally, all the building blocks were put together in Grenoble, because that is where the CO₂-electrolysis experiments were set up at the ILL neutron source and measured with the Munich detector.

J. Disch, L. Bohn, S. Koch, M. Schulz, Y. Han, A. Tengtini, L. Helfen, M. Breitwieser, S. Vierrath, High-resolution neutron imaging of salt precipitation and water transport in zero-gap CO₂ electrolysis, Nat. Commun. 13, 6099 (2022) DOI: 10.1038/s41467-022-33694-y



Neutron images show the change in water content in the cell, which in turn provides information about precipitated salts.

Understanding the structure of fuel cell membranes

Proton exchange membrane fuel cells (PEMFC) can be found, for example, in hydrogen cars and are therefore important in the transition to green energy. The core element of the cells is a proton exchange membrane. Japanese researchers have now investigated its complex structure in greater detail than ever before with the help of neutrons.

PEMFCs have been developed and in use since the 1960s. The proton exchange membrane (PEM for short) of the PEMFC is a very thin plastic membrane. It separates the two reaction partners, hydrogen and oxygen, from each other, and allows when hydrated only positively charged electrical particles, the protons, to pass through water-filled channels. Both sides of the membrane are coated with catalytically active electrodes. On one side, hydrogen molecules are oxidized to two protons each by the release of two electrons. These protons then cross the membrane with the help of the channels. On the other side of the membrane, electrons, which previously were able to perform electrical work in an external circuit, reduce oxygen. Together with the protons, water is formed.

Produce more efficient materials

Currently, perfluorosulfonic acid polymers such as Nafion® are the leading materials, as they show good stability at moderate operating temperatures while simultaneously demonstrating high conductivity over a wide range of relative humidity conditions. These properties, according to the latest research, result from the membranes' structure being made up of nanometer-sized domains. However, a complete picture of the microstructure of Nafion® was still lacking despite widespread use of the material including intensive studies. The aim of this study was to understand the mechanism by which ions are transported through the material and thus learn how to produce more efficient materials for different temperatures and humidity conditions.

Structure like a sponge

Researchers from the National Institutes for Quantum Science and Technology in Japan have now investigated the microstructure of hydrated Nafion® and the water-filled ion



Hydrogen cars contain proton exchange membranes, as investigated by the Japanese research team at the MLZ.

channels in more detail for the first time with the help of a special method of contrast variation neutron small-angle scattering at the KWS-2 at the MLZ. They interpreted the data using a decomposition method into partial scattering functions characteristic of each component, namely the main chain of the polymer, the side chain of the polymer and the water.

The researchers were able to quantitatively reconstruct the entire structure of the hydrated Nafion® membrane. Resembling a sponge soaked in water, the structure is self-similar, i.e. both the membrane as a whole and its components have a sponge-like structure. Additionally, there are crystalline and amorphous structural components. The measurements also showed that the water is homogeneously distributed over a large area of the material. This fits in well with the thesis that the high membrane conductivity of the membrane is based on a well-connected water network.

Y. Zhao, K. Yoshimura, T. Motegi, A. Hiroki, A. Radulescu, Y. Maekawa, Three-Component Domains in the Fully Hydrated Nafion Membrane Characterized by Partial Scattering Function Analysis, Macromolecules 54, 9, 4128 (2021) DOI: 10.1021/acs.macromol.1c00587

Neutrons explore more efficient hydrogen storage systems

Hydrogen plays an important role in the transition to a sustainable energy infrastructure. It is particularly promising as a potential energy storage medium because of its flexible applications, for example in mobility. However, the technology still faces major obstacles, especially in terms of efficiency and storage. Intensive research goes into developing solutions for these problems and neutrons are contributing to this effort.

The basic principle is simple: Hydrogen reacts with oxygen to form water, releasing energy in the process. If one manages to store the hydrogen, it can be brought to reaction later in order to release the stored energy. The problem is that pure hydrogen can only be stored at very high pressure or low temperatures. This brings practical problems for many applications, starting with transportation. For this reason, people have long been searching for solids that can bind the hydrogen chemically.

What happens microscopically?

These solids should be able to store hydrogen in high quantities, and the chemical reactions to release hydrogen should be fast and efficient. One type of solid has attracted a lot of interest in recent years: Compounds of light alkali and alkaline earth metals such as lithium or magnesium, and hydrogen-containing molecules. The key is the right mixture of several of these compounds in the hydrogen storage system: By cleverly combining them, it is possible to control via the applied temperature and pressure whether hydrogen is absorbed or released.

Neslihan Aslan, a PhD student at the Helmholtz-Zentrum Hereon at the MLZ, has taken a closer look at the compound $\text{Li}_4(\text{BH}_4)(\text{NH}_2)_3$, which is formed as a product in one of these compounds after hydrogen is released. While it is already known that this solid is a good hydrogen storage material, it is not understood why this is so at the microscopic level. This includes the crystal structure itself, as well as the motions of the hydrogen atoms within it.



Neslihan Aslan prepares the sample in powder form for analysis on the TOFTOF instrument. The powder is highly sensitive, so she must handle it under low-oxygen conditions in a glove box.

Neutrons reveal high mobility of hydrogen

Neslihan Aslan studied the crystal structure and its stability up to its melting point using synchrotron radiation. For the dynamical processes, she turned to the TOFTOF instrument at the MLZ for quasielastic neutron scattering. “This measurement at such a precision is not possible with any other method, because neutrons are ideal for studying hydrogen, and additionally they can resolve events in time and thus make them measurable,” explains Neslihan Aslan.

Her supervisor at GEMS, Dr. Sebastian Busch, is also very satisfied: “We were excited to see that the mobility of hydrogen is already very high within the solid,” he says, “before the neutron measurements, we had assumed that the material would have to melt first to allow the hydrogen to move so quickly.” The fast movement is important for a fast reaction. After all, nobody wants to wait a long time when fuelling up a hydrogen vehicle. The next step is to study the entire solid with measurements during the charging and discharging process to investigate the interaction of the individual components. Here, too, neutrons can provide a deep insight.

N. Aslan, G. Gizer, C. Pistidda, M. Dornheim, M. Müller, S. Busch, W. Lohstroh, High Hydrogen Mobility in an Amide-Borohydride Compound Studied by Quasielastic Neutron Scattering, Adv. Eng. Mater., 23 2100620 (2021) DOI: 10.1002/adem.202100620

Patent for a versatile valve

A new patent, developed at the MLZ and the Max Planck Institute for Solid State Research, makes so-called spin valves possible for the first time. These produce any resistance and could be used as artificial neurons, for example.

In contrast to transistors, where an applied voltage switches a large electrical resistance on and off, the resistance in spin valves is controlled by a magnetic field or, more precisely, its direction. So far, it has only been possible to realize collinear valves.

So far only two settings

Just like transistors, these can only switch between two values for the resistance. To do this, two ferromagnetic layers are decoupled from each other by a thin conductor so that both can be magnetized independently of each other. Magnetization involves exposing a ferromagnet to a magnetic field so that the spins inside it align and it maintains its own magnetic field. With relatively weak external fields, this self-produced magnetic field always points along the so-called “easy axis”, which is determined by the material. Both directions along this axis are possible, depending on the direction of the external magnetic field. The trick with binary spin valves is to fix the magnetization of one of the two ferromagnets so that an external magnetic field can only change that of the other. This way, the ferromagnets have the magnetization either in the same direction, which minimizes the resistance, or in the opposite direction, which leads to maximum resistance.

Invention makes arbitrary resistances possible

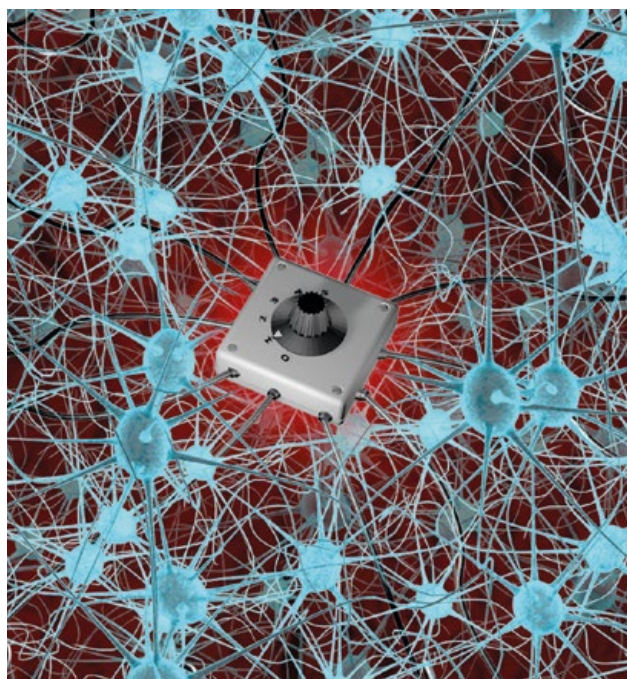
Could one also realize a continuous spin valve in which the two magnetizations can be arbitrarily rotated against each other and thus produce resistances between the two extreme values? Dr. Yuri Khaydukov from the Max Planck Institute for Solid State Research, until recently instrument scientist at the NREX of the MLZ, has submitted a patent describing how such a valve could work. The basic mode of operation is similar to that of the binary spin valve. However, he turns the tables by varying the direction of the fixed ferromagnetic layer through a clever choice of the materials used for the valve, without affecting the easy axis of the other ferromagnet. This means that all settings between the two extremes of the collinear spin valves are now possible.

Yuri Khaydukov came across this effect while investigating the interfaces between ferromagnets and superconductors with neutrons. He noticed in his measurements that the axis of magnetization seemed unexpectedly fixed, quickly recognized the potential of this discovery and endeavored to implement it in spin valves.

Candidates for artificial neurons

“With this method, it is now possible for the first time to have spin valves that reliably reproduce any resistances. And this makes the valves versatile,” Yuri Khaydukov explains the relevance of his patent. The first application that comes to his mind is the realization of artificial neural networks, where a series of input signals are linked together over several layers. The nodes at which input signals converge are the artificial neurons. Just like their biological counterparts, they give an output signal when the sum of the incoming signals exceeds a certain threshold. The neural network learns by constantly adjusting this threshold until it finds the optimum. This is exactly where the continuous spin valves can be used, by having the finely adjustable resistor act as an artificial neuron.

Description of the patent: <https://www.max-planck-innovation.com/technology-offers/technology-offer/non-collinear-spin-valve-2.html>



One possible application for continuous spin valves could be artificial neurons.

Super methods for superalloys

The newly developed superalloy VDM® Alloy 780 withstands temperatures of up to 750°C and endures enormous forces with ease. Such materials are real superheroes among alloys. And just like human superheroes, they have very special laboratories and methods with which they can improve their strength.

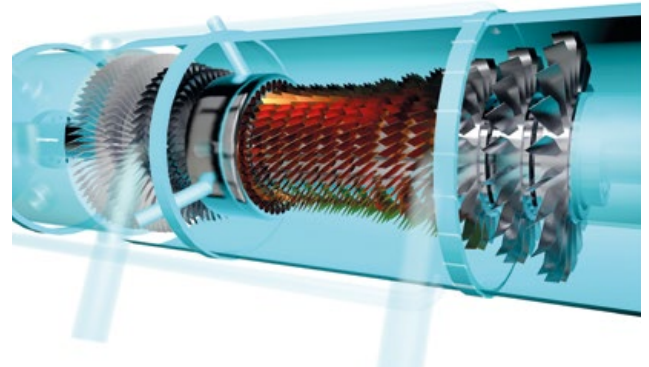
Superalloys owe their stability, among other things, to their internal structure, i.e. the way in which the atomic constituents arrange themselves. They form a regular crystal lattice, the so-called γ matrix, which forms the basic structure of the alloy. In addition, various substructures and other elements are embedded to increase the stability and heat resistance of the alloy. One of these processes is the generation of another phase, the so-called γ' phase. It consists of single-crystalline precipitates arranged within the alloy and embedded in the matrix.

These precipitates, typically of the order of nanometers, are formed when the alloy undergoes an appropriate temperature treatment. They increase the mechanical stability of the alloy because they act as barriers to atomic rearrangements. The VDM® Alloy 780 produced by the metallic materials company VDM Metals also owes its stability to this principle, and promises operating temperatures of up to 750°C. To better understand its properties, scientists from the BMBF HiMat project have studied the alloy with neutrons and X-rays in order to understand how the γ' matrix is formed (see p. 56 for more details).

How to defeat a superalloy?

But what happens to the γ' phase at temperatures well above the maximum operating temperature of the superalloy? Dr. Frank Kümmel, until recently a scientist at the MLZ, and his colleague Dr. Massimo Fritton have also used X-ray and synchrotron radiation to study the VDM® Alloy 780 alloy in order to understand its stability and longevity. The two methods differ essentially in their energy and thus in their depth of penetration. The former has energies that are conveniently generated using laboratory instruments, but can only penetrate a few micrometers deep into the alloy.

Synchrotron beams, on the other hand, are highly focused beams with much higher energy as conventional laboratory X-rays. They can thus penetrate several millimeters into



Superalloys from VDM Metals are used, for example, in gas turbines, where they have to withstand high temperatures and forces. Optimized superalloys can improve the durability and efficiency of such turbines.

the sample. They are generated at large research facilities, such as the German Electron Synchrotron (DESY) in Hamburg. Frank Kümmel and Massimo Fritton also made their measurements at the PETRA III synchrotron there. “With both methods, investigations are possible both on the surface and inside the sample, and by comparing them we can distinguish surface effects from effects inside the sample,” explains Frank Kümmel.

Full stability below 750°C

With the combined measurements, the two scientists were able to show that the γ' phase is retained throughout the alloy at temperatures below 750°C and thus exhibits full stability. Only at 800°C the precipitates begin to dissolve. They also observe this effect on the surface of the alloy together with small oxidation effects.

“These new findings are of great value for materials science but also for industry to further optimize the alloy,” says Ralph Gilles, coordinator of the BMBF HiMat project, where the two alloy investigations were conducted. After all, the superalloys from VDM Metals are used for example in gas turbines, where they have to withstand extreme temperatures, among other things. This could allow turbines to run more efficiently in the future.

F. Kümmel, M. Fritton, C. Solís, A. Kriele, A. Stark, R. Gilles, Near-Surface and Bulk Dissolution Behavior of γ' Precipitates in Nickel-Based VDM® Alloy 780 Studied with In-Situ Lab-Source and Synchrotron X-ray Diffraction, Metals 12, 1067 (2022)

DOI: 10.3390/met12071067

Less waste from lower enriched uranium targets

Nuclear medicine utilizes technetium-99m for tumor diagnostics. With over 30 million applications worldwide each year, it is the most widely used radioisotope. The precursor material, molybdenum-99, is mainly produced in research reactors. A study at the FRM II now illustrates options to significantly reduce the radioactive waste produced during processing to a medical product.

Coupled to suitable organic molecules, technetium is distributed throughout the body via the blood and accumulates in tumors, for example. When it decays there, the radiation released reveals the precise location of the tumor.

Technetium-99m (Tc-99m) is produced by irradiating uranium plates, so-called targets, with a high neutron flux that is practically only available at research reactors. Starting from uranium-235 this produces molybdenum-99 (Mo-99), which decays to Tc-99m with a half-life of 66 hours. With a half-life of six hours, the latter converts to Tc-99, emitting gamma radiation that can be measured.

More waste from low-enriched uranium

The political desire to replace highly enriched uranium with low-enriched uranium also applies to targets being used in the medical field. This is why the Mo-99 irradiation facility currently under construction at the FRM II is designed for targets with low-enriched uranium.



Dr. Tobias Chemnitz at the test facility for Mo-99 production at the FRM II.

“However, this gives rise to a severe problem: the less the uranium plates are enriched with uranium-235, the lower the specific yield of Mo-99 during irradiation,” says Dr. Tobias Chemnitz, instrument scientist at the MEDAPP medical irradiation facility at the MLZ.

To meet world-wide demand for Tc-99m, at least twice as many uranium plates must be irradiated and processed, depending on the technology used. This produces correspondingly higher volumes of waste. Chemnitz addressed this problem in his doctoral thesis at the Technical University of Munich.

New process avoids up to 15,000 liters of liquid radioactive waste

The final irradiated plates comprise only about 0.1 percent Mo-99. To ensure a purity sufficient for medical applications, the Mo-99 must be separated from the remaining material.

Since highly enriched targets have been substituted by low-enriched targets, the same molybdenum yield doubles the volume of the resulting aqueous, medium-level radioactive waste to an annual volume of up to 15,000 liters worldwide.

The solution: Get rid of the water

To alleviate this problem, Chemnitz and his colleague Riane Stene developed a new method for extracting Mo-99 without the use of aqueous chemistry.

In collaboration with the fluorine chemistry group at Philipps University of Marburg, the researchers developed a system in which the uranium-molybdenum test plates react with nitrogen trifluoride in a plasma. These plates had the same molybdenum content as would later be present in actual irradiated targets.

The Technical University of Munich has submitted a patent application for the process. Chemnitz is confident that this novel approach will provide a viable alternative to established processes in the medium term.

T. Chemnitz, Development of a dry-chemical extraction process for ⁹⁹Mo and plasma-aided synthesis of transition metal hexafluorides, Dissertation, TUM (2020)

How prefilled syringes become clogged

The hypodermic needles of prefilled syringes can clog if stored incorrectly. A research team with the pharmaceutical company Novartis has studied the process in detail and systematically, including via neutron radiography. The results should help to adapt production and storage conditions accordingly.

Prefilled syringes have become indispensable for the administration of therapeutic proteins (biopharmaceuticals) in particular, as they are now available as a therapeutic option for a number of diseases, such as cancer. They are easy to handle and allow exact dosing during application, which can thus also be carried out by the patients themselves. Recently, however, it has become apparent that under certain circumstances, which are still insufficiently understood, the needles can become clogged during storage, which can lead to incorrect dosing of the drugs during injection.

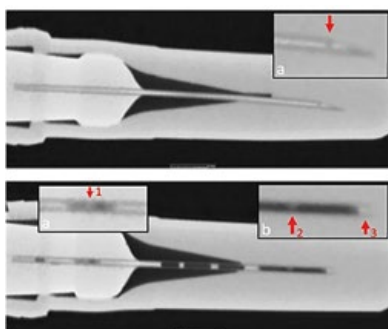
Neutrons reveal fluid in needle tip

"This is currently a topical problem that has attracted international attention not only from pharmaceutical manufacturers but also from regulatory authorities," says Prof. Dr. Stefan Scheler from the Swiss pharmaceutical company Novartis and Kaiserslautern University of Applied Sciences. Scheler and his colleague Dr. Alexander Zuern have for the first time developed a detailed and systematic study that mathematically models the processes involved in needle clogging, thus providing a better understanding of the background to this undesirable process. It also made use of the ANTARES neutron radiography facility at the MLZ.

Incorrect storage at too high a temperature

The trigger for clogging is that liquid penetrates the needle. The Novartis team wanted to investigate more closely which factors influence this. The researchers examined 27 differently treated prefilled syringes. Some were exposed to

Neutrons penetrate the metal of the needles easily and show a good contrast between liquid (dark) and air as seen in the radiographies (left pictures). The longer the storage time, the more water evaporates from the needle (right picture).



temperature fluctuations instead of being stored in the refrigerator as prescribed. The pharmacists also examined shaking and pressure fluctuations, to simulate air freight transport, as well as storage times of varying lengths.

"A major problem is certainly the gas permeability of the rubber cap on the syringe, which also allows diffusion of water vapor," Scheler explains. While the use of a denser rubber compound would be able to reduce evaporation, it would also protect the needle from entry of the microbicidal gas used to sterilize empty syringes before filling.

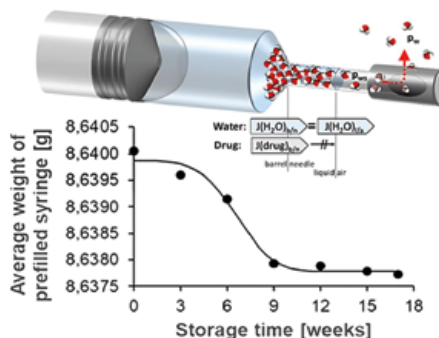
Needle blockages – A growing problem

"The neutron experiments clearly showed us the conditions under which liquid enters the needle," Scheler says. Overpressure inside the syringe relative to ambient air leads to faster clogging. Storage time and high temperatures also have a negative effect. "Needle clogging could happen more often in the future," predicts Scheler. This is because, in order to be able to administer high active ingredient doses subcutaneously in small volumes, the active ingredient concentrations in the syringes are being selected to be ever higher. This increases the risk of needle blockages.

Findings enable development of countermeasures

"We are now working to prevent this from happening in the manufacturing process," says Scheler. One possibility, he says, is to change the filling process and create a slight negative pressure in the syringe that prevents liquid from entering the needle during storage. To optimize such measures, further investigations with neutrons can be very helpful.

S. Scheler, S. Knappke, M. Schulz, A. Zuern, Needle clogging of protein solutions in prefilled syringes: A two-stage process with various determinants, Eur. J. Pharm. Biopharm. 176, 188 (2022)
DOI: 10.1016/j.ejpb.2022.05.009



Better vaccines against multi-resistant germs

Bacteria which are resistant to all conventional antibiotics cause more than one million deaths each year. Consequently, researchers around the world are looking for new therapeutic approaches against these pathogens. Recently, scientists analyzed precisely a promising vaccine against multi-resistant germs.

An international team in Grenoble identified an active ingredient suitable for producing a vaccine against multi-drug-resistant bacteria *Pseudomonas aeruginosa*. The vaccine has since been successfully tested in mice.

“As with many new vaccines, the active ingredient in this case is embedded in liposomes. Accurately characterizing and understanding these nanoscopic biomolecules is a key factor in the development and optimization of future vaccines,” explains Dr. Marco Maccarini, biophysicist at the Centre National de la Recherche Scientifique (CNRS). With his team and at the FRM II, he has now succeeded in analyzing the structure of the vaccine candidate against *Pseudomonas aeruginosa*.

The vaccine consists of biomolecules about 100 nanometers. These molecules consist mostly of lipids, substances similar to fats, which form small bubbles or liposomes because of their biochemical properties. These bubbles can in turn protect and transport the actual active ingredients. In the case of the vaccine against *Pseudomonas aeruginosa*, this active ingredient is the protein OprF. “In general, the active ingredient can dock on the liposome at various positions – for example internally or externally,” Maccarini explains. “But it is best recognized by the immune system when it is incorporated into the double lipid layer. Thus knowing the structure of the biomolecules is crucial for the effect of a vaccine.”

Wanted: Non-destructive radiation

“Neutron beams are ideal: they only interact with atomic nuclei, and thus cause no damage or structural changes. This way the samples can be investigated in their original condition,” Maccarini explains. At the MLZ in Garching, the researcher found everything he needed to analyze the new vaccine candidate: a high neutron flux, a well-equipped laboratory and Dr. Aurel Radulescu, an expert in small-angle measurements, a technology which can be used to study the nanometer-sized molecules in detail.



The vaccine consists of biomolecules about 100 nanometers. They were analyzed using neutrons.

Neutrons see hydrogen

“In our case the challenge was to distinguish between the proteins and the lipids in the sample,” recalls Radulescu, who oversees the KWS-2 neutron small-angle facility for Forschungszentrum Jülich. He adds that it took a trick to finally make this distinction work: “We conducted the measurements with different combinations of solvents – normal water and heavy water containing deuterium, mixed in various concentrations.” Because neutrons “see” normal hydrogen and deuterium differently, images of the sample were created with different contrasts containing different information.

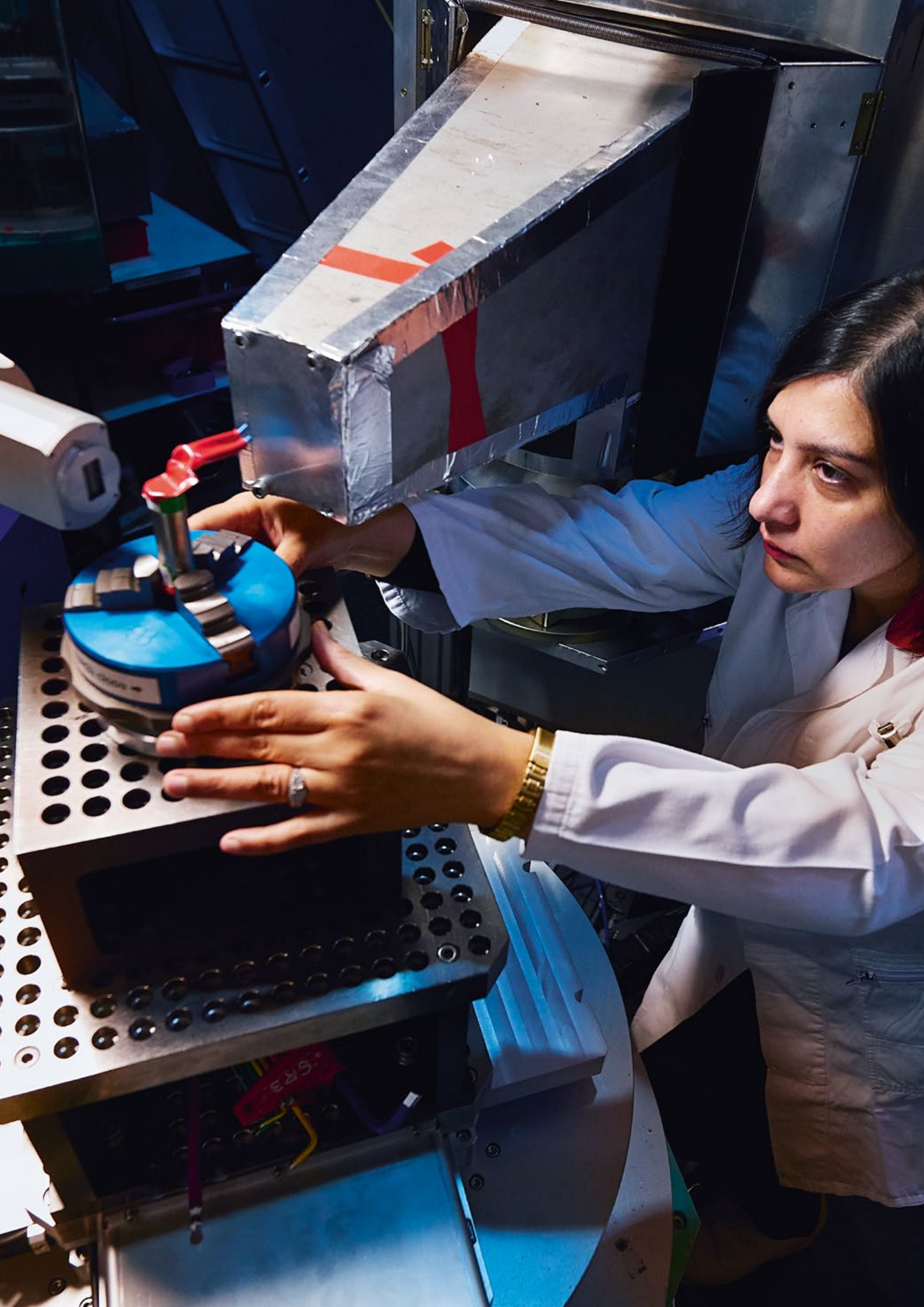
Computer model determines position

For the analysis, the research team developed a computer model which represents the structure of the candidate vaccine. “In this way, we were able not only to visualize the bilayer structure of the lipids, but also to determine the average position and amount of the OprF active ingredient embedded between the two lipid layers.

The new model can now also be used to explore the structure of new, liposome-based vaccines and optimize their development.

F. Spinozzi, J.-P. Alcaraz, M. G. Ortore, L. Gayet, A. Radulescu, D. K. Martin, M. Maccarini, Small-Angle Neutron Scattering Reveals the Nanostructure of Liposomes with Embedded OprF Porins of Pseudomonas aeruginosa, Langmuir 38, 15026 (2022)

DOI: 10.1021/acs.langmuir.2c01342





Scientific Reports



Effects of polymer coating mechanics at solid-electrolyte interphase for stabilizing lithium metal anodes

Z. Huang¹, N. Paul², S. Choudhury³, J.H. Thienenkamp⁴, P. Lennartz⁴, H. Gong³, P. Müller-Buschbaum^{2,5}, G. Brunklaus⁴, R. Gilles², Z. Bao³

¹Department of Materials Science and Engineering, Stanford University, Stanford, USA; ²Heinz Maier-Leibnitz Zentrum (MLZ), Technical University of Munich, Garching, Germany; ³Department of Chemical Engineering, Stanford University, Stanford, USA; ⁴Institute of Energy and Climate Research (IEK-12), Forschungszentrum Jülich GmbH at Helmholtz-Institute Münster (HI MS), Münster, Germany; ⁵Physics Department E13, Technical University of Munich, Garching, Germany

Lithium metal batteries (LMBs) are next generation energy storage devices that rely on the stable deposition of Li. A layer of polymer coating on Li can stabilize its deposition. In this work, we investigated the effect of the polymer mechanical property on Li deposition and found a viscoelastic layer results in homogeneous Li deposition and higher cycling performance.

The unstable interface between Li and the electrolyte hinders the commercialization of LMBs. A layer of solid electrolyte interphase (SEI), when Li is exposed to the liquid electrolyte, is often brittle, and can fracture during cycling. Heterogeneous Li deposition originates from these local defects, and is the root cause of capacity fading and cell failure in LMBs. While several works in the past have evaluated polymer coatings as an artificial coating layer for the Li electrode, the requirement for polymer design is still unclear.

Materials design and characterization

In this work, we investigate the effect of polymer dynamics on Li deposition. We design a PFPE (perfluoro polyether) based polymer network with evenly spaced H-bonding sites of various strengths, resulting in significant differences in the molecular ordering, as analyzed by SAXS measurements. The differences in the H-bonding strength directly impacted the mechanical properties of these materials, thus providing a controlled set of samples with a range of polymer dynamics for electrodeposition studies. We name the two types of hydrogen bonds as I unit and M unit. The H-bonds in the I unit are weak due to steric hindrance. The M unit has π - π stacking, leading to strong H-bonds. A polymer with a higher percentage of M units shows a more solid-like behavior. Finally, a systematic evaluation of the lithium metal electrodeposition quality with these polymers as negative electrode coatings showed that polymers with

flowability or faster polymer dynamics exhibited higher coulombic efficiency and a more homogenous Li deposition morphology. We found the optimal ratio between the M unit and the I unit is 1:3. This work demonstrates a design concept different from the conventional wisdom: an interface capable of suppressing heterogeneous Li growth needs to have a modulus higher than Li. These experimental findings provide rational design principles of soft polymer coatings on lithium metal electrodes.

[1] Z. Huang et al., *Effects of Polymer Coating Mechanics at Solid-Electrolyte Interphase for Stabilizing Lithium Metal Anodes*, *Adv. Energy Mater.* 12, 2103187 (2022)
DOI: 10.1002/aenm.202103187

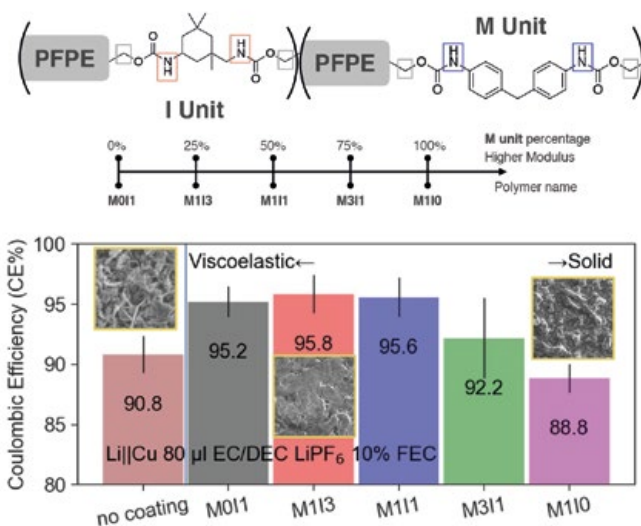


Figure 1: The chemical structure of the PFPE-based polymer with both the M and I unit linkers. The cycling C.E. of the coated Li||Cu cells and the top-view SEM images of Li deposited on Cu electrode. Electrolyte listed.

Study of H diffusion in Zircaloy-2 and Zr-2.5%Nb plates between 250°C and 350°C by neutron imaging

J. R. Santisteban^{1,2}, N. L. Buitrago^{1,2}, A. Moya Riffo^{1,2}, S. R. Soria^{2,3}, A. L. Baruj^{2,3}, M. Schulz⁴, M. Grosse⁵, V. Luzin⁶, M. Hache⁷, L. Barrow⁷, M. R. Daymond⁷

¹ Comisión Nacional de Energía Atómica, Laboratorio Argentino de Haces de Neutrones (LAHN) Argentina; ² Consejo Nacional de Investigaciones Científicas y Técnicas (CONICET), Argentina; ³ Comisión Nacional de Energía Atómica, Centro Atómico Bariloche, S. C. de Bariloche, Argentina; ⁴ Heinz Maier-Leibnitz Zentrum (MLZ), Technical University of Munich, Garching, Germany; ⁵ Institute for Applied Materials, Karlsruhe Institute of Technology, Karlsruhe, Germany; ⁶ Australian Center for Neutron Scattering, ANSTO, Lucas Heights, Australia; ⁷ Department of Mechanical and Materials Engineering, Queens University, Kingston, Canada

Zr alloys used in the nuclear industry for fuel cladding are susceptible to H degradation. The reactor core operates in high-pressure water at temperatures close to 300°C and H is incorporated by the waterside corrosion on Zr components. In the present work, H diffusion coefficients were determined in Zircaloy-2 and Zr-2.5%Nb rolled plates at 250°C, 300°C and 350°C by neutron imaging (NI) experiments at the ANTARES neutron imaging facility.

H diffusion was studied along the normal and rolling directions of Zircaloy-2 and Zr-2.5%Nb plates. Experiments were performed on small 4x10x10mm³ specimens machined from plates. H was incorporated by cathodic charge in an aqueous solution of H₂SO₄. The hydride layers from five of the faces were removed by mechanical polishing, keeping only a hydride layer on the remaining face of 10x10mm² that acts as the H source, creating one-dimensional diffusion profiles. Diffusion treatments at temperatures of 250°C, 300°C and 350°C were performed before the NI acquisition, using periods between 60–600 minutes.

NI were performed at the ANTARES using an L/D = 500, a Gd₂O₂S scintillator plate of 20 μm thickness, obtaining a pixel size of ~20 μm. The calibration line between the attenuation coefficient and H content was experimentally defined using samples with a homogeneous H contents between 11 and 366 wt. ppm.

Fig. 1 shows typical profiles of H content across the thickness of the specimens, for Zircaloy-2 and Zr-2.5%Nb specimens diffusion annealed at 250°C and 350°C, respectively. The profiles are plotted on a log-log scale, in order to reveal the different behaviors observed at three distinct zones: (i) initial hydride layer, (ii) transition zone with hydrides partially dissolved and (iii) H in solid solution into the matrix, where H from the hydride layer has diffused.

In Zircaloy-2 plates (α Zr), no substantial differences were observed in H diffusion along different directions or metallurgical conditions. By contrast, in hot rolled Zr-2.5%Nb plates (α+β Zr) the diffusion along the rolling direction was much faster than along the normal direction, very likely due to H diffusing along the continuous network of β filaments (fast diffusion paths) [1].

The non-destructive nature of the NI together with its technical advantages in terms of spatial resolution (40 μm), specimen geometry (4 mm) and measurement times (600 s) opens the possibility for several interesting future experiments that cannot be performed by other techniques.

[1] J. R. Santisteban et al., *Diffusion of H in Zircaloy-2 and Zr-2.5% Nb rolled plates between 250° C and 350° C by off-situ neutron imaging experiments*, *J. Nucl. Mater.* 561, 153547 (2022)

DOI: 10.1016/j.jnucmat.2022.153547

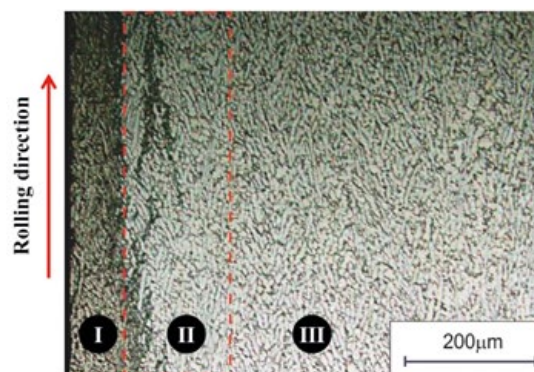
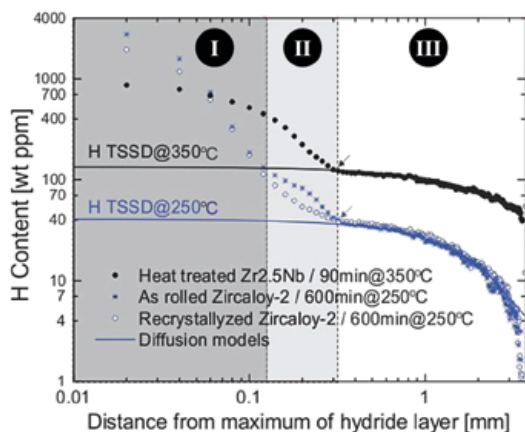


Figure 1: Left) Typical H content profiles measured by neutron imaging on the Zircaloy-2 and Zr-2.5Nb specimens. Right) optical microscopy of Zr-2.5%Nb specimen showing the different regions: (i) initial hydride layer, (ii) partial decomposition of hydrides in the transition zone and (iii) region of hydrogen dissolved in solid solution.

Monitoring the precipitation of the hardening phase in the new superalloy VDM® Alloy 780

C. Solís^{1,2*}, A. Kirchmayer³, I. da Silva⁴, F. Kümmel¹, S. Mühlbauer¹, P. Beran⁵, M. Hafez Haghghat⁶, B. Gehrman⁶, S. Neumeier³, R. Gilles¹

¹Heinz Maier-Leibnitz Zentrum (MLZ), Technical University of Munich, Garching, Germany; ²German Engineering Materials Science Centre (GEMS) at MLZ, Helmholtz-Zentrum hereon GmbH, Garching, Germany; ³Department of Materials Science and Engineering, Friedrich-Alexander-Universität Erlangen-Nürnberg, Erlangen, Germany; ⁴ISIS Facility, Science and Technology Facilities Council (STFC), Rutherford Appleton Laboratory, Didcot, U.K.; ⁵European Spallation Source ERIC, Lund, Sweden; ⁶VDM Metals International GmbH, Altena, Germany

The development of new alloys that can operate at higher temperatures is crucial for the reduction of the CO₂ emissions of gas turbines. In this work, we apply complementary neutron scattering and microscopy techniques to characterize in-situ the precipitation of the hardening phase in the new Ni-based VDM® Alloy 780 under a two-step heat treatment. The aim is to understand the precipitation to optimize the alloy for high temperature operation.

During the whole heat treatment process (8 h at 720°C + 8 h at 620°C), in-situ time-of-flight neutron diffraction (TOF-ND @GEM, ISIS) unambiguously identified the γ' phase, its volume fraction and the misfit with the γ matrix phase, while in-situ small-angle neutron scattering (SANS @SANS-1, MLZ) provided the size and volume fraction of the precipitates. Atom probe tomography (APT, Fig. 1a) and scanning electron microscopy (SEM) provided the microstructural characterization and chemical composition of samples at different precipitation stages, which were essential for proper neutron scattering data evaluation. In-situ SANS makes it possible to detect the formation of first precipitates after some minutes at 720°C (Fig. 1b) while one hour was needed to obtain data from TOF ND (Fig. 1c). However, volume fraction evolution with time is more precisely measured by TOF ND compared to SANS as the data obtained do not depend so strongly on the composition of precipitates, which continuously changes during the precipitation process. Time evolution of the volume fraction of the precipitates shows an Avrami's parameter of 1.2, which can be related to a decreasing nucleation rate during the holding for 8 h at 720°C. However, the growth kinetics of precipitates at 720°C depend on the heating rates and pre-heating history of the sample, and SANS data confirm the presence of a bimodal distribution of γ' in one of the samples. The subsequent heat treatment at 620°C seems not to alter the precipitates obtained at 720°C significantly.

Finally, the coarsening process during expected operation temperatures was studied in-situ. The Ostwald ripening process of the γ' precipitates was monitored by SANS on a full precipitation hardened sample at expected operating

temperatures (750°C). VDM® Alloy 780 showed a good performance with slower coarsening kinetics (0.0176 nm³/s at 750°C) than other reported Ni-based superalloys (0.104 nm³/s at 750 for Inconel 718).

[1] C. Solís et al., *Monitoring the precipitation of the hardening phase in the new VDM® Alloy 780 by in-situ high-temperature small-angle neutron scattering, neutron diffraction and complementary microscopy techniques*, *J. Alloys Compd* 928, 167203 (2022)

DOI: 10.1016/j.jallcom.2022.167203

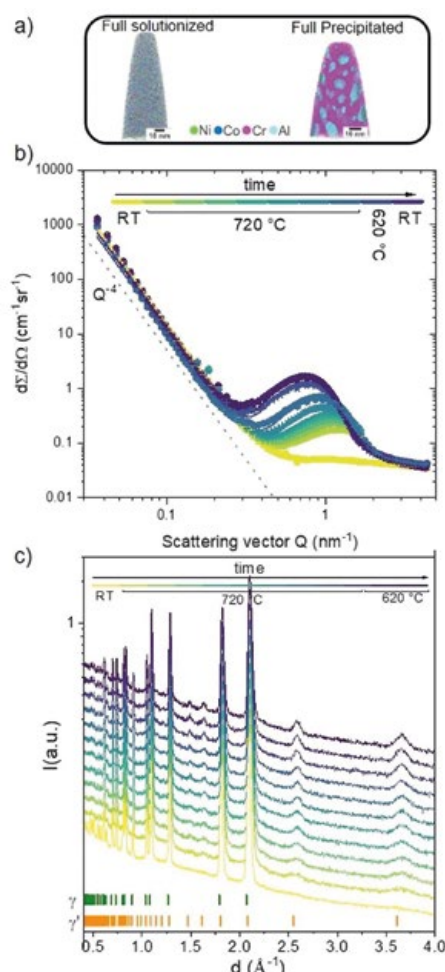


Figure 1: (a) 3D APT maps of fully solutionized sample and after two-stage precipitation heat treatment (8 h at 720°C + 8 h at 620°C); (b) in-situ SANS curves and (c) in-situ TOF ND patterns of a fully solutionized sample at RT and during the two-stage precipitation heat treatment at 720°C. With time, peaks related to the γ' precipitates appear, grow in intensity (vol. increase) and move to smaller Q values in SANS and get narrower in TOF ND (size growth).

Hydrogen detection in thin films by resonant neutron reflectometry

L. Guasco^{1,2}, Yu.N. Khaydukov^{1,2}, S. Pütter³, L. Silvi⁴, M.A. Paulin^{4,5}, T. Keller^{1,2}, B. Keimer¹

¹Max Planck Institute for Solid State Research, Stuttgart, Germany; ²Heinz Maier-Leibnitz Zentrum (MLZ), Technical University of Munich, Garching, Germany;

³Jülich Centre for Neutron Science (JCNS) at MLZ, Forschungszentrum Jülich GmbH, Garching, Germany; ⁴Helmholtz Zentrum Berlin (HZB), Berlin, Germany;

⁵Laboratorio Argentino de Haces de Neutrones (LAHN), CAB, CNEA, Bariloche, Argentina

A new methodology to measure *in situ* absorbed hydrogen concentration in thin films with increased sensitivity and faster measurement times with respect to conventional reflectometry methods was recently developed at the reflectometer NREX at the MLZ. The method is based on the linear relation between the incorporated hydrogen concentration and the shift in momentum transfer of a resonant mode arising due to waveguide effects.

The study of hydrogen diffusion and storage in different materials is crucial for the improvement of the functional materials needed for the implementation of so-called hydrogen economy. At the same time, hydrogen induced modification of the host film is at the core of proton-based solid state devices. In both cases, we are interested in knowing how much and how fast hydrogen is incorporated in a given material. Due to the high sensitivity of neutrons to hydrogen atoms, neutron scattering techniques are often used for this purpose. Neutron reflectometry in particular is demonstrated to be a powerful method for the study of hydrogen absorption in thin films for atomic concentrations of 5% and higher. In this work [1] we show a model-free method which makes it possible to measure lower (<5%) concentrations of hydrogen absorbed *in situ*, with shorter counting times and higher sensitivity. The method is based

on measuring the position of the resonance formed due to the contrast between the scattering potential of a layer and its neighbours. Hydrogen absorption leads to a change in this scattering potential and hence to a shift of the resonance position.

Method's proof-of-principle

Polarized neutron reflectometry experiments were conducted on Al₂O₃/Nb(25 nm)/Co(3 nm)/Nb(25 nm)/Pt(3 nm) thin films to prove the principle of the method. The scattering potential difference between the sapphire substrate and the hydrogen absorber Nb ensured the resonance formation, while the thin magnetic Co layer was used as a source of spin-flip scattering to detect the resonant enhancement. The thin Pt layer served as a catalyst for the splitting of H₂ molecules injected in the controlled atmosphere chamber. The *in situ* absorption process was monitored via the shift of the resonant peak, which in turn induced an intensity variation at fixed reflection angle, as shown in Fig. 1. This experiment demonstrated that the method reaches a sensitivity to hydrogen concentrations of around 1 at.% and allows one to measure absorption kinetics of a few seconds.

[1] L. Guasco *et al.*, *Resonant neutron reflectometry for hydrogen detection*, *Nat. Commun* 13 (1), 1486 (2022)
DOI: 10.1038/s41467-022-29092-z

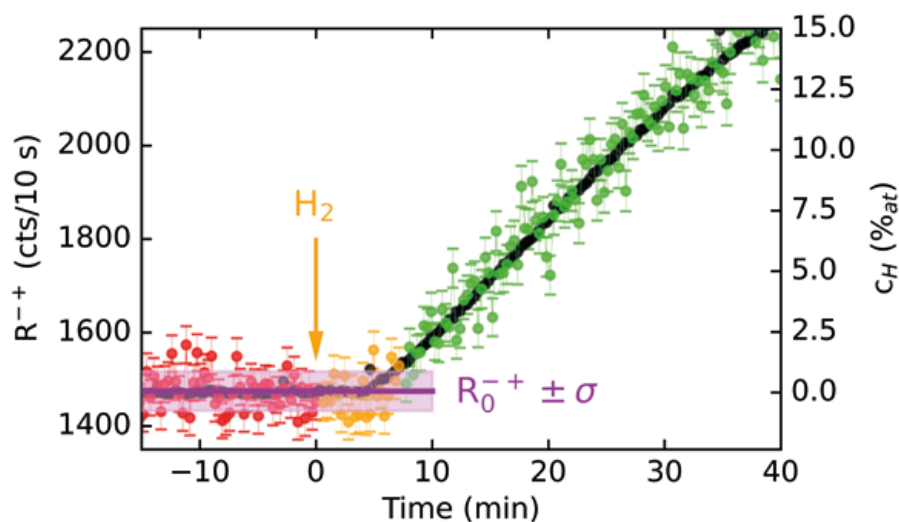


Figure 1: Variation of spin-flip reflected intensity (R^{-+}) due to resonance shift upon *in situ* hydrogen absorption in the Nb thin films. The intensity variation (left axis) is directly connected to hydrogen content c_H (right axis).

Formation of vacancies and metallic-like domains in photochromic YH_xO_y films studied using positrons

Z. Wu¹, T. de Krom¹, G. Colombi², D. Chaykina^{2,1}, G. van Hattem¹, H. Schut¹, M. Dickmann³, W. Egger³, C. Hugenschmidt⁴, E. Brück¹, B. Dam², S.W.H. Eijt¹

¹Department of Radiation Science and Technology, Faculty of Applied Sciences, Delft University of Technology, Delft, The Netherlands; ²Department of Chemical Engineering, Faculty of Applied Sciences, Delft University of Technology, Delft, The Netherlands; ³Institut für angewandte Physik und Messtechnik, Bundeswehr Universität München, Germany; ⁴Physics Department and Heinz Maier-Leibnitz Zentrum (MLZ), Technical University of Munich, Garching, Germany

PALS reveals the presence of Y mono-vacancies in as-prepared photochromic YH_xO_y films at concentrations of $\sim 10^{-5}$. In-situ illumination DB-PAS shows the irreversible formation of predominantly di-vacancies, in which formed anion mono-vacancies cluster with the Y mono-vacancies. Part of the photo-induced shifts in the Doppler parameters are reversible and correlate with the photochromic effect, pointing to the formation of metallic domains.

Yttrium oxyhydride (YH_xO_y) thin films show a color-neutral, reversible photochromic effect at ambient conditions, with potential applications in smart windows and sensors. Positron annihilation lifetime spectroscopy (PALS) studies were performed using PLEPS at NEPOMUC. Doppler broadening positron annihilation spectroscopy (DB-PAS) experiments were performed using the VEP instrument at the Reactor Institute Delft.

Vacancy defects in as-prepared YH_xO_y films

The lifetime spectrum of the YH_xO_y films was satisfactorily fitted by a four-lifetime-component analysis using POSWIN (Fig. 1a). We attribute the first component to a reduced bulk lifetime. The dominant second component of 266 ps is related to positron trapping in Y mono-vacancies, with a lifetime that is $\sim 11\%$ larger than the bulk lifetime extracted using a two-defect positron trapping model. The third lifetime of ~ 500 ps suggests the presence of larger vacancy clusters. Finally, the longest lifetime of ~ 1.6 ns indicates the presence of nanopores with an average radius of ~ 0.25 nm according to the Tao-Eldrup model.

The variation in the S and W parameters of the Y-based films seen by DB-PAS reflect the changes in their electronic structure, going from metallic Y, $\text{YH}_{-1.9}$, semiconducting YH_xO_y to insulating Y_2O_3 films (Fig. 1b). The nanostructural evolution in photochromic YH_xO_y films upon illumination was studied by in-situ DB-PAS. A partially reversible shift of the S-W point in the direction of the S-W point of $\text{YH}_{-1.9}$ is observed during photo-darkening, indicating the formation of metallic domains inside the YH_xO_y films during illumination. Subsequently, the S-parameter remains high during ~ 38 h

bleaching. This suggests that anion mono-vacancies are formed during illumination by removal of anions from their lattice positions, leading to the formation of stable di-vacancies as some of the anion vacancies cluster with Y mono-vacancies present in the film.

[1] Z. Wu et al., *Formation of vacancies and metallic-like domains in photochromic rare-earth oxyhydride thin films studied by in-situ illumination positron annihilation spectroscopy*, *Phys. Rev. Mater.* **6**, 065201 (2022)

DOI: 10.1103/PhysRevMaterials.6.065201

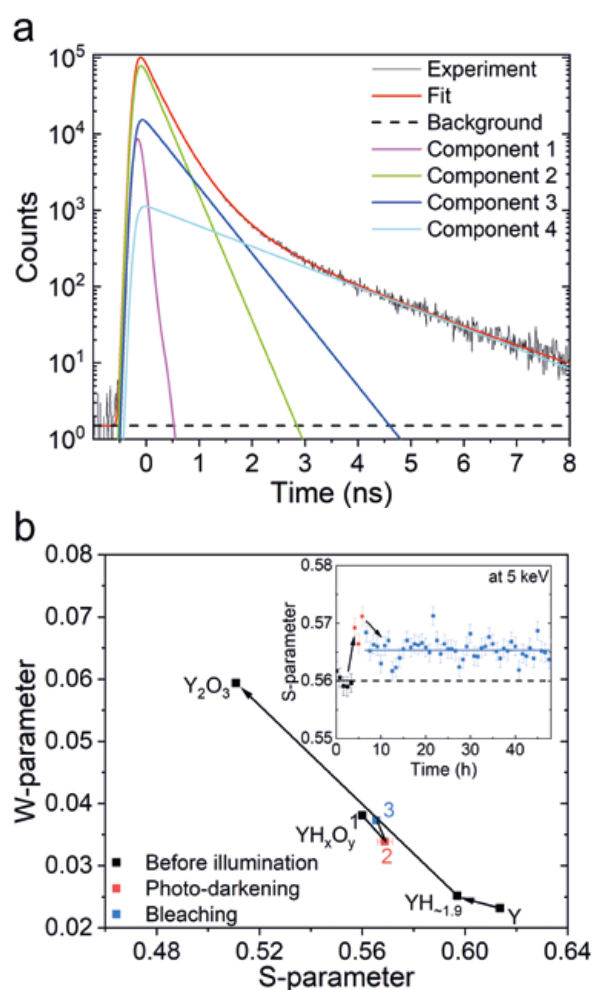


Figure 1: a. PALS spectrum of a YH_xO_y film collected at a positron implantation energy of 4 keV together with a 4-component analysis using POSWIN; b. S and W values for the YH_xO_y film before illumination (1, black), upon illumination for 2.5 hours (2, red) and after illumination in the bleaching state (3, blue), compared with Y, $\text{YH}_{-1.9}$ and Y_2O_3 films. The inset shows the corresponding time-dependence of the S-parameter collected at 5 keV.

Prompt Gamma Activation Analysis of nuclear graphite impurities to support decommissioning operations

E. Mossini^{1*}, Z. Revay²

¹Department of Energy, Politecnico di Milano, Milano, Italy; ²Heinz Maier-Leibnitz Zentrum (MLZ), Technical University of Munich, Garching, Germany

The use of nuclear graphite is often accompanied by gaps in knowledge. In this work, the analysis of virgin-graphite impurities was completed using Prompt Gamma Activation Analysis, which proved complementarity with mass spectrometry techniques. The bulk concentrations of the main activation precursors were determined and proved consistent with the literature benchmark. Moreover, N and Cl depth distributions were measured for the first time.

Assessment of nuclear graphite impurity distribution by PGAA to foster radiological characterization

The decommissioning of irradiated nuclear graphite is challenging due to the large amount of this radioactive material that may have undergone mechanical distortion and degradation by neutron damage, including Wigner energy accumulation. The task of radiological characterization could be achieved by neutron activation models. In this work, to bridge the gaps in knowledge regarding historical nuclear-grade graphite composition, PGAA has been exploited to determine the bulk concentration and depth distribution profiles of light and volatile elements hardly measurable by other techniques, such as Li, B, N and Cl, that are neutron activation precursors of ³H, ¹⁴C, and ³⁶Cl radionuclides.

To determine the depth distribution profiles, cylindrical slices were cut from a virgin AGOT graphite rod at increasing depth from the surface. The PGAA measurements were conducted under vacuum at the Heinz Maier-Leibnitz Zentrum (MLZ), in a cold neutron beam using a Compton-suppressed HPGe detector system. To correct for the spectral background from scattered neutrons, an equivalent amount of heavy water was also measured.

Whenever a comparison was possible, the results obtained showed consistency with the literature data. Hence, PGAA proved to be an effective and complementary technique for completing an accurate elemental characterization of pure materials in support of radiological characterization. All elements were found to be homogeneously distributed with the depth, except for N and Cl showing a decreasing trend (see Fig. 1). This unprecedented outcome may facilitate the decommissioning of graphite-moderated nuclear reactors by driving more accurate activation code simulations, explain-

ing ¹⁴C depth distribution and fractional release, and improving irradiated graphite waste management through surface decontamination processes to declassify part of the inventory.

This study opens the door to further work in the decommissioning field. Being a generic approach, it could be applied to other situations and materials to optimize their management.

[1] E. Mossini et al., *Determination of nuclear graphite impurities by prompt gamma activation analysis to support decommissioning operations*, *J Radioanal Nucl Chem* 331, 3117 (2022)

DOI: 10.1007/s10967-022-08381-3

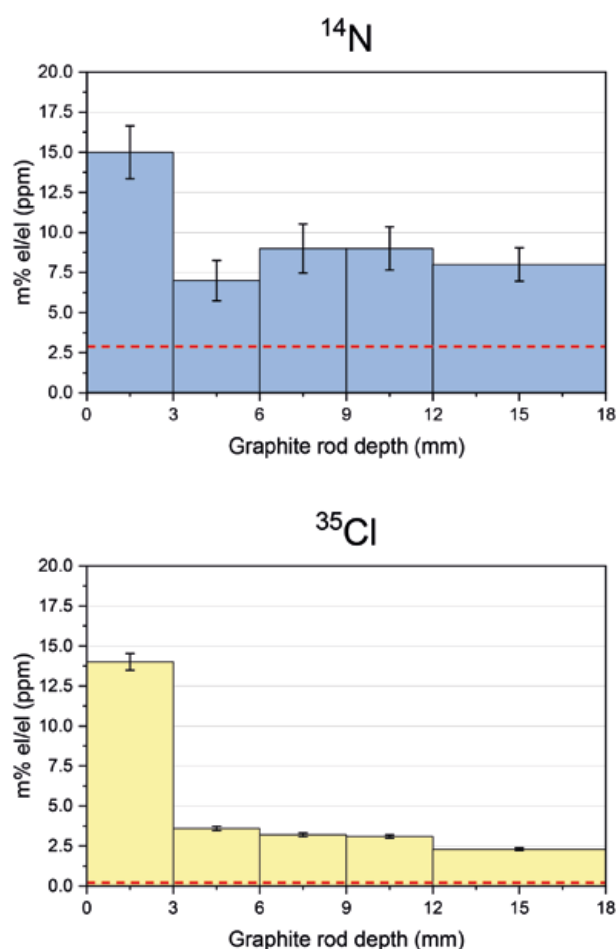


Figure 1: PGAA measurements of ¹⁴N (a) and ³⁵Cl (b) concentrations in AGOT graphite as a function of depth. The red dotted lines denote the detection limits. Four cylindrical samples with a thickness of about 3 mm each and mass ranging from 1.5 g to 1.8 g were collected at increasing depth from the graphite rod surface; a fifth sample was collected downward with a thickness of about 1.2 cm and mass of about 6 g.

DISEMM: a software package for investigation of elasto-plastic behavior of polycrystalline samples using X-ray and neutron diffraction

A. Heldmann¹, M. Hofmann¹, M. Hoelzel¹

¹Heinz Maier-Leibnitz Zentrum (MLZ), Technical University of Munich, Garching, Germany

DISEMM is designed to analyze diffraction data obtained on polycrystalline samples under mechanical stress to determine single-crystal elastic constants (SECs). Furthermore, the SECs calculated can be used as input parameters for an elasto-plastic self-consistent (EPSC) modelling of lattice strains.

In-situ diffraction makes it possible to elucidate deformation mechanisms during elastic and plastic loading. Using a dedicated experimental setup consisting of a unique rotatable test rig in combination with high-resolution powder diffraction, even SECs can be derived from polycrystalline samples under external uniaxial stress using appropriate models for the grain-to-grain interactions. This technique offers the possibility of deriving SECs in technical alloys as well as multi-phase materials that are not available as single-crystals. Measuring lattice strains by diffraction under mechanical load above the yield stress allows an analysis of the plastic anisotropy. The interpretation of experimental data in terms of deformation mechanisms can be supported by plasticity models such as elasto-plastic self-consistent (EPSC) simulations.

DISEMM (Diffraction assisted mechanical modelling) is a software tool to analyse neutron or X-ray diffraction data on polycrystalline samples collected under mechanical load, combining the determination of SECs and the methods of EPSC modelling in one package [1].

DISEMM implements routines to fit single-crystal elastic constants from single- and multi-phase alloys, considering texture and the stress distribution among different phases from diffraction data recorded in situ during a tensile test, shown in Fig. 1. It provides packages to visualize and quantify anisotropy, such as the Zener anisotropy. The program also contains a package implementing a routine for EPSC modelling using the results of the elastic evaluation as input parameters. DISEMM is designed to enable a comparison between experimental and calculated data, regarding macroscopic stress-strain curves as well as lattice strain data. DISEMM was validated on ferrous metals to obtain elastic constants and lattice strains in good agreement with literature data. Furthermore, it was possible to determine all eight single-crystal elastic constants of the *hcp* and *bcc* phases in the two-phase Ti alloy Ti-6Al-2Sn-4Zr-6Mo using DISEMM. Moreover, the stress distribution between the phases, i.e. the load transfer between the softer β phase and the stiffer α phase, could be quantified using an approach implemented in DISEMM. In general, DISEMM can be used for data analysis on any neutron or synchrotron diffractometer that can be equipped with an appropriate tensile rig. So far, it has been used for data collected at the MLZ instruments STRESS-SPEC and SPODI as well as D20 (ILL, Grenoble) and HEMS (DESY, Hamburg).

[1] A. Heldmann et al., *DISEMM: a tool for the investigation of elasto-plastic behaviour on polycrystalline samples using X-ray and neutron diffraction*, *J. Appl. Cryst.* 55, 656 (2022) DOI: 10.1107/S1600576722003314



Figure 1: Screenshot of the peak-fitting window of DISEMM, including plot of the fit, plot of deviation between calculated and measured intensities, peak list and values of selected refineable parameters.

In-situ diffraction analysis of elasto-plastic characteristics of industrial steel sheets

S. Vitzthum¹, J. Rebelo Kornmeier², M. Hofmann², M. Gruber¹, E. Maawad³, A. C. Batista⁴, C. Hartmann¹, W. Volk¹

¹Chair of Metal Forming and Casting, Technical University of Munich, Garching, Germany; ²Heinz Maier-Leibnitz Zentrum (MLZ), Technical University of Munich, Garching, Germany; ³Institute of Materials Physics, Helmholtz-Zentrum hereon GmbH, Geesthacht, Germany; ⁴Department of Physics, Centre for Physics of the University of Coimbra (CFisUC), Coimbra, Portugal

The elasto-plastic behavior of modern steels deviates strongly from theory and this leads to challenges in predictions of the springback effect in sheet metal forming. The most plausible explanations for that have their origin on the microstructural level. Therefore, in situ diffraction analysis is necessary to understand the elasto-plastic characteristics of industrial steels.

Diffraction experiments, under load, were performed at DESY at the beamline P07 to analyze correlations of the macroscopic onset of yielding with the microstructural material behavior. The macroscopic strain, load and specimen temperature were measured time synchronously to microstructural quantities, such as lattice strains and dislocation densities. Given this, a microstructural validation of a new temperature-based determination of the onset of yielding using the ferritic steel, HC260Y, was possible.

The lattice strains are evaluated based on the peak shift of several lattice planes and the dislocation density is estimated based on the micro strains extracted from the peak broadening analysis. The thermoelastic effect indicates the dependency of temperature and volume change in the material and, due to the heat release during plastic deformation, a temperature minimum occurs in the region of the onset of yielding (Fig. 1 left). The assumption is made that

during purely elastic loading, the temperature decreases linearly. Consequently, a deviation of the temperature behavior from linearity means that plastic deformation starts. For this purpose, the onset of yielding is divided into three phases as a function of temperature and the respective limits are represented by the parameters YS_0 and YS_{Tmin} . In the first phase, pure elastic, the measured lattice strains increase rapidly and there is no increase in the dislocation density (Fig. 1 right). The stress-strain curve increases linearly while the temperature decreases linearly. At a certain point the temperature deviates from linearity, which implies that the sample is heated by slight plastic deformation, but this heating is still less than the elastic cooling. This point is called yield stress at zero plastic strain YS_0 . Finally, YS_{Tmin} occurs when the equilibrium between elastic cooling and plastic heating is achieved and from here on the temperature rises and approaches a linear behavior once more.

In comparison with the currently used but somewhat arbitrary RP0,2 limit for determination of the elastic modulus, the YS_0 is an easily measurable, physically based and unbiased upper limit for the elastic region in metals.

[1] S. Vitzthum et al., *In-situ Analysis of the Thermoelastic Effect and its Relation to the Onset of Yielding of Low Carbon Steel*, *Materials and Design* 219, 110753 (2022)
DOI: 10.1016/j.matdes.2022.110753

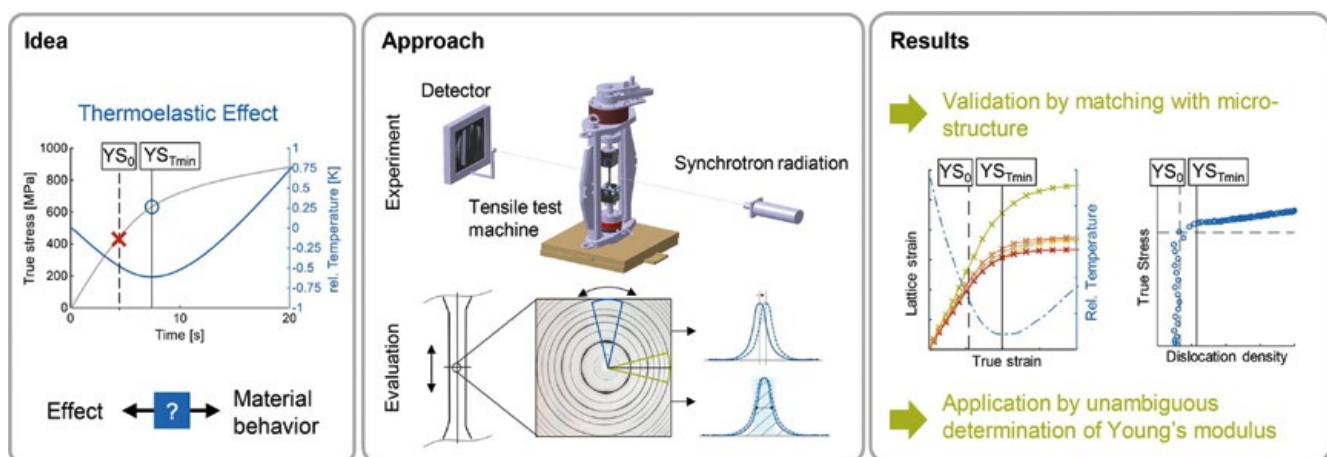


Figure 1: Experimental validation of the thermoelastic effect through mechanical material behavior by macro and micro characterization.

Chiral spin liquid ground state in $\text{YBaCo}_3\text{FeO}_7$ W. Schweika^{1,2}, M. Valldor³, J. D. Reim^{4,2}, U. Rößler⁵

¹European Spallation Source ERIC, Lund, Sweden; ²Quantum Materials and Collective Phenomena (JCNS-2/PGI-4), Forschungszentrum Jülich GmbH, Jülich, Germany; ³Centre for Materials Science and Nanotechnology, Department of Chemistry, University of Oslo, Oslo, Norway; ⁴Institute of Multidisciplinary Research for Advanced Materials, Tohoku University, Sendai, Japan; ⁵Leibniz Institute for Solid State and Materials Research Dresden (IFW), Dresden, Germany

We studied the spin-liquid state in the layered Kagome system $\text{YBaCo}_3\text{FeO}_7$ and determined the chiral spin correlations by diffuse polarized neutron scattering. We observed cycloidal spin correlations originating from sites with 3-fold symmetry due to the antisymmetric exchange in this non-centrosymmetric and polar structure. According to our theory this is a classical lump-like chiral ground state preventing conventional long-range order.

Spin liquids are a topical and fascinating subject in condensed matter physics, fueled by the hope of creating novel ground-states of matter. Typically, the combination of antiferromagnetic interactions with strong frustration leads to a rich variety of highly correlated spin states rather than to conventional order.

As known from previous experiments on powder samples, the layered Kagome system $\text{YBaCo}_3\text{FeO}_7$ exhibits a spin-liquid state at low temperatures. In this single crystal study, we undertook a new search for the vector chirality and non-collinear properties in this spin-liquid state with polarized neutrons.

Unraveling of the vector spin chirality

The scattering experiments with polarized neutron were performed at the DNS at the MLZ Munich. We measured the diffuse scattering in the $(hk0)$ plane of a single domain crystal at low temperature, in spin-flip mode and with polarization reversal along the scattering vector \mathbf{Q} . In an extension to the conventional XYZ method and analysis, the related intensity difference yields the chiral scattering,

which shows a characteristic antisymmetry, see Fig. 1 (left). A model description is found by the Fourier transform of the vector chirality $\mathbf{C} = \mathbf{S} \times \mathbf{S}'$ in terms of cycloidal spin correlations. These cycloidal spin correlations emanate from trigonal sites with threefold rotational symmetry around the polar c -axis and spread out into the adjacent Kagome layers forming a solitonic, lump-like structure. An approximate picture of the spin lump pattern is displayed in Fig. 1 (right). The observed intensity and proposed lump structure can be traced back to the underlying antisymmetric exchange in the system.

This novel observation of a liquid-like magnetic ground state with a very peculiar vector chirality and non-collinear solitonic structure is supported by a fundamental theoretical analysis with a classical mechanism based on anti-symmetric exchange, which arises from broken symmetry along the exchange paths.

The present scenario displays similarities to the avoided phase transition in coupled gauge and matter fields for sub-nuclear particles. Chiral properties are invisible to conventional neutron scattering, but show up in the antisymmetric scattering of polarized neutrons. There are many frustrated spin systems with a non-centrosymmetric structure, where the lack of long-range order may originate from a similar yet hidden chirality.

[1] W. Schweika et al., *Chiral Spin Liquid Ground State in $\text{YBaCo}_3\text{FeO}_7$* , *Physical Review X* 12, 021029 (2022)
DOI: 10.1103/PhysRevX.12.021029

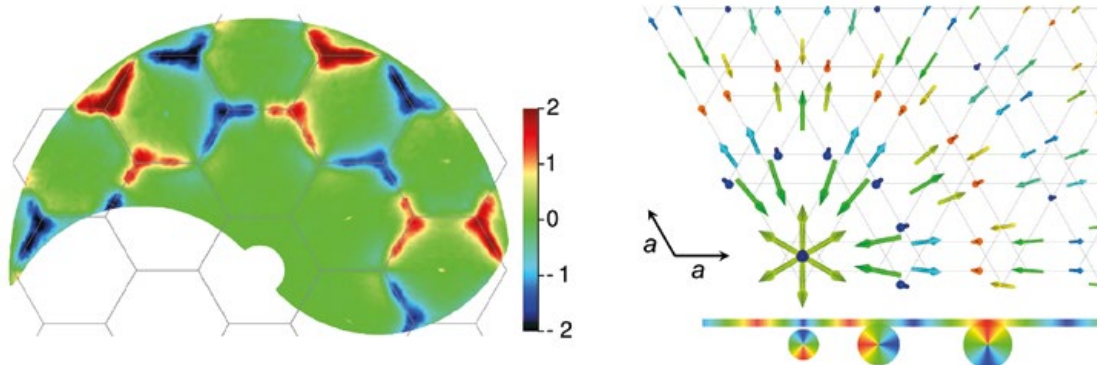


Figure 1: Observed chiral scattering and chiral spin liquid ground state in $\text{YBaCo}_3\text{FeO}_7$. (left) Antisymmetry of the diffuse chiral scattering in the $(hk0)$ plane at $T = 4\text{K}$, obtained in spin-flip mode from polarisation reversal along \mathbf{Q} . (right) A cylindrical wave composed of three cycloids emanate from a trigonal site between adjacent Kagome layers, which provides an approximate picture of the proposed chiral spin lumps in a classical short-range ordered ground state.

Neutron depolarization due to ferromagnetism and spin freezing in $\text{CePd}_{1-x}\text{Rh}_x$

M. Seifert¹, P. Schmakat^{1,2}, M. Schulz², P. Jorba¹, V. Hutanu², C. Geibel³, M. Deppe³, C. Pfleiderer^{1,4,5}

¹Physik-Department E21/E51, Technical University Munich, Garching, Germany; ²Heinz Maier-Leibnitz Zentrum (MLZ), Technical University of Munich, Garching, Germany; ³Max-Planck-Institute for Chemical Physics of Solids, Dresden, Germany; ⁴Centre for Quantum Engineering (ZQE), Technical University of Munich, Garching, Germany; ⁵Munich Center for Quantum Science and Technology (MCQST), Technical University of Munich, Garching, Germany

We provide experimental evidence of the formation of a Kondo cluster glass in the vicinity of a quantum phase transition in $\text{CePd}_{1-x}\text{Rh}_x$ around a critical concentration of $x^* \approx 0.6$. The evolution of the neutron depolarization as a function of temperature with different magnetic field histories supports the reentrant temperature dependence of the magnetization suggested in previous studies and reveals particular length and time scales defined by the neutron wavelengths used.

The investigation of Quantum phase transitions (QPTs), defined as zero-temperature phase transitions, represents a well-established roadmap in the search for new properties of correlated electron systems. Perhaps the simplest example of a magnetic QPT is associated with the suppression or emergence of long-range ferromagnetic (FM) order as a function of a nonthermal control parameter (pressure, magnetic field, chemical composition). In clean materials a variety of escape routes to FM quantum criticality were identified. Several studies suggest an intricate interplay of mechanisms at microscopic and mesoscopic length scales at QPTs that are experimentally difficult to determine and characterize. Here, neutron depolarization (ND) is an ideal tool with which to study the involved length scales and texture sizes in bulk systems.

Our neutron depolarization (ND) measurements at ANTARES provide experimental evidence of the suppression of long-range ferromagnetism and the concomitant emergence of magnetic irreversibilities and spin freezing in $\text{CePd}_{1-x}\text{Rh}_x$ around $x^* \approx 0.6$. By tracking the temperature versus field history of the ND, we find clear signatures of long-range Ising ferromagnetism below a Curie temperature T_C for $x = 0.4$. For compositions $x > x^*$ we find an absence of depolarization for $T > T_{F1}$ characteristic of a freezing of small, rapidly

fluctuating clusters. However, for temperatures $T_{F1} > T > T_{F2}$ a reentrance of depolarization under zero field-cooling/field heating reveals a thermally activated increase of cluster size in the spin frozen state. The sensitivity of our setup makes it possible to estimate the length scale of FM correlations, which provides microscopic information consistent with the formation of a Kondo cluster glass below T_{F1} adjacent to a FM quantum phase transition at x^* , initially proposed on the basis of the bulk properties elsewhere. Taken together, our observations in $\text{CePd}_{1-x}\text{Rh}_x$ underscore the potential of neutron depolarization as a microscopic probe in the search for FM QPTs and concomitant escape routes.

[1] M. Seifert et al., *Neutron depolarization due to ferromagnetism and spin freezing in $\text{CePd}_{1-x}\text{Rh}_x$* , *Phys. Rev. Research* 4, 043029 (2022)

DOI: 10.1103/PhysRevResearch.4.043029

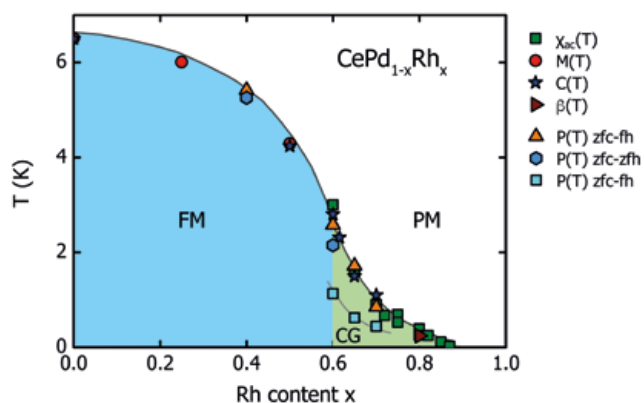


Figure 1: Magnetic phase diagram of $\text{CePd}_{1-x}\text{Rh}_x$. Shown are values of T_C , T_{F1} , and T_{F2} as inferred from the neutron polarization $P(T)$ recorded in our study, and the ac susceptibility $\chi_{ac}(T)$, magnetization $M(T)$, specific heat $C(T)$ and thermal volume expansion $\beta(T)$ of the same samples reported elsewhere. With increasing x ferromagnetism (blue shading) is suppressed and spin-frozen behavior characteristic of a Kondo cluster glass (green shading) emerges.

Bulk domain Meissner state in the ferromagnetic superconductor $\text{EuFe}_2(\text{As}_{0.8}\text{P}_{0.2})_2$: Consequence of compromise between ferromagnetism and superconductivity

W. Jin¹, S. Mühlbauer², P. Bender³, Y. Liu⁴, S. Demirdis⁵, Z. Fu⁶, Y. Xiao⁷, S. Nandi⁸, G.-H. Cao⁹, Y. Su⁵, T. Brückel^{8,5}

¹School of Physics, Beihang University, Beijing, China; ²Heinz Maier-Leibnitz Zentrum (MLZ), Technical University of Munich, Garching, Germany; ³Physics and Materials Science Research Unit, University of Luxembourg, Luxembourg, Grand Duchy of Luxembourg; ⁴College of Science, Zhejiang University of Technology, Hangzhou, China; ⁵Jülich Centre for Neutron Science (JCNS) at MLZ, Forschungszentrum Jülich GmbH, Garching, Germany; ⁶Neutron Platform, Songshan Lake Materials Laboratory, Dongguan, China; ⁷School of Advanced Materials, Peking University Shenzhen Graduate School, Shenzhen, China; ⁸Jülich Centre for Neutron Science JCNS-2 and Peter Grünberg Institut PGI-4, Jülich, Germany; ⁹Department of Physics, Zhejiang University, Hangzhou, China

The antagonistic nature of ferromagnetism (FM) and superconductivity (SC) makes the coexistence of these two states of matter quite rare. Recently, the observation of an intriguing coexistence of bulk SC and strong FM in the EuFe_2As_2 -family iron pnictides (Eu-122) has attracted much attention. Neutron diffraction experiments have confirmed the ferromagnetic ordering of localized Eu^{2+} moments with a huge moment of $\sim 7 \mu_B$ per Eu atom in the superconducting ground state, induced either by chemical doping into the parent compound or the application of hydrostatic pressure.

To probe the delicate interplay between FM and SC in the ferromagnetic superconductor $\text{EuFe}_2(\text{As}_{0.8}\text{P}_{0.2})_2$ ($T_{sc} = 22.5$ K), small-angle neutron scattering (SANS) measurements were performed on the instrument SANS-1 at the MLZ. The q dependencies of the integrated magnetic SANS intensity at different temperatures for the zero-, longitudinal-, and transverse-field cases, respectively, are summarized in Fig. 1. A clear signature of large ferromagnetic domains is found

below the ferromagnetic ordering temperature $T_c = 18.5$ K, supported by an overall sloping background with the power-law behavior of $I(q) \propto q^{-4}$. In a small temperature interval of ~ 1.5 K below T_c , an additional SANS signal is observed, of which the indirect Fourier transform (IFF) reveals characteristic length scales in between ~ 80 nm and ~ 160 nm, as shown in Fig. 1(F). These nanometer-scaled domain structures are identified to result from an intermediate inhomogeneous Meissner effect denoted the domain Meissner state (DMS), which was recently observed on the surface of $\text{EuFe}_2(\text{As}_{0.79}\text{P}_{0.21})_2$ crystals by means of magnetic force microscopy, assigned to the competition between FM and SC. Our measurements clearly render the domain Meissner state as a bulk phenomenon and provide a key solution to the mystery regarding the intriguing coexistence of strong FM and bulk SC in these compounds [1].

[1] W. Jin et al., *Bulk domain Meissner state in the ferromagnetic superconductor $\text{EuFe}_2(\text{As}_{0.8}\text{P}_{0.2})_2$* , *Phys. Rev. B* **105**, L180504 (2022)

DOI: 10.1103/PhysRevB.105.L180504

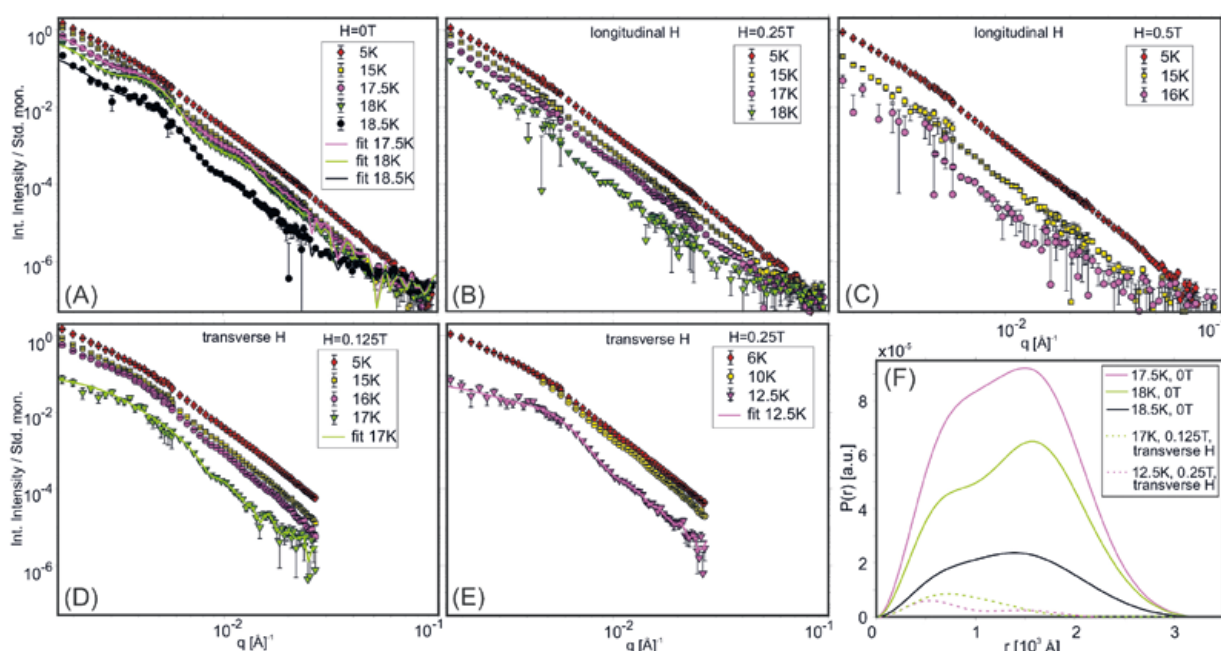


Figure 1: The q dependencies of the radially integrated magnetic SANS intensity at different temperatures in zero magnetic field (a), longitudinal field of $H_i = 0.25$ T (b) and $H_i = 0.5$ T (c), and in a transverse field of $H_i = 0.125$ T (d) and $H_i = 0.25$ T (e). (f) The extracted real-space pair distance distribution function $P(r)$ taken from the fitting of the $I(q)$ curves with a double-hump feature (panels a,d and e) measured at the intermediate temperatures just below T_c for the zero-field and transverse-field case. It reveals the existence of the DMS at intermediate temperatures closely below T_c .

Frustration model and spin excitations in the helimagnet FeP

A. S. Sukhanov¹, Y. V. Tymoshenko¹, A. A. Kulbakov¹, A. S. Cameron¹, V. Kocsis², H. C. Walker³, A. Ivanov⁴, J. T. Park⁵, V. Pomjakushin⁶, S. E. Nikitin⁷, I. V. Morozov², I. O. Chernyavskii², S. Aswartham², A. U. B. Wolter², A. Yaresko⁸, B. Büchner^{1,2}, D. S. Inosov¹¹Institute for Solid State and Materials Physics, Technische Universität Dresden, Dresden, Germany; ²Leibniz Institute for Solid State and Materials Research Dresden (IFW), Dresden, Germany; ³ISIS Facility, STFC, Rutherford Appleton Laboratory, Didcot, Oxfordshire, UK; ⁴Institut Laue-Langevin, Grenoble, France; ⁵Heinz Maier-Leibnitz Zentrum (MLZ), Technical University of Munich, Garching, Germany; ⁶Laboratory for Neutron Scattering and Imaging (LNS), Paul Scherrer Institute (PSI), Villigen, Switzerland; ⁷Paul Scherrer Institute (PSI), Villigen, Switzerland; ⁸Max Planck Institute for Solid State Research, Stuttgart, Germany

In the metallic compound FeP, the double-helix spin structure is driven by magnetic frustration. Neutron spectroscopy supported by linear spin-wave theory helped us reveal the frustration mechanism and quantify the magnetic interactions. Despite the 3D crystal structure, the magnon modes display strongly anisotropic dispersions, revealing a quasi-one-dimensional character of the magnetic interactions in FeP with the dominating ferromagnetic interaction along the b axis. Much weaker antiferromagnetic interactions in the plane orthogonal to the rigid ferromagnetic chains drive the magnetic frustration and are responsible for the helical order.

In many magnetic compounds, the hierarchy of magnetic interactions can be roughly deduced from the crystal structure. For example, layered materials are expected to have weak interlayer coupling compared to in-plane interactions, whereas in three-dimensional materials the interactions, and hence the magnon band width, should be approximately the same in all three spatial directions. The metallic helimagnet FeP is a prominent exception to this empirical

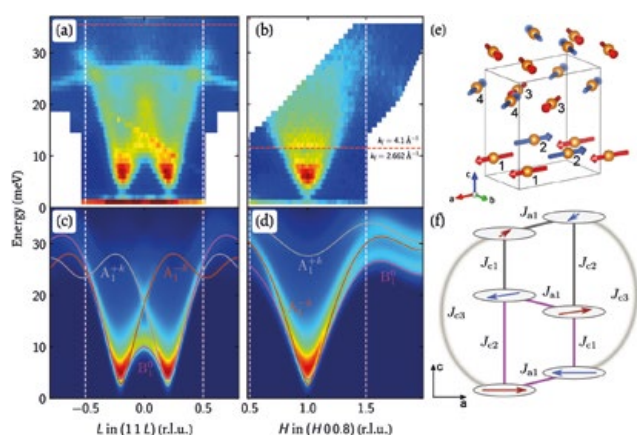


Figure 1: (a, b) The inelastic neutron-scattering data collected using triple-axis spectrometers IN8 (ILL) and PUMA (MLZ) on the same sample of FeP along two orthogonal directions in momentum space. (c, d) Linear spin-wave theory simulations of the magnon spectra according to our newly proposed spin model. (e) The double-helix spin structure of FeP. (f) The effective two-dimensional frustrated spin model of FeP. The strongest coupling J_b along the ferromagnetic chains is not shown.

rule. Without any obvious chain-like structures in the lattice, this material exhibits exceptionally high magnetic stiffness along the b direction, with the spin waves reaching about 500 meV. This is one order of magnitude higher than in the ac plane, where the magnon band width is only 35 meV. This results in an essentially two-dimensional spin model that consists of rigid ferromagnetic chains running along the b direction.

The interactions among the Fe moments are frustrated, resulting in a helimagnetic ground state known as the double spin spiral, which is shown in Fig. 1(e). It consists of two approximately antialigned sublattices, twisted into a helix along the c axis. To explain the frustration mechanism, a simple spin model was previously proposed, consisting of one ferromagnetic and three antiferromagnetic interactions forming a trapezoid. Using inelastic neutron scattering in combination with linear spin-wave theory, we show that this model is inconsistent with the experimental data and offer an alternative frustration mechanism that can describe the experimental neutron spectra with high accuracy (cf. Figs. 1(a,b) and Fig. 1(c,d)). Our resulting model, shown in Fig. 1(f), is reminiscent of the well-known model of frustrated antiferromagnetic chains, where frustration arises from the competition between the nearest- and the next-nearest-neighbor antiferromagnetic exchange interactions. These chains run along the c direction and consist of macroscopic moments formed by the rigidly bound ferromagnetic b -axis chains (shown with single arrows). Thus, the strongly pronounced hierarchy of exchange energies allowed us to introduce an effective low-dimensional spin model for a structurally three-dimensional material, explaining the origin of the spin-spiral order and the frustration mechanism. Our model can be used in future studies of the similar double-helix magnets such as FeAs, CrAs, and MnP.

[1] A. S. Sukhanov et al., *Frustration model and spin excitations in the helimagnet FeP*, *Phys. Rev. B* 105, 134424 (2022)
DOI: 10.1103/PhysRevB.105.134424

Spin stripe fluctuations in antiferromagnetic $\text{Pr}_{2-x}\text{Sr}_x\text{NiO}_{4+\delta}$ A. Maity¹, R. Dutta^{2,3}, W. Paulus⁴

¹Heinz Maier-Leibnitz Zentrum (MLZ), Technische Universität München, Garching, Germany; ²Institut für Kristallographie, RWTH Aachen Universität, Aachen, Germany; ³Jülich Centre for Neutron Science (JCNS) at MLZ, Forschungszentrum Jülich GmbH, Garching, Germany; ⁴Institute Charles Gerhardt Montpellier (ICGM), CNRS, ENSCM, Montpellier, France

Spin and charge stripe correlations and their dynamics have been well explored in the superconducting La-based 214-cuprates and hole-doped 214-nickelates in an attempt to understand the possible role of stripe correlation in high- T_c superconductivity. Considering the amount of experimental work put forward characterizing the spin stripe ordering and dynamics of 214-nickelates and theoretical calculations presenting various aspects of the ground state, what remains less explored is the fluctuating state of the spin stripes, including their dynamical correlation from which the long-range static spin stripes develop upon cooling.

We have performed inelastic neutron scattering (INS) measurements at the thermal triple-axis spectrometer PUMA at the MLZ on a hole doped $\text{Pr}_{2-x}\text{Sr}_x\text{NiO}_{4+\delta}$ ($x \approx 0.125$, $\delta \approx 0.1$) sample with stripe incommensurability $\mathcal{E} = 0.33$. Our results for the spin stripe fluctuations clearly indicate that the presence of static charge stripe order is essential for the spin stripe fluctuations to persist [1].

From the temperature dependent elastic scans through the spin and charge stripe reflections at different Brillouin zones, we have obtained the spin and charge stripe ordering temperature $T_{so} \approx 190$ K and $T_{co} \approx 255$ K respectively (see Fig. 1a). The inelastic measurements of the spin stripe

fluctuations measured at $(3, -0.33, 0)$ just above T_{so} show a non-dispersive character and can be detected up to 10 meV (see Fig. 1b, c).

However, we were unable to observe any significant anisotropy of the spin stripe fluctuations along the h and k directions. Additionally, we could not detect any anomalous behavior in the spin stripe fluctuations, suggesting no significant interaction between the spin stripe fluctuations and the dynamical charge stripes. The peak position of the non-dispersive spin stripe fluctuations do not shift in Q , leaving the incommensurability of the stripes invariant, which suggests that the spin and charge stripes can maintain an instantaneous correlation even when the static spin stripe order is absent above T_{so} .

Nonetheless, the spin stripe fluctuations are strongly diminished below the charge stripe melting temperature $T_{co} \approx 255$ K (see Fig. 1d), which clearly indicates that the formation of static charge order is not driven by spin stripe fluctuations, but rather suggests that the presence of static charge stripe order is a prerequisite for the spin stripe fluctuations to exist.

[1] A. Maity et al., *Spin stripe fluctuations in antiferromagnetic $\text{Pr}_{2-x}\text{Sr}_x\text{NiO}_{4+\delta}$* , *Phys. Rev. B* **106**, 024414 (2022)
DOI: 10.1103/PhysRevB.106.024414

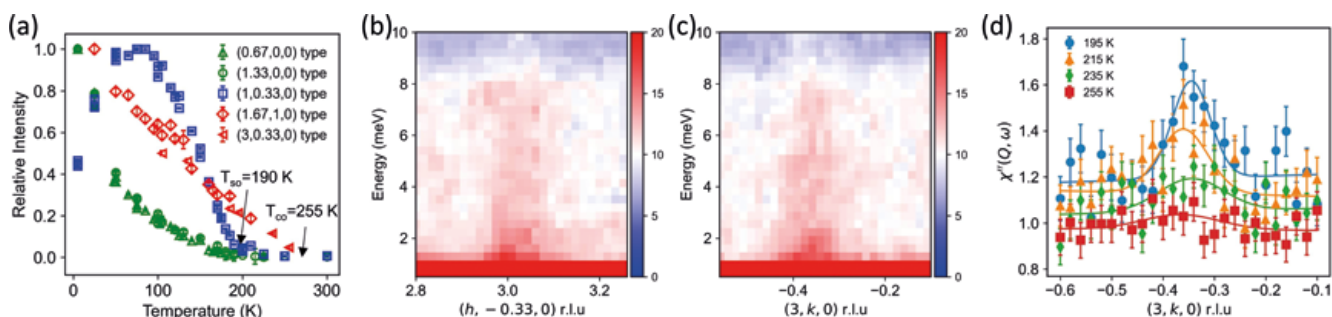


Figure 1: (a) T dependence of the relative intensities from the spin and charge stripe reflections from different Brillouin zones. (b, c) The respective color maps of the spin stripe fluctuations measured along h and k directions at $(3, -0.33, 0)$ at 195 K just above T_{so} . (d) T-dependent inelastic scans through the spin and charge stripe overlapped satellite position at $(3, -0.33, 0)$ at energy transfer $E = 3$ meV.

Fermi surface modeling of light-rare-earth hexaborides
using positron annihilation spectroscopyJ. Ketels¹, M. Leitner^{1,2}, P. Böni¹, C. Hugenschmidt^{1,2}, M. Sekania³, A. D. N. James⁴, J. A. E. Bonart³, N. Unglert³, L. Chioncel³¹Physics Department, Technical University of Munich, Garching, Germany; ²Heinz Maier-Leibnitz Zentrum (MLZ), Technical University of Munich, Garching, Germany; ³Theoretical Physics III, University of Augsburg, Germany; ⁴H. H. Wills Physics Laboratory, University of Bristol, United Kingdom

2D angular correlation of annihilation radiation (2D-ACAR) spectra were measured for LaB₆ and compared with density functional theory (DFT) calculations. The electronic structure obtained agrees with quantum oscillation results and the Fermi surface (FS) has similar “necks” with significantly larger radii than those of SmB₆. The similarities found for LaB₆ and CeB₆ allow one to infer that both compounds are topologically trivial correlated metals.

The 2D-ACAR experiments performed in the NEPOMUC group offer answers to some fundamental questions of whether the electron momentum density in a specific material possesses FS breaks. Through this technique, one may provide guidance in searching for a suitable theoretical description of the electronic structure and thus help in developing an understanding of the mechanism responsible for the occurrence of specific effects, topological features also being among them. Alternatively, the accuracy of any specific electronic structure model can in principle be assessed by comparing the computed 2D-ACAR spectra with the corresponding measurements. On the theoretical side, such comparisons have already been made using the most advanced LDA+DMFT method for simple transition metals. However, its extension to correlated multiorbital 4f-systems with strong spin–orbit coupling is not currently available.

Experimental and theoretical results

In the present study, we carried out 2D-ACAR measurements on single-crystalline LaB₆ along three high-symmetry directions. The experimental spectra in both the p-space (see Fig. 1) and k-space were compared with LDA calculations and showed good agreement. In particular the quantitative results extracted from the experiment are in excellent agreement with the corresponding theoretical values of the FS along the X-M and X-R directions; the higher experimental value found for X- Γ , however, is attributed to the fact that this direction is experimentally not directly accessible.

Based on the results presented and the combined theoretical and experimental (for LaB₆) analysis, we conclude that the “ellipsoid” cross sections (α -orbit) and neck sizes increase; hence, the γ - and ϵ -hole orbits of LaB₆ and CeB₆ are significantly reduced in size in comparison with SmB₆. This is in agreement with the quantum oscillation measurements and supports the idea that these two compounds are topologically trivial but correlated metals.

Financial support by the Deutsche Forschungsgemeinschaft through TRR80 (project E2) project number 107745057 is gratefully acknowledged.

[1] J. Ketels et al., *Fermi Surface Modeling of Light-Rare-Earth Hexaborides using Positron Annihilation Spectroscopy*, *Phys. Stat. Sol. B* 259, 2100151 (2021)

DOI: 10.1002/pssb.202100151

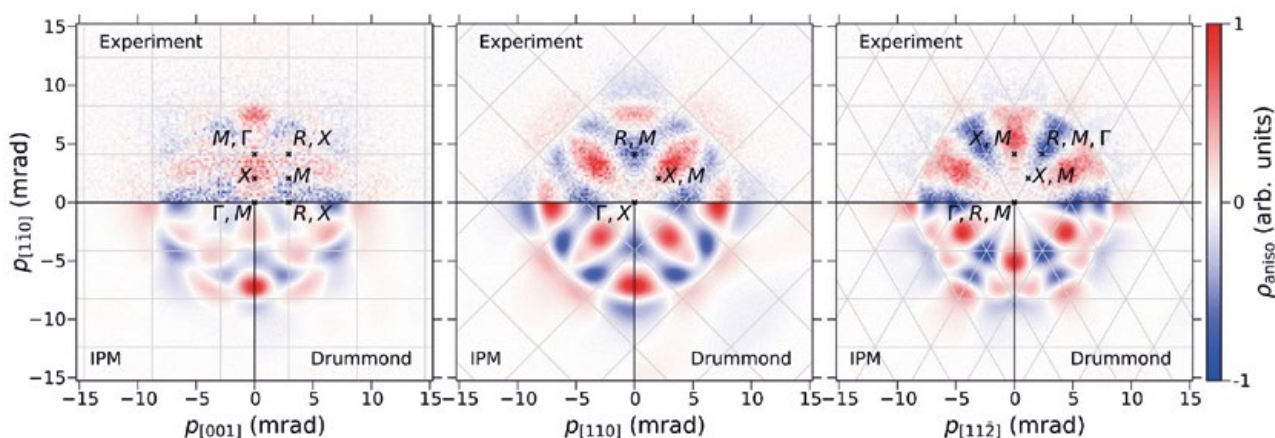


Figure 1: Radial anisotropy of measured and symmetrized LaB₆ ACAR spectra (top) and theoretical spectra calculated in the independent particle model (IPM, bottom left) and with the Drummond enhancement (bottom right). The spectra from first-principle calculations are convolved with a Gaussian accounting for the experimental resolution of 0.60 mrad. The borders of the projected first BZ in a repeated zone scheme are plotted as gray lines.

Current-induced self-organization of mixed superconducting states

X. S. Brems^{1,2}, S. Mühlbauer¹, W. Y. Córdoba-Camacho³, A. A. Shanenko^{3,4}, A. Vagov^{4,5}, J. A. Aguiar³, R. Cubitt²

¹Heinz Maier-Leibnitz Zentrum (MLZ), Technical University of Munich, Garching, Germany; ²Institut Laue-Langevin, Grenoble, France;

³Departamento de Física, Universidade Federal de Pernambuco, Recife, Brazil; ⁴HSE University, Moscow, Russia;

⁵Institute of Theoretical Physics III, University of Bayreuth, Bayreuth, Germany

The elemental superconductor Niobium hosts the intermediate mixed state (IMS) where flux-free Meissner state domains and mixed state domains filled with supercurrent vortices form a two-domain structure. A sufficiently large current can depin vortices in a SC. We used a combined small angle neutron scattering and transport measurement setup to study the non-trivial current-induced self-organization of the IMS to a stripe-like superstructure.

The superconductor (SC) Niobium, found on the cusp between type I and type II superconductivity, hosts the intermediate mixed state (IMS) where flux-free Meissner state domains coexist with mixed state domains, filled with supercurrent vortices. This two domain structure is an ideal model system for universal domain physics as it is readily tunable via temperature and magnetic field. A sufficiently large current can depin vortices in a SC. In contrast to the pure mixed state of a conventional type II SC, this turns into a non-trivial scenario in the IMS as, due to Ampere's law, the current in the IMS is constrained to areas filled with vortices, meaning that in the IMS we find a highly heterogeneous current distribution leading to non-trivial ordering phenomena. In this work we report combined small-angle neutron scattering (SANS) and transport measurements studying the effect of an applied current on the IMS in a single-crystal bulk sample of the SC Nb.

SANS unveils non-trivial ordering phenomena

Fig. 1 (a) shows a schematic drawing of the experimental setup of the experiment at the Institut Laue-Langevin using D33 with the sample dimension, field direction B , current I , vortex movement v_L and the voltage V_{ff} . The scattering pattern exhibits two distinct contributions: (i) the vortex lattice within the mixed state results in Bragg peak scattering and (ii) the IMS domain structure leads to diffuse VSANS power-law scattering, the tail of which can be observed in the vicinity of the blacked out direct beam.

As a main result, we find that the initially random IMS domain structure is self-organizing into a stripe-like structure consisting of parallel Meissner state and mixed state strips. These are oriented along the movement of vortices. The rearrangement is manifested by a change from isotropic VSANS scattering in zero applied current to a clear anisotropy in the horizontal direction when a current is applied as depicted in Fig. 1 (b) showing the 2D SANS pattern with zero (left) and a current of 40 A applied to the sample (right).

[1] X. S. Brems et al., *Current-induced self-organisation of mixed superconducting states*, *Supercond. Sci. Technol.* **35**, 035003 (2022)

DOI: 10.1088/1361-6668/ac455e

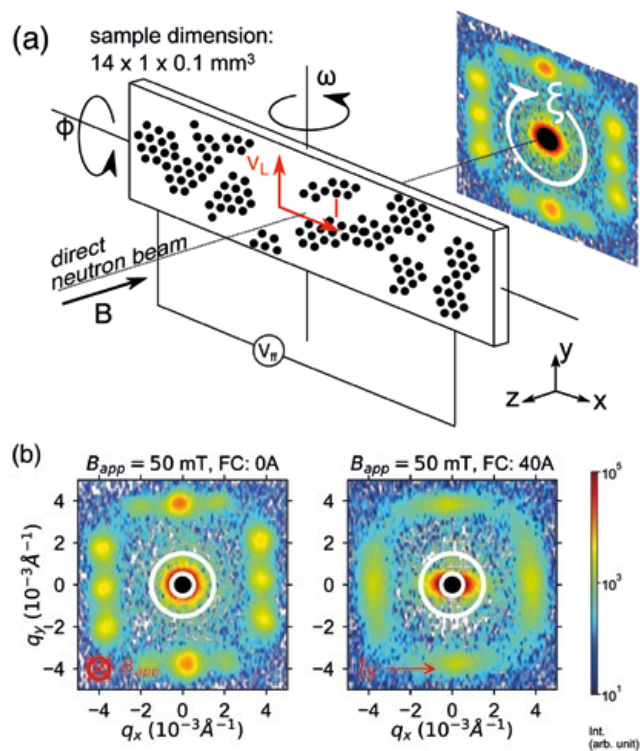


Figure 1: (a) Schematic drawing of the experimental setup with the sample dimension and orientation, magnetic field direction B , current I , vortex movement v_L and the voltage V_{ff} . (b) 2D SANS pattern with zero current (left) and $I = 40$ A (right) inducing flux flow. The VSANS from the IMS domain structure is marked in between the white circles and changes from isotropic to anisotropic for $I = 40$ A. This is consistent with a stripe-like superstructure of the IMS.

Quantifying the solution structure of metal nanoclusters
using small-angle neutron scatteringX. Liu¹, H. Yang², Y. Chen³, Y. Yang⁴, L. Porcar⁵, A. Radulescu⁶, S. Guldin⁴, R. Jin³, F. Stellacci⁷, Z. Luo¹

¹Department of Biomedical Engineering, Southern University of Science and Technology, Shenzhen, China; ²Department of Medicine, Shenzhen University, Shenzhen, China; ³Department of Chemistry, Carnegie Mellon University, Pittsburgh, United States; ⁴Department of Chemical Engineering, University College London, London, United Kingdom; ⁵Institut Laue-Langevin, Grenoble, France; ⁶Jülich Center for Neutron Science (JCNS) at MLZ, Forschungszentrum Jülich GmbH, Garching, Germany; ⁷Institute of Materials, École Polytechnique Fédérale de Lausanne, Lausanne, Switzerland

Small-angle neutron scattering (SANS) can directly quantify the overall structure parameters of nanoclusters in solution without the requirement of crystallization or gas phase ionization. A series of silver and gold nanoclusters were studied with SANS (on KWS-2), demonstrating good agreement with crystallographic data in both the shape and size as well as the molecular weight information.

Metal nanoclusters (NCs) are an emerging type of nanomaterial with unique optical, magnetic, and catalytic properties. Due to the quantum size effects and the extremely high surface-to-volume ratio, NCs exhibit fundamentally different properties from their plasmonic counterparts. The same goes for their characterization. While TEM is the standard technique for nanoparticles, it fails to provide enough resolution for the ultrasmall NCs. To date, a complete characterization of NCs is only possible if a single crystal can be obtained and resolved, which is limited to only a fraction of the NCs.

We report a systematic study on the neutron scattering of atomically precise NCs in solution using KWS-2.[1] Adopting an ellipsoid core-shell model, we successfully fitted the SANS data of a series of silver and gold NCs, including Ag₁₆, Ag₃₈, Ag₄₄, Ag₆₃, Ag₁₃₆, Ag₃₇₄ as well as Au₃₈, Au₁₀₄, Au₁₄₄. Both the size and geometry parameters calculated from SANS were found to be consistent with the crystallographic results

for these NCs. And for NCs, whose single crystal structures have not yet been resolved, such as Au₁₀₄, the calculated results of metal core and ligand shell act as the reference for future experimental and theoretical analysis of those NCs. Interestingly, for some NCs that carry multiple intrinsic charges, such as Ag₄₄, the overall diameter appeared significantly larger than other NCs with similar numbers of metal atoms. We attribute this observation to the presence of counter-ions in solution. Therefore, SANS could not only provide quantitative structure information without the need for crystallization but also allow for the examination of the surrounding molecules of NCs in solution.

Furthermore, using the contrast variation SANS, we also established a power-law relationship between the scattering invariants and the molecular weights of the NCs. As in the molecular weight calculation with SAXS, a deviation of < 10% was observed with SANS analysis on the M_w of the ligand shell. Considering the number of ligands on nanoclusters being in the order of 10-100, such deviation means that SANS could achieve molecular precise information (1-10 molecules) demonstrating the potential of SANS to serve as a supplementary technique for mass spectrometry.

[1] X. Liu et al., *Quantifying the Solution Structure of Metal Nanoclusters Using Small-Angle Neutron Scattering*, *Angew. Chem. Int. Ed.* 61, e202209751 (2022)
DOI: 10.1002/anie.202209751

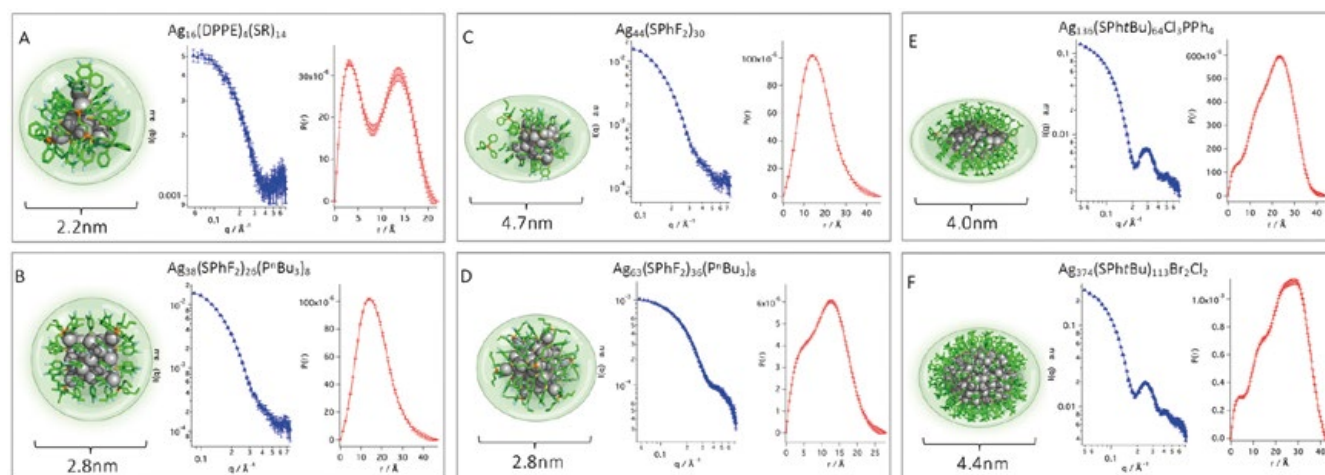


Figure 1: Comparison between the single crystal structures of Ag NCs, their SANS data and corresponding $P(r)$ analysis for (A) Ag₁₆(DPPE)₄(SC₆H₃F₂)₁₄, (B) Ag₃₈(SPhF₂)₂₆(PⁿBu₃)₈, (C) Ag₄₄(SPhF₂)₃₀, (D) Ag₆₃(SPhF₂)₃₆(PⁿBu₃)₈, (E) Ag₁₃₆(SPhtBu)₆₄Cl₃PPh₄, and (F) Ag₃₇₄(SPhtBu)₁₁₃Br₂Cl₂.

Polymeric nanocapsules from well-defined zwitterionic vesicles as template

H. Yalcinkaya^{1,5}, G. Mangiapia², M.-S. Appavou³, I. Hoffmann⁴, M. Gradzielski¹

¹Stranski-Laboratory for Physical and Theoretical Chemistry, Institute of Chemistry, Technical University of Berlin, Berlin, Germany;

²German Engineering Materials Science (GEMS) at MLZ, Helmholtz-Zentrum hereon GmbH, Garching, Germany; ³Jülich Centre for Neutron Science (JCNS) at MLZ, Forschungszentrum Jülich GmbH, Garching, Germany; ⁴Institut Max von Laue-Paul Langevin (ILL), Grenoble, France;

⁵Evonik Operations GmbH, Essen, Germany

The formation of highly monodisperse, rather small polymeric nanocapsules originating from a self-assembled vesicle system is monitored using small angle neutron scattering. SANS provided a full picture of the formation path of these structures from micelles to monomer-loaded vesicles and, subsequently, the fixation of the vesicles via the polymerization in a very systematic way.

Polymeric nanocapsules have a wide field of application. However, their preparation is challenging due to the difficulty of controlling the formation of homogeneous, uniform, small structures. An effective and non-aggressive method for controlled synthesis is by initiating them from vesicles and fixating by polymerization. In our approach, we initially dissolved monomers in surfactant micelles, which were transformed spontaneously into well-defined vesicles upon mixing with a second surfactant. Subsequently, the monomer-loaded vesicles were polymerized via UV-initiated polymerization. The structural evolution from micelles to monomer-loaded vesicles and, later, the polymerized vesicles were investigated using SANS performed on KWS1. Scattering curves of the monomer dissolved micelles were analyzed by modelling with a cylindrical geometry which for high concentrations shifts to a spherical one.

When the second surfactant has been mixed with the monomer containing micelles, the characteristic patterns of the scattering curves change completely. A q^{-2} slope in the middle q and q^{-4} slope at high q indicate the presence of bilayers and sharp interfaces, respectively. Applying the spherical shell model, one sees the initial radius decreasing from 36 (in good agreement with previous results) to 24 nm, which is also clear from the shift of the form factor minimum. This means the system rearranges itself to form a new more favored equilibrium structure of smaller vesicles. Porod analysis confirms the successful monomer incorporation within the bilayers. Moreover, the pronounced form factor minima confirm that the initial low polydispersity ~ 0.1 is retained (Fig. 1). SANS curves of the polymer fixated vesicles are very similar to those before polymerization, concluding that polymerization was able to retain the initial template vesicles completely.

In conclusion, this is a versatile way to obtain polymeric nanocapsules under ambient conditions. Their small size and high monodispersity render them interesting for potential applications like carrier vehicles.

[1] H. Yalcinkaya et al., *Polymeric Nanocapsules from Well-Defined Zwitterionic Vesicles as a Template*, *Macromolecules* 55 (17), 7869 (2022)

DOI: 10.1021/acs.macromol.2c01023

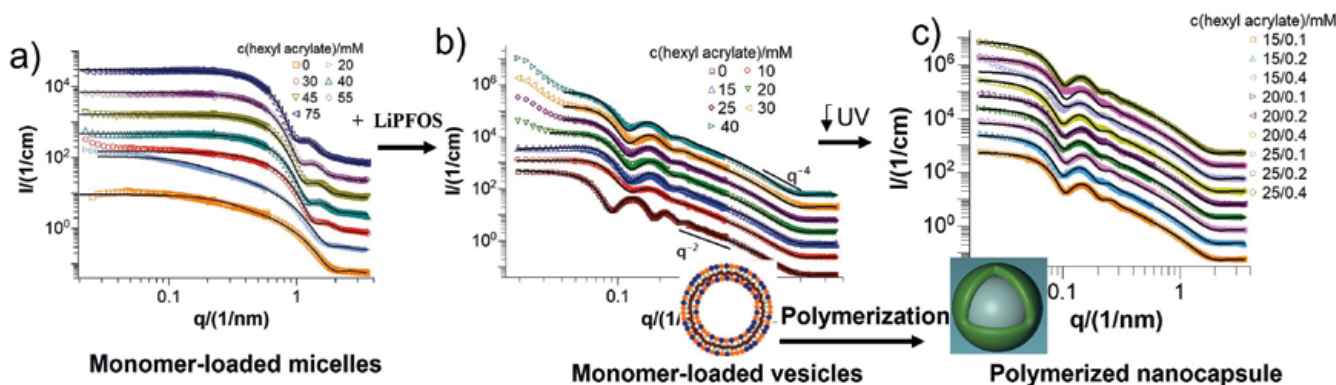


Figure 1: SANS curves of samples: (a) Hexyl acrylate (HA) monomer dissolved in 50 mM TDMAO/0.5 mM L35 micelles (b) unpolymerized vesicles of 27.5 mM TDMAO/0.275 mM L35/22.5 mM LiPFOS/HA (c) polymerized vesicles of 27.5 mM TDMAO/0.275 mM L35/22.5 mM LiPFOS/HA mixtures. (colored symbols: measured data; solid black line: fitted data) For clarity, subsequent data sets were each multiplied with a scale factor of 3.

Structure analysis of graft-type proton exchange membranes by SANS partial scattering function

Y. Zhao¹, K. Yoshimura¹, S. Sawada¹, T. Motegi¹, A. Hiroki¹, A. Radulescu², Y. Maekawa¹

¹Department of Advanced Functional Materials Research, Takasaki Advanced Radiation Research Institute, National Institutes for Quantum Science and Technology (QST), Takasaki, Gunma, Japan; ²Jülich Centre for Neutron Science (JCNS) at MLZ, Forschungszentrum Jülich GmbH, Garching, Germany

Partial scattering function analysis was used to visualize and quantify the exact structure of individual components in hydrated radiation-grafted proton exchange membranes at multiple length scales. In addition, the correlation between two components was explored to establish their locations. Structural insights into the membrane properties were provided.

Radiation-grafted proton exchange membranes (PEMs), made of poly(styrenesulfonic acid)-grafted poly(ethylene-co-tetrafluoroethylene) (ETFE-g-PSSA), are promising alternatives to Nafion[®] membranes for electrochemical applications such as electrodialysis and fuel cells. To improve the membrane performance, a thorough understanding of the structure-property relationship, investigated by techniques such as small-angle neutron scattering (SANS), is essential. However, SANS intensity profile measured conventionally contains contributions of all components in the sample like the hydrophobic polymer, hydrophilic polymer, ions, and water molecules, and fails to provide the detailed structure of the individual components. This undesirable original data problem can be solved by partial scattering function (PSF) analysis.

Hydrated ETFE-g-PSSA membranes were treated as a three-component system comprising the ETFE base polymer (BP), PSSA graft polymer (GP), and absorbed water (W). Using PSF analysis through contrast variation SANS experiments performed on the instrument KWS-2, the structure pattern of the PEM was constructed as shown in Fig. 1. On a large length scale the formation of polymer grains with a radius of gyration (Rg) of ~150 nm through the aggregation of phase-separated GP domains in the BP matrix with

a mass fractal structure having a dimension of 2.4 was observed. Each GP domain has an average Rg of 9.5 nm and was made up of homogeneously distributed water and GP, characterized by a bicontinuous-like local structure with a mean separation distance of ~2 nm. This indicated the formation of a well-connected ion channel network, which is a crucial factor in improving membrane conductivity. Furthermore, the PSF analysis revealed the repulsion between the water and GP at a molecular length scale of less than 3 nm, leading to a lower hydration number compared to Nafion[®] membranes. The results showed that the PSF analysis provides a mechanistic insight into membrane conductivity and structure correlations, illuminating a path forward toward establishing superior design rules for fuel cell membranes.

[1] Y. Zhao et al., *Unique Structural Characteristics of Graft-Type Proton-Exchange Membranes Using SANS Partial Scattering Function Analysis*, *Macromolecules* 55 (16), 7100 (2022)

DOI: 10.1021/acs.macromol.2c00333

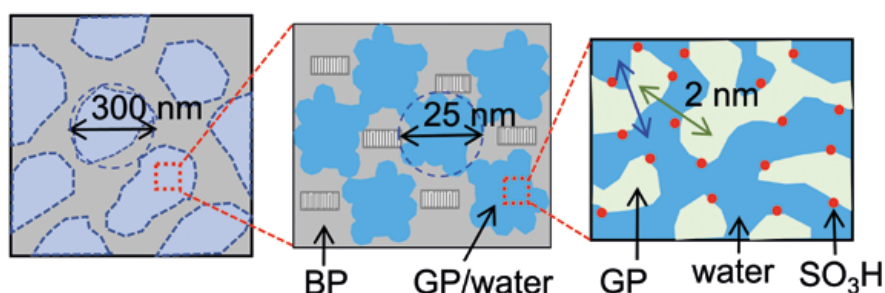
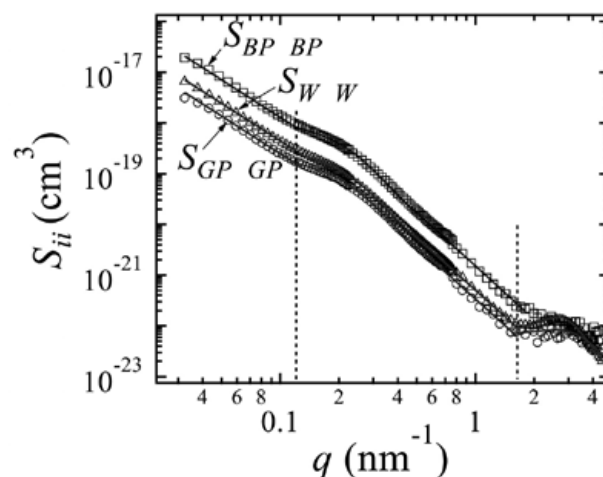


Figure 1: (Top) PSFs obtained through contrast variation SANS: the PSF for BP-BP correlation (S_{BP-BP}), the PSF for GP-GP correlation (S_{GP-GP}), and the PSF for W-W correlation (S_{W-W}); (Bottom) Schematic of the hierarchical structure of BP, GP and water domains in the fully hydrated ETFE-g-PSSA PEMs at multiple length scales.

Simulating the dynamics of supported membrane stacks on the nanosecond timescale

D. W. Hayward¹, S. Jaksch¹, M. Fomina¹, P. S. Dubey¹, H. Frielinghaus¹, O. Holderer¹, M. Monkenbusch²

¹Jülich Centre for Neutron Science (JCNS) at MLZ, Forschungszentrum Jülich GmbH, Garching, Germany; ²Jülich Centre for Neutron Science (JCNS-1), Forschungszentrum Jülich GmbH, Jülich, Germany

The dynamic structure factor of a solid-supported membrane stack has been calculated, extending the calculation of the static structure factor by Romanov and Ul'yanov. The physical properties of supported phospholipid bilayers can be studied in this way and can be related to measured intermediate scattering functions from grazing-incidence neutron spin-echo spectroscopy experiments.

Phospholipid bilayer stacks are of great biological importance and neutron spin-echo spectroscopy has the means of providing insight into the dynamics on length scales and time scales relevant for thermally driven fluctuations of phospholipid membranes. Grazing-incidence neutron spin-echo spectroscopy (GINSES) is unique in the sense that it provides access to the solid-liquid interface and, in this way, makes it possible to study membrane stacks supported by a flat silicon waver. The constraint of the flat solid interface has an influence on the fluctuation spectrum of lipid bilayers. Experiments on phospholipid membrane stacks with GINSES showed a part of the intermediate scattering function, which oscillates in time, and which might be visible due to the very precise geometrical conditions where the part of the scattering vector Q lying in the plane of the membrane is very small (corresponding to large length scales) and is therefore sensitive to relatively large scale motions.

MembraneDyn calculates membrane properties

The interpretation of these experimental observations triggered the development of a Fortran code, called MembraneDyn, which allows one to calculate the intermediate scattering function as a function of the scattering vector parallel and perpendicular to the membrane normal, and the physical parameters of the membrane such as the bending rigidity κ , the layer compression modulus B , the layer sliding viscosity η_s and the number of layers.

The static scattering, i.e. the structure of a stack of membranes supported by a flat rigid interface has been described in detail by Romanov and Ul'yanov [Romanov & Ul'yanov, *Phys. Rev. E*, 66, 06170 (2022)]. This procedure has been extended into the time domain. The effect of the different parameters as well as requirements for the numerical cal-

culations are described in detail in the paper. These calculations therefore help to understand and discuss GINSES experiments on supported lipid bilayers.

[1] D. W. Hayward et al., *MembraneDyn: simulating the dynamics of supported membrane stacks on the nanosecond timescale*, *Acta Crystallogr D Struct Biol.* 78 (10), 1249 (2022)

DOI: 10.1107/S2059798322008701

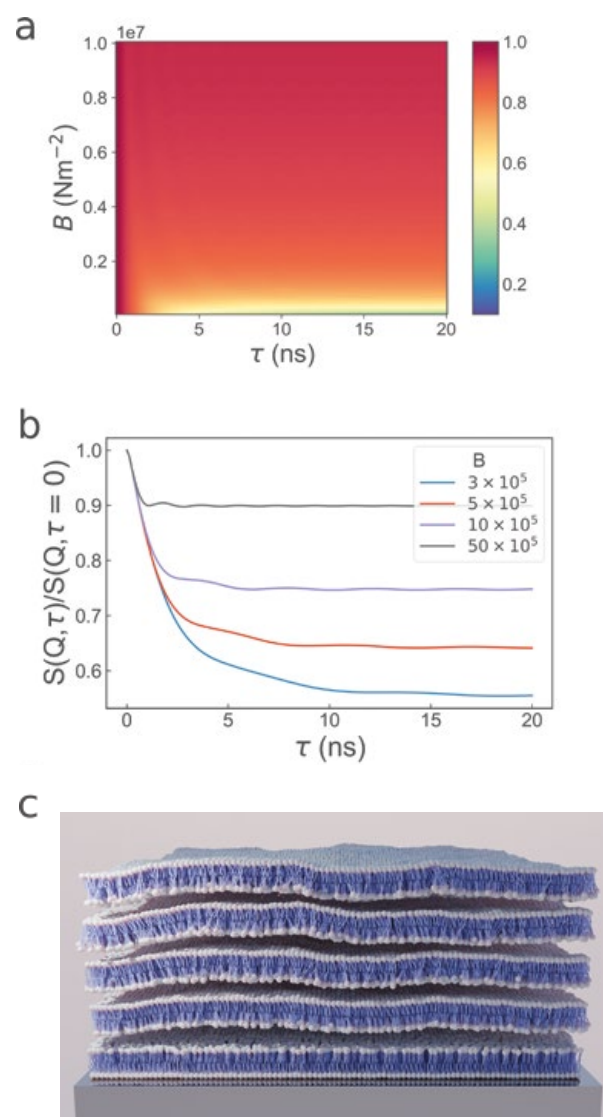


Figure 1: Results of the calculation of $S(Q, \tau)/S(Q, 0)$, here as an example as a function of the compression modulus as 2D plot (a), a cut for different B (b) and an artist's drawing of a supported lipid bilayer membrane stack (c).

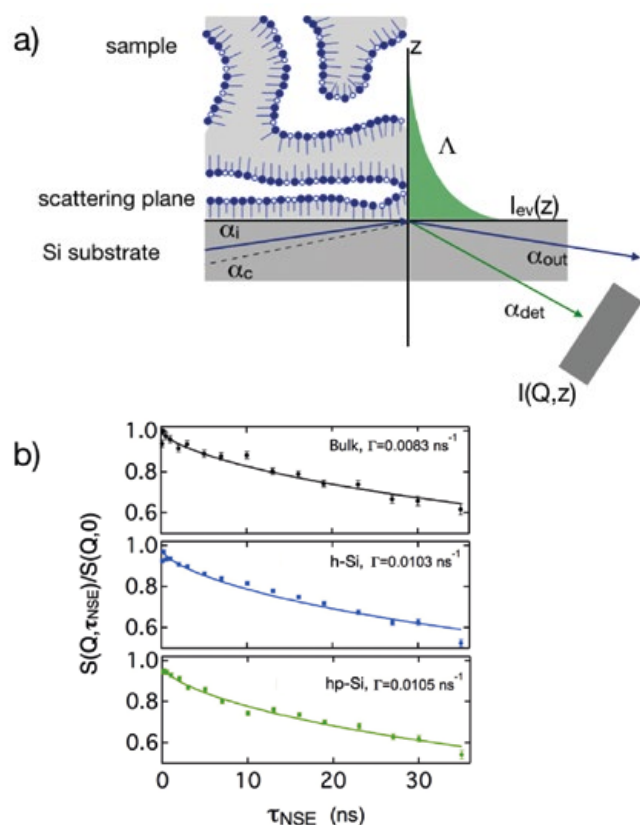
A combined wetting and scattering study of the near surface ordering in sugar surfactant based bicontinuous microemulsions at hydrophilic and hydrophobic surfaces

S. Wellert¹, R. Stehle^{2,3}, S. Micciulla⁴, M. Dahl¹, R. Steitz², T. Hellweg³, O. Holderer⁵

¹Department of Chemistry, Technische Universität Berlin, Berlin, Germany; ²Helmholtz Zentrum Berlin, Berlin, Germany; ³Physikalische und Biophysikalische Chemie, Universität Bielefeld, Bielefeld, Germany; ⁴Institut Laue-Langevin, Grenoble, France; ⁵Jülich Centre for Neutron Science (JCNS) at MLZ, Forschungszentrum Jülich GmbH, Garching, Germany

The commercial availability of natural surfactants and the solubilization of plant and food grade oils extends the field of application for microemulsions. To study potential confinement effects on the structure and dynamics in a microemulsion, neutron reflectometry and neutron spin echo spectroscopy under grazing incidence have been used. These measurements at a hydrophilic and hydrophobic surface are compared and show a similar wetting behavior and near surface structuring.

The use of environmentally friendly and sustainable microemulsions is very attractive in various applications. An important question in this context is the effect of rigid interfaces, which are ubiquitous in nature and applications, always providing some kind of confinement for the microemulsion, which might affect the structure and the fluctuation dynamics on microscopic length scales, but may by this means also modify the macroscopic properties of the microemulsion.



The influence of the chemical nature of the confining surface on the near surface structure and dynamics of a sugar surfactant based microemulsion is addressed in the paper presented here. A quaternary phase system is investigated with a sugar-based surfactant, pentanol as co-surfactant, water, and cyclohexane as oil phase, which is frequently used as a solvent in chemical and industrial applications.

Interface fluctuations

With grazing incidence neutron spin echo spectroscopy (GINSES) measured at J-NSE, thermal fluctuations of the surfactant layer are probed in the vicinity of the interface with an evanescent neutron wave.

The structure in surface normal direction is probed using neutron reflectometry. Surface wetting properties are investigated via contact angle measurements. The latter showed that these microemulsions wet hydrophilic and hydrophobic silicon surfaces. Neutron reflectometry revealed that the structure at the interface was very similar to the bulk phase, a slight increase of the correlation length being observed. The dynamics was altered by the interface but identical for both types of interface. The characteristic length of around 3 nm between the first microemulsion layer and wall is the outcome of the GINSES experiment, and showed that the microemulsion interacts in a very similar manner with the interface.

It could be concluded that this type of microemulsions does not form extended lamellar phases at the interface, as has been observed in other microemulsions.

[1] S. Wellert et al., *A Combined Wetting and Scattering Study of the Near Surface Ordering in Sugar Surfactant Based Bicontinuous Microemulsions at Hydrophilic and Hydrophobic Surfaces*, *Front. Soft. Matter* 2, 887610 (2022)
DOI: 10.3389/frsfm.2022.887610

Figure 1: a) Experimental conditions with a bicontinuous microemulsion at a rigid silicon interface, probed from the silicon side by the neutron beam under grazing incidence conditions. b) GINSES measurements of the bulk microemulsion (top) compared to the microemulsion at a hydrophilic (middle) and hydrophobic (bottom) interface.

Tuning the uniaxial rotational dynamics of oleic acid by grafting on nanoparticles

A. Sharma¹, M. Kruteva¹, M. Zamponi², S. Ehlert¹, D. Richter³, S. Förster^{1,2}

¹Jülich Centre for Neutron Science (JCNS-1) and Institute for Biological Information processing (IBI-8), Forschungszentrum Jülich GmbH, Jülich, Germany;

²Jülich Centre for Neutron Science (JCNS) at MLZ, Forschungszentrum Jülich GmbH, Garching, Germany; ³Jülich Centre for Neutron Science (JCNS-2) and Peter Grünberg Institute (PGI-4), Forschungszentrum Jülich GmbH, Jülich, Germany

Quasielastic neutron scattering reveals that the dynamics of oleic acid could be tuned by grafting it onto the spherical nanoparticles. With a decrease in temperature, the grafted molecules exhibit selective bond rotations and a change in the rotational diffusivity. We present a modified uniaxial rotational diffusion model to quantitatively capture the temperature dependent diffusivity, radius of rotation and the elastic contribution to the scattering.

We study oleic acid in a purely melted state as well as in a nanoparticle (iron oxide) grafted state by employing quasielastic neutron backscattering (QENS) experiments performed using SPHERES operated by JCNS at the MLZ.¹ We employed three temperatures: 250, 275 and 300 K. The pure oleic acid crystallizes at $T \sim 286$ K hence, we only observe translational diffusion dynamics of oleic acid at 300 K. By fitting a stretched exponential function, we obtain average translational diffusivity 2.25×10^{-10} m²/s, which agrees with the literature. On the other hand, for nanoparticle grafted oleic acid we observe dynamics even at 250 and 275 K due to unfeasible crystallization of grafted molecules.

Selective bond rotation dynamics

Along with the dynamic processes, we also observe elastic scattering indicating dynamic constraints (Fig. 1). Accounting for the grafting density (3 chains/nm²) and the dimensions

of the oleic acid molecule, we conclude that the dynamics observed for grafted oleic acid is due to the uniaxial rotation of a molecule around its axis. As the stretched exponential function cannot explain the physics of such a dynamics process, we modify the original uniaxial rotational diffusion model to obtain the rotational diffusivity, radius of rotation and elastic contribution from the dynamics of grafted oleic acid. The radius of rotation obtained at 300 K matches the lateral dimension of the oleic acid molecule and the grafting density induced geometrical constraints (Fig. 1 insert). With a decrease in temperature, the radius of rotation decreases. This interesting result asserts that a decrease in temperature leads to the cessation of certain bond rotations. When we fix the radius of rotation for all temperatures to the molecular radius, we obtain a continuous increase in the diffusivity with the temperature, as well as a decrease in the elastic contribution. This proves that in the case of nanoparticle grafted oleic acid, temperature dependent selective bond rotation could be induced. This important quantitative result is useful for tuning the dynamics of oleic acid.

[1] A. Sharma et al., *Quasielastic Neutron Scattering Reveals the Temperature Dependent Rotational Dynamics of Densely Grafted Oleic Acid*, *J. Chem. Phys.* 156 (16), 164908 (2022)

DOI: 10.1063/5.0089874

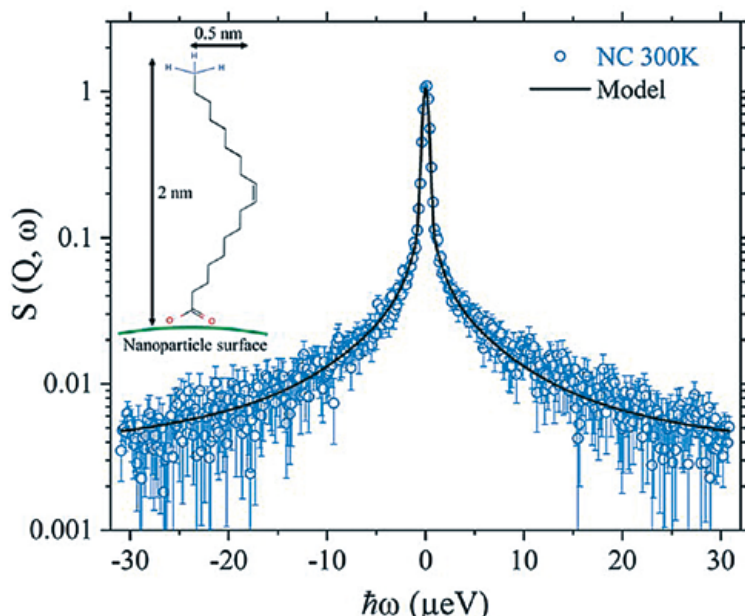


Figure 1: Representative quasielastic neutron backscattering spectrum for oleic acid grafted onto iron oxide nanoparticles obtained at 300 K, $Q = 1.12 \text{ \AA}^{-1}$ shows dynamic broadening at high energy transfers as well as the elastic scattering at zero energy transfer. Black line represents the fit using the modified uniaxial rotational diffusion model. Inset shows the schematic of oleic acid grafted onto nanoparticle surface along with its dimensions.

Structure formation of PNIPAM microgels in foams and foam films

M. Kühnhammer¹, K. Gräff¹, E. Loran¹, O. Soltwedel¹, O. Löhmann¹, H. Frielinghaus², R. von Klitzing¹

¹Institute for Condensed Matter Physics, Technische Universität Darmstadt, Darmstadt, Germany; ²Jülich Center for Neutron Science (JCNS) at MLZ, Forschungszentrum Jülich GmbH, Garching, Germany

Responsive aqueous foams are interesting for applications like foam flooding or foam flotation. Thermoresponsive microgels (MGs) made from poly(N-isopropyl-acrylamide) (PNIPAM) with varying cross-linker content are used as foam stabilisers. The foams are thermoresponsive and are destabilised at elevated temperatures. The structure of the foam films is investigated using small-angle neutron scattering (SANS) and in a thin film pressure balance (TFPB).

Foams are abundant in every day life as food, personal care products or household cleaning agents and are also important for industrial processes like flotation or textile manufacturing. Aqueous foams are dispersions of gas in water and the structure of their continuous liquid phase is often described as hierarchical with differently sized building blocks at different length scales. These building blocks are: foam films, which are liquid films separating two bubbles, plateau borders that are made up of three foam films and nodes, which are the connection of plateau borders.

SANS measurements

Foams were produced from microgel dispersions in D₂O by bubbling N₂ gas through a porous glass plate at the bottom of the cell [1]. Once this steady-state was reached, SANS measurements at different foam heights ($h=2, 9.5$ and

16 cm) were performed (Fig. 1a). From the SANS analysis in a Porod representation, the MGs, adsorbed at a single air/water interface, adopt very well defined long-ranged hexagonal structures even at low surface pressures. In combination with the results obtained for individual foam films in a TFPB, the following picture arises: Foam films in MG stabilised foams are inhomogeneous in thickness. Only the thinner parts of the foam films (grey areas in Fig. 1b) are detectable by SANS. The foam film's inhomogeneity is also the reason for the rather exact Porod decay of the scattered intensity as the thicker parts of the foam films are too large to display a distinct form factor and are only detectable as single interfaces by the neutrons.

The foam films are inhomogeneous and form a network-like structure, in which thin and MG depleted zones with a thickness of ca. 30 nm are interspersed in a continuous network of thick MG containing areas with a thickness of several 100 nm. The thickness of this continuous network is related to the elastic modulus of the individual MGs. Both the elastic moduli and foam film thicknesses indicate a correlation to the network elasticity of the MGs predicted by the affine network model.

[1] M. Kühnhammer et al., *Structure formation of PNIPAM microgels in foams and foam films*, *Soft Matter* 18 (48), 9249 (2022)

DOI: 10.1039/D2SM01021F

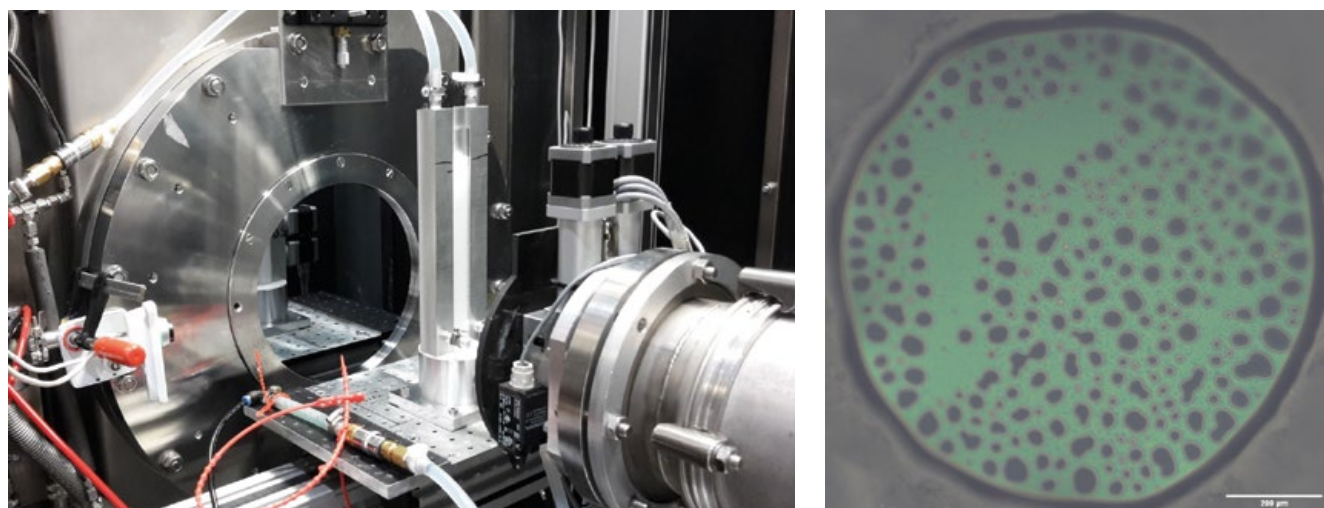


Figure 1: (a) Single foam cell installed at the KWS-1 beamline at the MLZ. (b) Photograph of foam films inside the TFPB stabilized by MG dispersions (with a cross linker parameter of 7.5) at a concentration of $w = 0.3\text{wt}\%$.

Controlled LCST and structural variety of alternating amphiphilic copolymers in water

E. Kostyurina¹, J. U. De Mel², A. Vasilyeva¹, M. Kruteva¹, H. Frielinghaus⁴, M. Dulle¹, L. Barnsley⁴, S. Förster^{1,4}, G. J. Schneider^{2,3}, R. Biehl¹, J. Allgaier¹¹Jülich Centre for Neutron Science (JCNS-1) and Institute for Biological Information processing (IBI-8), Forschungszentrum Jülich GmbH, Jülich, Germany; ²Department of Chemistry, Louisiana State University, Baton Rouge, Louisiana, United States; ³Department of Physics & Astronomy, Louisiana State University, Baton Rouge, Louisiana, United States; ⁴Jülich Centre for Neutron Science at MLZ, Forschungszentrum Jülich GmbH, Garching, Germany

We widely and systematically studied non-ionic alternating amphiphilic polymers (AAPs) from the perspectives of solubility behavior and structure formation in water. The structures which AAP form in water were closely investigated by small angle X-ray and neutron scattering. It was found that, depending on the AAP composition, molecular weight and concentration, the polymers either dissolve in water as free chains or form micelles and gels. The study demonstrates how the structure of AAP, namely the length of the hydrophilic and the hydrophobic blocks, can be systematically varied to adjust the thermal solution properties such as the LCST over a wide range.

The AAPs containing dicarboxylic acids as hydrophobic (C_m) and polyethylene glycol (EG_n) as hydrophilic blocks show a lower critical solution temperature (LCST) behavior in water. We show that the transition temperature, which is a measure of AAP hydrophobicity, can be tuned in the range from 0 to 100°C by changing the AAP composition [1]. The structures which such polymers form in water were closely investigated by SAXS in JCNS and SANS at KWS-1 at MLZ. It was found that, depending on the AAP composition, molecular weight and concentration the polymers either dissolve in water as free chains or form micelles and gels (Fig. 1).

Free chains and micellar structures of AAP

In short, hydrophobic blocks (C_m) need sufficiently long EG_n block to keep the polymers water-soluble. The copolymers behave as free chains, forming loops because of hydrophobic intrachain block attractions. SANS was used to clarify the details of free chain structure. With increasing the hydrocarbon chain length and keeping the polymers water-soluble, the polymers can form compact objects, such as partially collapsed chains or micelles. The micelles formed by the AAP differ structurally from micelles formed by block copolymers or surfactants, where the core is formed exclusively by the hydrophobic units.

The AAP micelles have a pronounced core constructed by the hydrophobic domains embedded in a PEG-rich and water-poor matrix, whereas the micellar shell consists of a smaller number of PEG end groups or internal PEG units forming loops. SAXS is more sensitive to the micellar hydrophobic core and therefore to the micellar self-assembly and intra-core structure. When the PEG length is not long enough to keep the polymers water-soluble, the polymers aggregate into a gel which is formed by the micellar structures described above.

In conclusion, the ability to tune polymer solubility behavior and structural properties by changing temperature, AAP composition, molecular weight and concentration, makes AAP materials highly interesting for various applications.

[1] E. Kostyurina et al., *J. Controlled LCST Behavior and Structure Formation of Alternating Amphiphilic Copolymers in Water*, *Macromolecules* 55 (5), 1552 (2022)

DOI: 10.1021/acs.macromol.1c02324

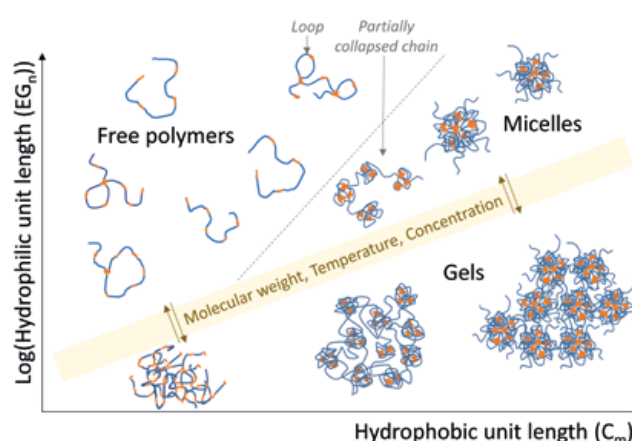


Figure 1: Qualitative diagram representing the solubilization states and conformations of the AAP measured by SANS at KWS-1 at MLZ depending on their composition.

Open-bundle structure as the unfolding intermediate of cytochrome c'

T. Yamaguchi¹, K. Akao¹, A. Koutsioumpas², H. Frielinghaus², T. Kohzuma¹

¹Institute of Quantum Beam Science, Graduate School of Science and Engineering, Ibaraki University, Mito, Ibaraki, Japan

²Jülich Centre for Neutron Science (JCNS) at MLZ, Forschungszentrum Jülich GmbH, Garching, Germany

The dynamic structural changes, including the unfolding, dimerization, and transition from the compact to the open-bundle unfolding intermediate structure of Cytochrome c' (Cyt c'), were detected by small-angle neutron scattering (SANS). The protein was investigated in buffer/D₂O solution at acidic (pD = 1.7), neutral (pD = 6.4), and alkaline (pD ≈ 9.6; pD ≈ 13) states. The structures obtained range from a random coil over dimers to an open-bundle structure.

A protein molecule is folded into a distinctive structure to express the unique role it plays in biological systems. Anfinsen showed that most small proteins fold spontaneously into their specific functional structure. Many protein-folding/unfolding experiments have been performed to date to reveal protein self-assembly mechanisms, and several general mechanisms have been proposed. The “energy landscape” model is a widely accepted hypothesis for describing protein folding pathways. This model proposes that the protein folding reaction explores exothermic conformational arrangements of the polypeptide along the potential energy surface, leading to the native protein structure.

SANS measurements

Cyt c' was extracted from *Alcaligenes xylosoxidans* (Fig. 1, left) and purified by cation exchange chromatography and size-exclusion chromatography, followed by re-crystalliza-

tion according to a previous method. The purity of Cyt c' was checked by sodium dodecyl sulfate polyacrylamide gel electrophoresis. Samples for SANS experiments at KWS-1 were prepared at pD 6.4 and 9.6 with 20 mM phosphate buffer. The sample solutions at pD 1.7 and ~13 were prepared by the addition of a small amount of DCI and NaOD to the phosphate buffer, respectively.

The forward scattering of the SANS measurements directly indicated unimers at pD 1.7 and ~13, while dimers were observed at neutral and slightly alkaline pD values. For pD 1.7, a random coil structure perfectly describes the SANS data. Using the program DENFERT, a static real-space bead model was obtained from the SANS measurements (Fig. 1, right). Clearly, dimer structures could be identified at pD 6.4 and 9.6 with two compact proteins being attached to each other. At pD ~13, a static, rather long structure was obtained that could be connected to an elongated open bundle structure. A more detailed analysis (Fig. 1, left) connected the open bundle structure either to an analytic model with four fluctuating joint clubs formed by the helices, or to a fluctuating protein model using the software BUNCH.

[1] T. Yamaguchi et al., *Open-Bundle Structure as the Unfolding Intermediate of Cytochrome c' Revealed by Small Angle Neutron Scattering*, *Biomolecules* 12(1), 95 (2022)
DOI: 10.3390/biom12010095

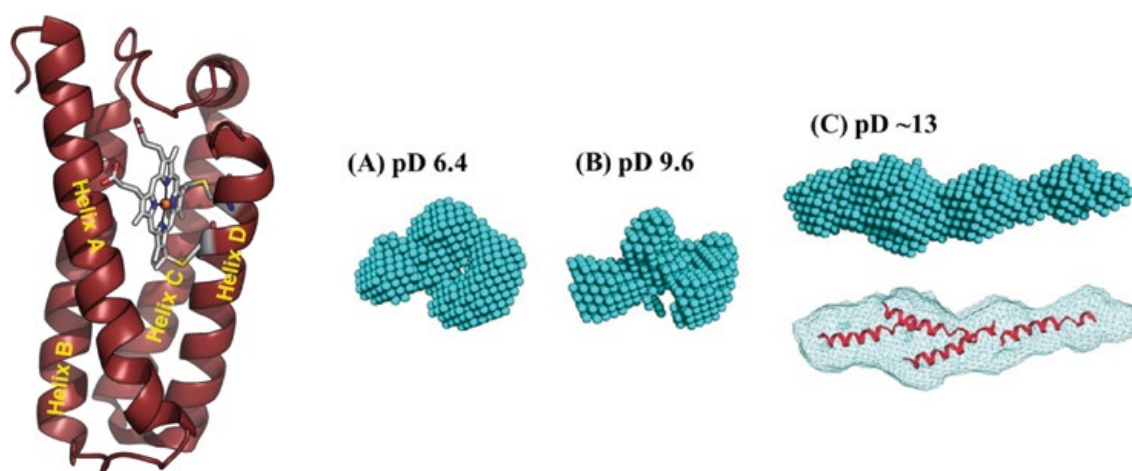


Figure 1: (left) Structure of Cyt c' monomer from *Alcaligenes xylosoxidans* NCIMB 11015. (right) The ab initio bead models generated by the program DENFERT at pD 6.4 (A), 9.6 (B), and ~13 (C). The four B helices were docked in the volumetric map for (C) using the program Situs.

Structural analysis of the nucleotide-binding domain of Hsp72 in complex with ADP

T. Yokoyama¹, S. Fujii¹, A. Ostermann², T.E. Schrader^{3,2}, Y. Nabeshima¹, M. Mizuguchi¹

¹Faculty of Pharmaceutical Sciences, University of Toyama, Toyama, Japan; ²Heinz Maier-Leibnitz Zentrum (MLZ), Technical University of Munich, Garching, Germany; ³Jülich Centre for Neutron Science (JCNS) at MLZ, Forschungszentrum Jülich GmbH, Garching, Germany

Neutron crystallographic analysis of the heat-shock protein Hsp72 in complex with adenosine diphosphate (ADP) revealed the protonation states of the catalytic residues and ADP, as well as the structure of water clusters inside the protein. An enzymatic assay and a X-ray crystallographic analysis of a Hsp72 mutant provided further insights into the relationship between a water cluster and the enzymatic activity of Hsp72.

Protonation states and water cluster in Hsp72

The neutron crystal structure of the nucleotide-binding domain of Hsp72 in complex with ADP was solved at a resolution of 2.2 Å using the single crystal diffractometer BIODIFF. The structure analysis revealed that three catalytically important acid residues are present in the deprotonated state. Also, the phosphate group of the bound ADP molecule was found in the fully deprotonated state. The study made it possible to characterize the detailed structure of a water cluster located near the binding pocket of ADP (see Fig. 1). This cluster is composed of seven water molecules which display low Debye-Waller-factors, indicating a well-ordered state.

Study of the ATPase activity with a Hsp72 mutant

The amino acid tyrosine 149 (Y149) is in direct contact with the water cluster and is also involved in the conformational change between the ATP- and ADP-bound states. We conducted an enzymatic assay and X-ray crystallographic analysis of the mutant Y149A where the tyrosine is replaced by the smaller and nonpolar amino acid alanine. The ATPase activity of the Y149A mutant was found to be lower than that of the wild-type protein. An X-ray crystallographic analysis of Y149A-Hsp72 revealed that the Y149A mutation disrupts the hydrogen bond network of the water cluster and results in the incorporation of an additional magnesium ion at the catalytic site. These results suggest that Y149 contributes to the intrinsically lowered ATPase activity by stabilizing the water cluster.

[1] T. Yokoyama et al., *Neutron crystallographic analysis of the nucleotide-binding domain of Hsp72 in complex with ADP*, *IUCrJ*, 9(Pt 5), 562 (2022)

DOI: 10.1107/S2052252522006297

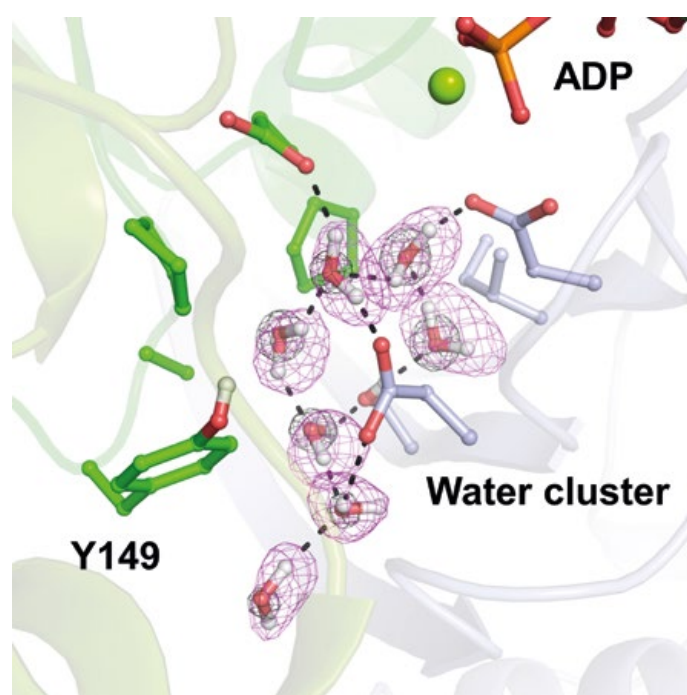


Figure 1: Structure of the water cluster in the Hsp72-ADP complex. A neutron scattering length density map (deuterium omit Fo-Fc difference Fourier map at 5 σ) and an X-ray electron density map (2Fo-Fc, 3 σ) are shown as magenta and black mesh, respectively.

Magnetic phase diagram of HoFeO₃ by neutron diffraction

A. K. Ovsianikov¹, I. A. Zobkalo², V. Hutanu^{1,3}, S. N. Barilo⁴, N. A. Liubachko⁴, T. Chatterji⁵,
M. Meven^{1,3}, P. J. Brown⁵, G. Roth¹, L. Peters¹

¹Institute of Crystallography, RWTH Aachen University, Aachen, Germany; ²Petersburg Nuclear Physics Institute by B. P. Konstantinov of NRC “Kurchatov Institute”, Gatchina, Russia; ³Jülich Centre for Neutron Science (JCNS) at MLZ, Forschungszentrum Jülich GmbH, Garching, Germany; ⁴Scientific-Practical Materials Research Centre NAS of Belarus, Minsk, Belarus; ⁵Institut Laue-Langevin (ILL), Grenoble, France

Long range magnetic order in HoFeO₃ single crystals was studied using neutron diffraction under external magnetic fields. The interplay between the external magnetic fields, Dzyaloshinsky-Moria antisymmetric exchange, isotropic exchange interactions between Fe/Ho sublattices and within the Fe sublattice alone results in a rich magnetic phase diagram. As a result, eight different magnetic phases were found either induced or suppressed, depending on the external field.

The crystal structure of HoFeO₃ is described by the space group *Pnma* (or *Pbnm* in another setting), where the compound exhibits two spin-reorientation transitions. The first transition takes place at $T_{SR1} = 53$ K where the moments of the Fe³⁺ ions rotate in plane from the *c* axis to the *a* axis. The second transition takes place at $T_{SR2} = 35$ K, where the strongest component of the magnetic moment tends to orient along the *b* axis. The Ho³⁺ ordering takes place at $T_{NR} \approx 10$ K. The neutron diffraction experiments were performed at the diffractometer POLI, operating with both polarized and non-polarized neutrons. For the present studies, we used a non-polarized setup with the 8 T dedicated magnet.

Magnetic scattering dependence on magnetic fields

In the HoFeO₃ unit cell, the Fe³⁺ ions occupy the special site *4b*, creating certain restrictions for the contribution of different magnetic modes to Bragg reflections with corresponding Miller index parity. The temperature dependence of their integral intensities was measured in external magnetic fields. For all of these reflections, a change in intensity with the temperature was monitored. A set of magnetic phases was identified and described by a selection of magnetic irreducible representations. The phases obtained differ in direction and magnitude for the components of the magnetic moments. One can identify eight different magnetic phases, either induced or suppressed by the magnetic field. The rich resulting magnetic phase diagram is the consequence of a subtle balance of exchange interactions in the crystal and the external magnetic field. The close values of the determined exchange parameters $J_{Ho-Ho} = 0.036$ meV and $J_{Ho-Fe} = -0.026$ meV are the reason for the transition at $T = 24$ K, where the direction of the ferromagnetic component of Ho changes its sign (see Fig. 1 a). A magnetic field above 1 T destroys this balance, and suppresses this phase (Fig. 1 b). Fields above 4 T stabilize canting of the Ho moments, which gives them a non-zero y-component (Fig. 1 c). The full analysis of all magnetic phases in HoFeO₃ can be found in [1].

[1] A. K. Ovsianikov et al., *Magnetic phase diagram of HoFeO₃ by neutron diffraction*, *J. Magn. Magn. Mater.* 557, 169431 (2022)
DOI: 10.1016/j.jmmm.2022.169431

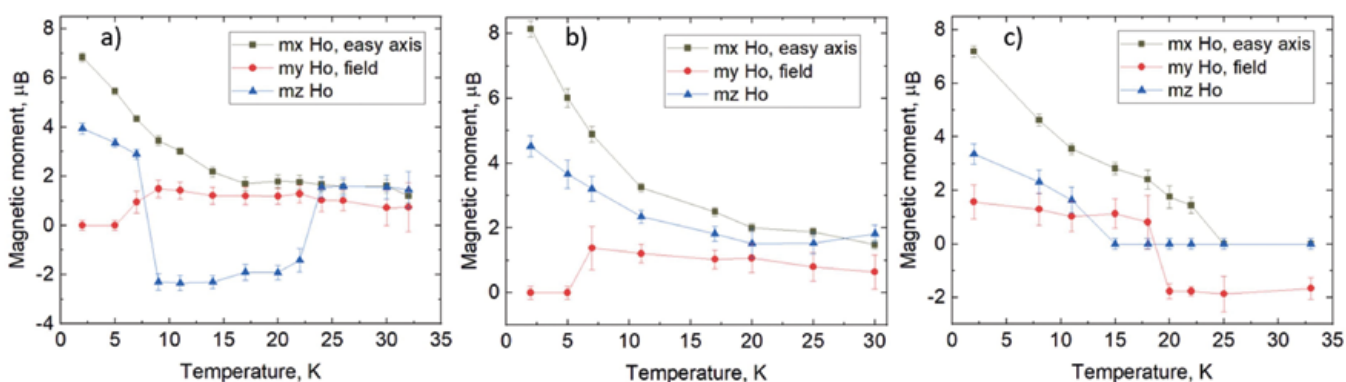


Figure 1: Temperature dependence of the x, y and z components of the Ho magnetic moments in fields of a) 0.5 T, b) 1.25 T and c) 5 T.

Secondary phase effect on the thermoelectricity by doping Ag in SnSe

J. Wu¹, L. Zhang⁴, R. Vasudevan¹, Z. Cheng⁴, J. Wang⁴, S. Lin⁵, F. Zhu⁶, Y. Zhang^{1,7}, Y. Pei⁵, X. Tong^{2,3}, J. Ma¹, Q. Ren^{1,2,3}, M. Hoelzel⁸

¹School of Physics and Astronomy, Shanghai Jiao Tong University, Shanghai, China; ²Institute of High Energy Physics, Chinese Academy of Sciences (CAS), Beijing, China; ³Spallation Neutron Source Science Center, Dongguan, China; ⁴Institute for Superconducting and Electronic Materials, University of Wollongong, New South Wales, Australia; ⁵Interdisciplinary Materials Research Center, School of Materials Science and Engineering, Tongji University, Shanghai, China; ⁶Jülich Centre for Neutron Science (JCNS) at Heinz Maier-Leibnitz Zentrum (MLZ), Forschungszentrum Jülich, Garching, Germany; ⁷Wenzhou Institute, University of Chinese Academy of Sciences, Wenzhou, China; ⁸Heinz Maier-Leibnitz Zentrum (MLZ), Technical University of Munich, Garching, Germany

Thermoelectric materials attract increasing attention, as they can directly and reversibly convert a temperature gradient into electrical energy. SnSe is a group of promising thermoelectric materials with excellent electrical properties and very low lattice thermal conductivity. In general, the optimization of thermoelectric performance in SnSe strongly relies on doping elements, like Na and Ag dopants. Nonetheless, introducing dopants in SnSe matrix would inevitably bring a secondary phase. However, the concomitant lattice and transport properties are yet understood.

Crystal structure

In this work, we used the high-resolution powder diffractometer SPODI at the Heinz Maier-Leibnitz Zentrum (MLZ) to study the crystal structures of pristine-SnSe (p-SnSe) as a function of temperature. The neutron powder diffraction (NPD) patterns over the temperature range of 300–950 K in Fig. 1(a) illustrate a phase transition from low symmetry *Pnma* (no. 62, Fig. 1(b)) to high symmetric *Cmcm* (no. 63, Fig. 1(c)). At 300 K, p-SnSe has the *Pnma* space group with $a = 11.44083 \text{ \AA}$, $b = 4.13168 \text{ \AA}$, and $c = 4.42467 \text{ \AA}$. The positions of Se and Sn atoms are located at $4c (x, 1/4, z)$

sites. Above 775 K, p-SnSe crystallizes in the *Cmcm* structure with $a = 4.27367 \text{ \AA}$, $b = 11.64371 \text{ \AA}$, and $c = 4.29595 \text{ \AA}$. The Sn and Se atoms occupy the $4c (0, y, 1/4)$ positions. The unit cell volume varies continuously across the phase transition, but the b/c trend exhibits a turning behavior. The observed phase transition significantly affects the thermoelectric performance. As shown in Fig. 1(d), the electrical transport property of the pristine sample shows a noticeable increase following the phase transition, which might be attributed to the different band structures between the low- T *Pnma* and high- T *Cmcm* structures.

Doping with Ag

Besides the structural studies on the P-SnSe, the effects of doping Ag in SeSn on the structures and thermoelectric properties are also investigated with X-ray diffraction and bulk property measurements. The doping of Ag into SnSe could favor the electrical transport properties and hence the thermoelectric performance (Fig. 1d). However, further increase in the Ag doping concentration would introduce an AgSnSe_2 secondary phase, which is harmful to the carrier concentration and mobility as well as lattice thermal conductivity. Therefore, an optimal Ag doping concentration is desirable to balance the enhancements in transport properties and the harmfulness of the secondary phase.

[1] R. Vasudevan et al., *Secondary phase effect on the thermoelectricity by doping Ag in SnSe*, *J. Alloys Comp.* 923, 166251 (2022)

DOI: 10.1016/j.jallcom.2022.166251

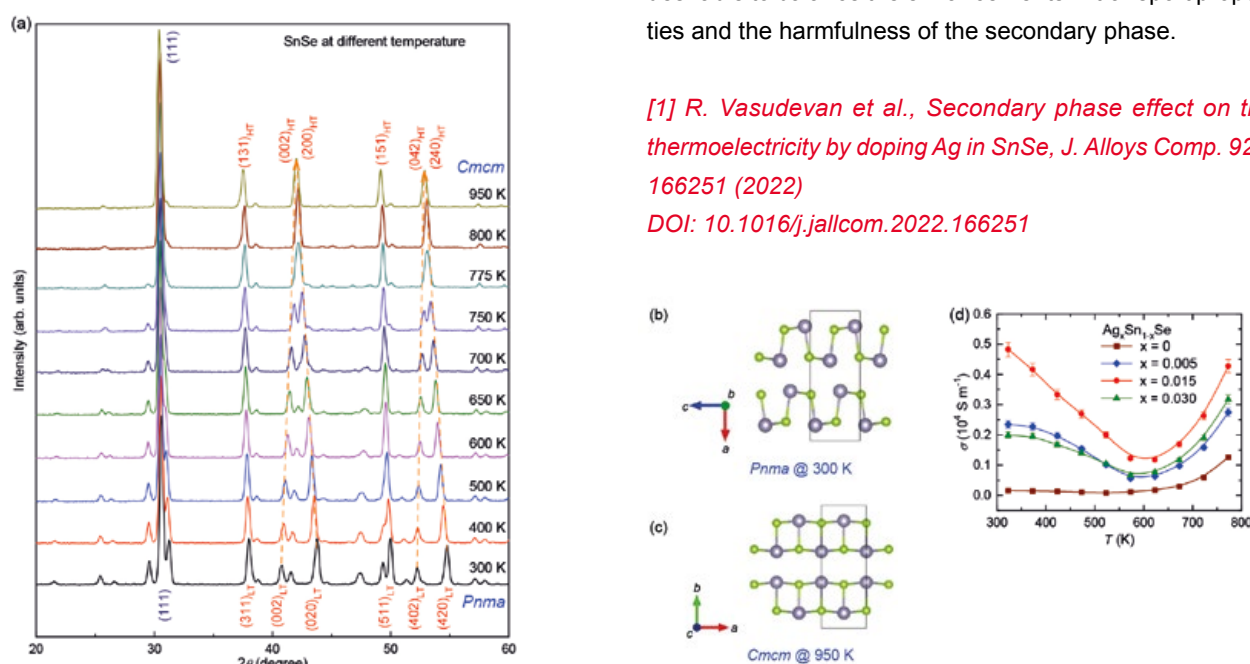


Figure 1(a) Temperature-dependent neutron powder diffraction (NPD) patterns of pristine-SnSe (p-SnSe). The crystal structures at (b) 300 K and (c) 950 K, as determined from the Rietveld refinement fitting of NPD patterns. (d) The temperature – dependent electrical conductivity of $\text{Ag}_x\text{Sn}_{1-x}\text{Se}$.

Non-collinear magnetic structures in the magnetoelectric Swedenborgite $\text{CaBaFe}_4\text{O}_7$

N. Qureshi^{1,2}, B. Ouladdiaf¹, A. Senyshyn³, V. Caignaert⁴, M. B. Valldor^{5,2}

¹Institut Laue-Langevin, Grenoble, France; ²II. Physikalisches Institut, Universität zu Köln, Köln, Germany; ³Heinz Maier-Leibnitz Zentrum (MLZ), Technical University of Munich, Garching, Germany; ⁴CRISMAT, UMR 6508, CNRS-ENSICAEN, Caen, France; ⁵Centre for Materials Science and Nanotechnology (SMN), Department of Chemistry, University of Oslo, Oslo, Norway

Geometrical frustration can lead to exotic spin configurations with fascinating properties. The Swedenborgite lattice is host to a plethora of magnetic ground states ranging from spin liquids to complex magnetic structures. As a result of competing single-ion anisotropy and exchange interactions, $\text{CaBaFe}_4\text{O}_7$ reveals a multi-q conical structure which adds a piece to the understanding of its magnetoelectric effect under magnetic fields.

Complex spin order leading to magnetoelectric effect

The orthorhombically distorted Swedenborgite $\text{CaBaFe}_4\text{O}_7$ – with Fe atoms forming Kagome planes separated by Fe layers with trigonal symmetry – orders magnetically close to room temperature and magnetocurrent measurements proved the magnetoelectric effect under the application of an external magnetic field for which a complex spin order was claimed to be responsible. Our work on powder (SPODI@FRM-II) and single-crystal (D10@ILL) samples is the first neutron diffraction study devoted to the details of the involved magnetic structures and reveals yet another type of magnetic ordering, adding to the rich diversity of examples within the Swedenborgite family.

In agreement with macroscopic measurements, our data show two magnetic phase transitions, the first at $T_{N1} = 274$ K into a ferrimagnetic structure with antiferromagnetic canting

perpendicular to the easy direction c (Fig. 1a and 1b). While the canting is stabilized by single-ion anisotropy, it cannot satisfy all exchange interactions on the triangular motifs and, due to the temperature-dependent competition with the exchange interactions, a second phase transition takes place at $T_{N2} = 202$ K where the b component changes from a collinear to a cycloidal arrangement resulting in a tripled unit cell along the a axis. Symmetry-compatible magnetic structure models were calculated and refined using the *Mag2Pol* program revealing a conical magnetic structure at low temperatures (Fig. 1c and 1d). The strong coupling within the planes and the 120° spin arrangement on triangular plaquettes above and below a triangular Fe spin (open triangles in Fig. 1) suggest that the magnetic structure is governed by the super-exchange interactions within these units. The interactions between the clusters (filled triangles) are not perfectly fulfilled and – in turn – seem less dominant in the energy balance.

The details of the complex magnetic structures are an important step towards an understanding of the magnetoelectric effect under magnetic fields in this polar ferrimagnet.

[1] N. Qureshi et al., *Non-collinear magnetic structures in the magnetoelectric Swedenborgite $\text{CaBaFe}_4\text{O}_7$ derived by powder and single-crystal neutron diffraction*, *SciPost Phys. Core* 5, 007 (2022)

DOI: 10.21468/SciPostPhysCore.5.1.007

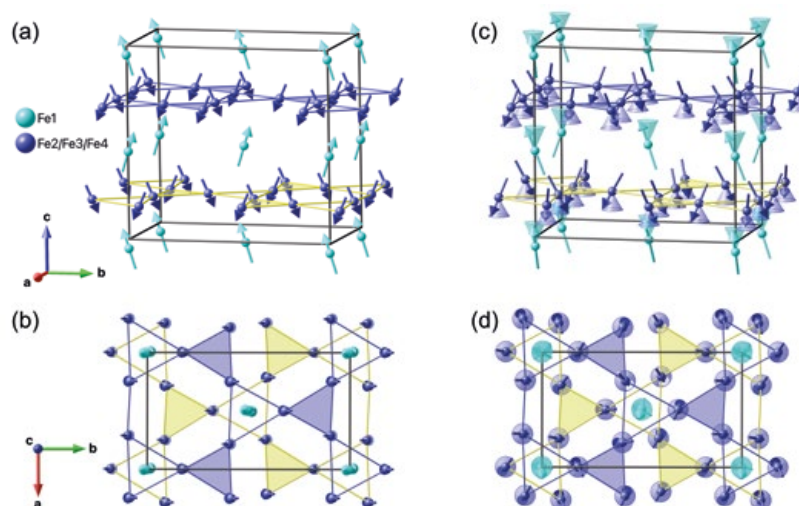


Figure 1: Magnetic structures at 220 K (left column) and 15 K (right column) in a perspective view (first row) and viewed along the c axis (second row). Yellow and blue bonds distinguish the Kagome planes at $z \sim 0.2$ and $z \sim 0.7$, while filled triangles emphasize the more isolated structure units between the vertically connected spin clusters shown by open triangles.

Study of exchange interactions in the single crystal of TbFeO₃ by inelastic neutron scattering

A. K. Ovsianikov¹, I. A. Zobkalo², A. Maity³, M. Meven^{1,4}, G. Roth¹

¹Institute of Crystallography, RWTH Aachen University, Aachen, Germany; ²Petersburg Nuclear Physics Institute by B. P. Konstantinov of NRC “Kurchatov Institute”, Gatchina, Russia; ³Heinz Maier-Leibnitz Zentrum (MLZ), Technical University of Munich, Garching, Germany; ⁴Jülich Centre for Neutron Science (JCNS) at MLZ, Forschungszentrum Jülich GmbH, Garching, Germany

Terbium orthoferrite, TbFeO₃, was studied using inelastic neutron scattering. The low temperature evolution of the energy gap was explored. The exchange parameters between the nearest neighbors for Fe³⁺ in TbFeO₃ were determined and discussed as a result of the energy balance between the Heisenberg exchange interactions, Dzyaloshinsky-Moriya interaction (DMI), anisotropy and external magnetic fields.

The rare earth orthoferrite family RFeO₃, where R is a rare earth element, demonstrates a remarkable variety of magnetic properties. Its compounds crystallize in an orthorhombic perovskite structure with the space group *Pnma*. At the Neel temperature which is typically in the range $T_N = 600 - 700$ K, the iron magnetic moments form a canted antiferromagnetic phase, where the DMI is responsible for the canting of the Fe-sublattice. With temperature decrease, the increasing exchange interaction between Fe³⁺ and R³⁺ ions leads to a rebalance of energies of the magnetic interactions, which causes spin reorientation transitions.

TbFeO₃: inelastic neutron scattering studies

High-energy excitations in a TbFeO₃ single crystal were studied on the thermal neutron spectrometer PUMA at the Heinz Maier-Leibnitz Zentrum (MLZ). Data collection was performed at temperatures corresponding to different magnetic phases: at the temperatures $T = 15$ K and $T = 5$ K, which correspond to the magnetic representations Γ_4^+ and Γ_2^+ of the Fe-sublattice, respectively. Before the measurements, the dispersion curves were simulated. This allowed us to choose the optimal scanning range in the experiment.

In TbFeO₃ the exchange interactions inside the Fe-sublattice determine the magnetic structure at temperatures above $T_{SR1} = 8.5$ K. The magnetic moments of iron lie within

the *ac* plane with a small canting around 0.15 μ B along the *b* direction. Below $T_{SR1} = 8.5$ K the Fe magnetic moments tend to align along the *b* direction. The intensities of inelastic neutron scattering obtained (Fig. 1) have been found to be almost unaffected by the decreasing temperatures, pointing to the unchanged character of exchange interactions between Fe ions. Thus, the exchange interaction between Fe and Tb ions J_{ij}^{Fe-Tb} is responsible for the spin reorientation transition. The full set of parameters of the exchange interactions in TbFeO₃ can be found in [1].

[1] A. K. Ovsianikov et al., *Inelastic neutron studies and diffraction in magnetic fields of TbFeO₃ and YbFeO₃*, *J. Magn. Mater.* 563, 170025 (2022)
DOI: 10.1016/j.jmmm.2022.170025

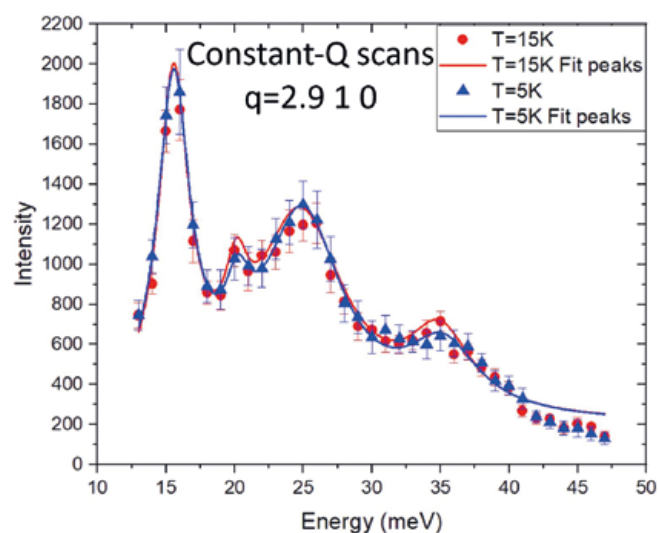


Figure 1: Typical inelastic neutron scattering scans on TbFeO₃, obtained at PUMA at $T = 15$ K and $T = 5$ K: measurement in “constant-*q*” mode.

Lithium intercalation mechanism in layered $\text{H}_2\text{V}_3\text{O}_8$ high-capacity cathode material for lithium-ion batteries

A. Kuhn¹, J. C. Pérez-Flores², J. Prado-Gonjal³, E. Morán³, M. Hoelzel⁴, V. Díez-Gómez⁵, I. Sobrados⁵, J. Sanz⁵, F. García-Alvarado¹

¹Fac. Farmacia, Dept. Química y Bioquímica, Univ. CEU San Pablo, Madrid, Spain; ²Renewable Energies Inst., Univ. Castilla-La Mancha, Albacete, Spain;

³Fac. Química, Dept. Inorg. Chemistry, Univ. Complutense, Madrid, Spain; ⁴Heinz Maier-Leibnitz Zentrum (MLZ), Technical University of Munich, Garching, Germany;

⁵Inst. Ciencia Materiales-CSIC, Madrid, Spain

A combination of synchrotron and neutron diffraction techniques made it possible to describe the crystal structures of both pristine and lithiated layered vanadium oxides, $\text{Li}_x\text{H}_2\text{V}_3\text{O}_8$ ($x = 0$ and 1). Additionally, DFT calculations and MAS-NMR spectroscopy helped to establish the role played by water in network stabilization. These results could explain the excellent electrochemical performance in rate capability and cycle life, shedding light on the Li^+ conduction pathways.

$\text{H}_2\text{V}_3\text{O}_8$ (HVO) is a promising high-capacity and high energy cathode material for lithium-ion batteries with a theoretical capacity of 378 mAh g^{-1} at an average voltage of 2.5 V resulting from a reversible two-electron transfer during the reversible lithium cycling processes (Fig. 1a). Although these excellent electrochemical lithium storage properties have been frequently reported in the literature, neither structural changes during the intercalation process nor the crystallographic positions occupied by the guest species have yet been published.

As an in-depth understanding of structural changes in cathode materials during Li intercalation is essential for cathode materials improvement, high-resolution synchrotron X-ray (SXR, *beamline BM25A, ESRF*) and neutron diffraction (NPD, *instrument SPODI, MLZ*) were applied to determine the crystal structures of $\text{Li}_x\text{H}_2\text{V}_3\text{O}_8$ ($x = 0$ and 1) samples. Thus, while NPD is advantageous in determining accurately

the positions of Li and H atoms, SXR has high sensitivity for V determination. Therefore, the complementary information given by NPD and SXR allowed for an exhaustive structural analysis of both samples. It has been found that hydrogen is located on one single-crystallographic site in a water-like arrangement, through which bent asymmetric hydrogen bonds across adjacent $\text{V}_3\text{O}_8^{2-}$ chains are established (Fig. 1b).

Increase in Li-mobility

DFT provided further evidence for the network stabilization by water whilst MAS-NMR spectroscopy revealed an increase in Li-ion mobility in the crystal host due to structural water. Based on NPD results, conduction pathways for Li ions were deduced from differential bond-valence mapping. The hydrogen bonds mitigate the volume expansion/contraction of vanadium layers during Li intercalation/deintercalation, resulting in an improved long-term structural stability (Fig. 1b). These structural studies explain the excellent performance in rate capability and cycle life for this cathode material and suggest that a rich variety of hydrated materials can be promising candidates for electrode applications [1].

[1] Kuhn et al., *Lithium Intercalation Mechanism and Critical Role of Structural Water in Layered $\text{H}_2\text{V}_3\text{O}_8$ High-Capacity Cathode Material for Lithium-Ion Batteries*, *Chem. Mater.* **34**, 694 (2022)

DOI: 10.1021/acs.chemmater.1c03283

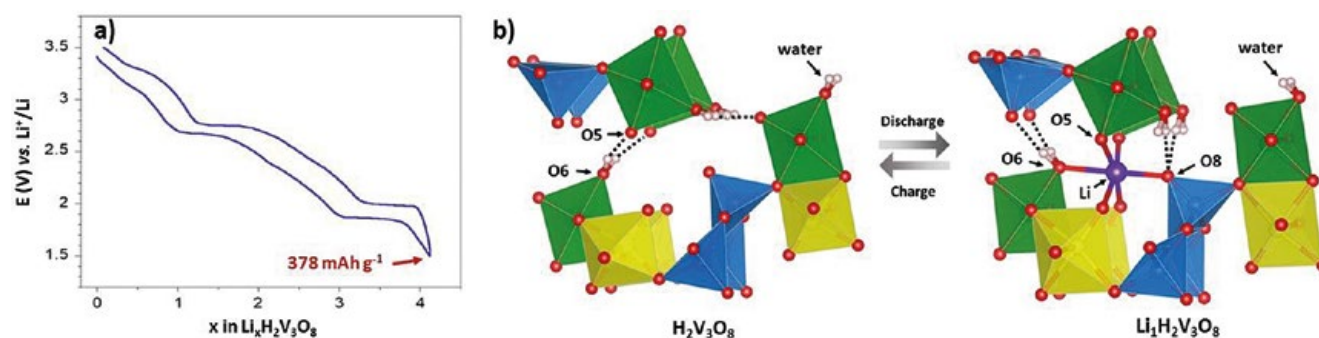


Figure 1: a) Electrochemical galvanostatic discharge-charge profile of a $\text{H}_2\text{V}_3\text{O}_8$ vs. Li cell at C/20 rate in the $3.75\text{--}1.50 \text{ V}$ range. b) Crystal structures of pristine and lithiated samples showing inter-slabs asymmetric hydrogen bonds (V1/V2-O_6 , yellow and green octahedra; V3-O_6 , blue square pyramids; H, white spheres; Li, purple sphere, respectively).

Spatially resolved diffraction study of the uniformity of a Li-ion pouch cell

D. R. Sørensen^{1,2}, M. Heere^{3,4}, A. Smith⁴, C. Schwab⁴, F. Sigel⁴, M. R. Vogel Jørgensen^{1,2}, V. Baran^{3,5}, A. Schökel⁵, M. Knapp⁴, H. Ehrenberg⁴, A. Senyshyn³

¹Department of Chemistry & iNANO, University of Aarhus, Aarhus C, Denmark; ²MAX IV Laboratory, Lund University, Lund, Sweden; ³Heinz Maier-Leibnitz Zentrum (MLZ), Technical University of Munich, Garching, Germany; ⁴Institute for Applied Materials (IAM), Karlsruhe Institute of Technology (KIT), Eggenstein-Leopoldshafen, Germany; ⁵Deutsches Elektronen Synchrotron (DESY), Hamburg, Germany

A Li-ion battery pouch cell is investigated using the combination of *in-operando* neutron powder diffraction (NPD) and spatially resolved powder X-ray diffraction (SR-PXRD). NPD allowed for extraction of the electrode structures as a function of state-of-charge (SOC). This was used to analyze the electrode homogeneity in the fully charged state as measured by SR-PXRD. The structural anode inhomogeneity was more pronounced than that of the cathode.

Understanding the lithiation inhomogeneity that is caused from charging Li-ion cells at high current rates is important to improve the performance of the battery. In this work, using neutron and X-ray powder diffraction together gave unique insights into how the electrode reactions proceed at different charging speeds.

Inhomogeneity in the electrode lithiation of Li-ion batteries is generally recognized to be detrimental to the long-term health of the battery. Importantly, it can result from fast charging of the battery. It is therefore important to investigate the conditions leading to inhomogeneity and the severity of it. Here, a Li-ion pouch cell was measured on using *in-operando* NPD conducted at SPODI, MLZ, while

the cell was rotated to average out geometrical effects. Patterns were obtained every 30 minutes during slow cycling and are shown in Fig. 1a alongside the voltage curve. Clear changes can be seen in the solid phases in the battery, which includes the $\text{LiNi}_{1/3}\text{Mn}_{1/3}\text{Co}_{1/3}\text{O}_2$ (NMC111) cathode and the graphite anode. Rietveld refinement of the patterns allowed for correlation of the electrode structures with the SOC.

Fast charging vs. slow charging

SR-PXRD was conducted on the cell in the fully charged state at P02.1, DESY. The measurement was performed both after fast (2C) and slow charging (C/2). A grid with 1 mm steps was set up and 10 s patterns were obtained at each grid point. Refinement of the patterns, aided by the NPD results, allowed for extracting the electrode lithiation at each grid point. The result is shown in Fig. 1b–e. Fast charging results in a significant degree of inhomogeneity in the anode where the center of the cell is more lithiated than the edges. The cathode is significantly more homogeneous. Slow charging still results in inhomogeneity in the anode, but the whole electrode participates more in the reaction and the center contains fewer spikes in lithiation. The cathode is now almost completely homogeneous. This shows that the anode is likely the electrode limiting fast charging.

[1] D. R. Sørensen et al., *Methods—Spatially Resolved Diffraction Study of the Uniformity of a Li-Ion Pouch Cell*, *J. Electrochem. Soc.* 169, 030518 (2022)
DOI: 10.1149/1945-7111/ac59f9

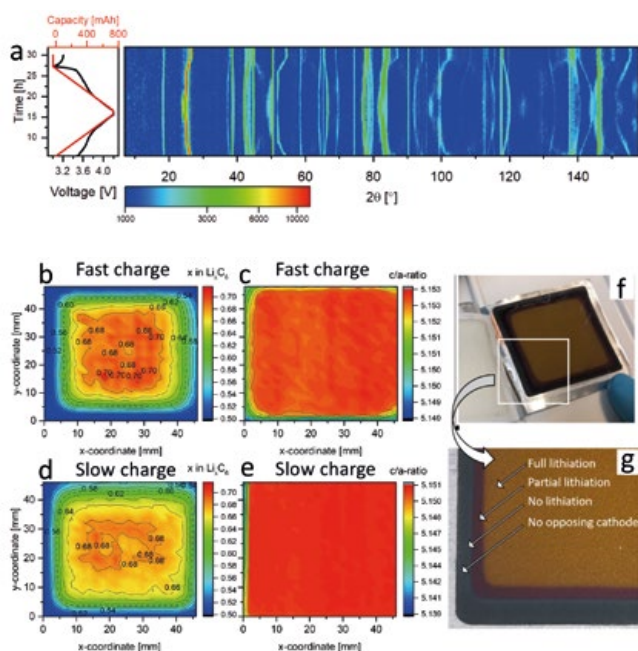


Figure 1: a) Stack of NPD patterns (log intensities in arbitrary units, $\lambda = 1.5482 \text{ \AA}$) collected during cell charge/discharge. The diffractograms are correlated with the charge/discharge curves on the left (voltage curves in black; capacity curves in red). b) Anode lithiation calculated as x in Li_xC_6 for the fast charge and (d) slow charge. Li_0C_6 is shown in a dotted line. (c) Cathode lithiation represented by the c/a -ratio of the NMC111 unit cell for the fast charge and (e) slow charge. (f) Photograph of an anode sheet in the opened pouch cell in the fully charged state. (g) Zoom-in on the corner of the anode sheet.

Energy landscape for Li-ion diffusion in the garnet-type solid electrolyte $\text{Li}_{6.5}\text{La}_3\text{Zr}_{1.5}\text{Nb}_{0.5}\text{O}_{12}$ (LLZO-Nb)

S. Strangmüller¹, M. Avdeev^{2,3}, V. Baran⁴, A. Kirchberger⁵, P. Walke⁵, T. Nilges⁵, A. Senyshyn¹

¹Research Neutron Source Heinz Maier-Leibnitz (FRM II), Technical University of Munich, Garching, Germany; ²Australian Centre for Neutron Scattering, Australian Nuclear Science and Technology Organisation, Sydney, Australia; ³School of Chemistry, University of Sydney, Sydney, Australia; ⁴Deutsches Elektronen-Synchrotron (DESY), Hamburg, Germany; ⁵Department of Chemistry, Synthesis and Characterization of Innovative Materials Group, Technical University of Munich, Garching, Germany

Solid electrolytes (SEs) feature promising properties, such as a high ionic conductivity, making them suitable for an application in next-generation batteries. Their detailed investigation is one of the key strategies to expand the understanding of corresponding structure-property-relationships which then allows for further tailoring of the materials properties. Therefore, further research on materials like garnet-type SEs is of great interest and relevance.

To obtain more detailed information on the diffusion mechanism within the well-known and commercially available material $\text{Li}_{6.5}\text{La}_3\text{Zr}_{1.5}\text{Nb}_{0.5}\text{O}_{12}$ (LLZO-Nb) on the atomic scale, we combined a series of characterization methods including powder X-ray and powder neutron diffraction (PXRD and PND) as well as temperature-dependent synchrotron powder diffraction experiments. Basic properties like the crystal structure and the thermal expansion of the material as well as the purity of the sample have been evaluated using PXRD and synchrotron data – collected at beamline P02.1 at the Deutsches Elektronen-Synchrotron (DESY). Furthermore, PND data – collected using the high-resolution powder diffractometer “ECHIDNA” at the Australian Centre for Neutron Scattering (Lucas Heights, Australia) – allowed for analysis and visualization of the energy landscape for Li-ion diffusion within LLZO-Nb. [1]

Visualization of Li-ion diffusion in LLZO-Nb using neutrons

In the material investigated, only lithium (in its natural isotope composition) possesses a negative scattering length, which limits the consideration to negative components of nuclear scattering density and is thereby beneficial in obtaining accurate information for the study of lithium diffusion pathways. The data evaluation was carried out by applying the maximum entropy method (MEM) as well as the one-particle potential (OPP) to the experimentally obtained negative nuclear densities, revealing three-dimensional diffusion pathways via face-sharing tetrahedral and octahedral sites featuring considerably low activation barriers between the partially occupied Li sites (Fig. 1).

According to this, further research is required to optimize the microstructure of membranes and bulk materials as the upper limit of the ionic conductivity of LLZO-Nb could be even higher than the so far highest reported values reported to date.

[1] S. Strangmüller et al., *Energy landscape for Li-ion diffusion in the garnet-type solid electrolyte $\text{Li}_{6.5}\text{La}_3\text{Zr}_{1.5}\text{Nb}_{0.5}\text{O}_{12}$ (LLZO-Nb)*, *Z. Naturforsch. B* 6, 453 (2022)

DOI: 10.1515/znb-2022-0068

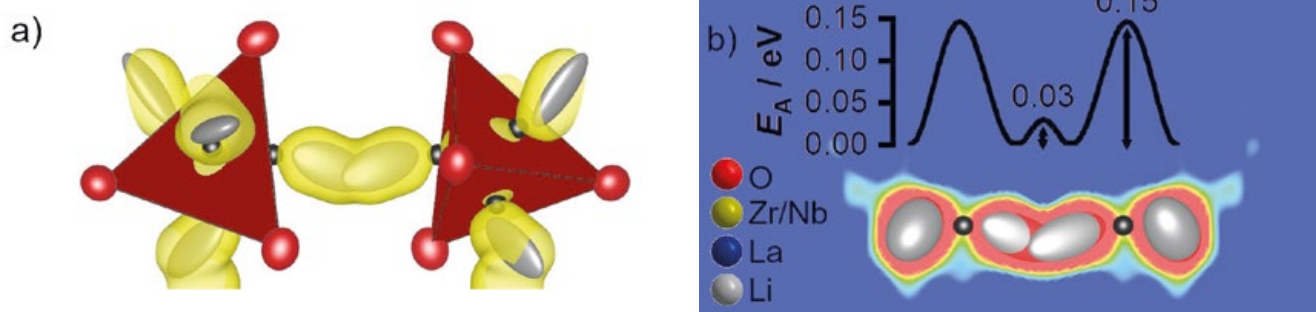


Figure 1: a) 3D negative nuclear density distribution along the sequence Li1–Li2–Li2–Li1 including intermediate positions (•) connecting neighboring sites Li1 and Li2, with LiO_4 -tetrahedra (red). b) Activation energy for Li-ion motion along the sequence Li1–Li2–Li2–Li1 within the 2D section cut of the OPP (red ≠ low, blue ≠ high) of LLZO-Nb. Zr/Nb, La, and Li atoms are drawn as red, olive, and gray ellipsoids, respectively.

Emission of fast neutron induced prompt gamma rays
from (n,n'), (n,p) and (n, α) reactions on CaCO₃N. Ophoven^{1,2}, Z. Ilic^{1,3}, E. Mauerhofer¹, T.H. Randriamalala¹, E. Vezhlev¹, C. Stieghorst⁴, Z. Révay⁴, T. Brückel^{1,3}, J. Jolie², E. Strub²¹Jülich Centre for Neutron Science (JCNS-2), Forschungszentrum Jülich GmbH, Jülich, Germany; ²Mathematisch-Naturwissenschaftliche Fakultät, Universität zu Köln, Köln, Germany; ³Lehrstuhl Für Experimentalphysik IVc, RWTH Aachen University, Aachen, Germany; ⁴Heinz-Maier-Leibnitz Zentrum (MLZ), Technical University of Munich, Garching, Germany

Within the framework of building up a comprehensive catalogue of (n,n' γ) reactions required for non-destructive elemental analysis, prompt gamma radiation emitted in fast-neutron-induced reactions by irradiation of a CaCO₃ sample with a beam of fission neutrons was measured using an upgraded version of the FaNGaS instrument. The relative intensities and fast neutron spectrum averaged partial gamma-ray production cross sections of 38 identified gamma rays as well as detection limits are presented.

Prompt gamma rays induced by fast neutron reactions on CaCO₃ were investigated via a new version of FaNGaS [1]. The shielding of the HPGe detector (50% relative efficiency and 2.1 keV energy resolution at 1.33 MeV) was upgraded for further reduction of the beam background and to facilitate access to the electromechanically cooled detector. Additionally, due to a new multi-leaf collimator at the MEDAPP facility, the distance between the sample and the neutron source (uranium converter plate) was increased, leading to a reduction of 20% in the fast neutron flux at the irradiation position compared to the previous geometry ($1.13 \times 10^8 \text{ cm}^{-2} \text{ s}^{-1}$ vs. $1.40 \times 10^8 \text{ cm}^{-2} \text{ s}^{-1}$). The distance between the sample and the detector is kept unchanged at 67 cm. The measurement was performed at an angle of 90° between the neutron beam direction and the detector. The sample was tilted by an angle of 45° with respect to the neutron beam axis.

Fast neutron reactions on CaCO₃

A total of 38 prompt gamma lines were detected. Of these, 20 gamma lines were assigned to the ⁴⁰Ca(n,p)⁴⁰K reaction, 15 lines to (n,n' γ) reactions (12 in Ca, 1 in C and 2 in O) and another 3 to the ⁴⁰Ca(n, α)³⁷Ar reaction. Relative intensities (using the 3905-keV line of ⁴⁰Ca and the 1982-keV line of ¹⁸O as reference), fast neutron spectrum averaged cross sections and elemental detection limits were determined. Compared to the work of Demidov et al., 6 new lines of Ca were observed due to improved detector resolution and different shape of the fast neutron spectrum (fission spectrum with an average neutron energy $E_n = 2.3 \text{ MeV}$ in our case vs. reactor-based spectrum with $E_n = 0.6 \text{ MeV}$). The relative intensities of the prompt gamma lines measured in our work agree well (1.2 σ level) with the values listed in the Demidov Atlas (see Fig. 1). For a counting time of 12 hours the derived detection limits of Ca, C and O are 5, 13 and 64 mg, respectively.

This work shows that FaNGaS is particularly well suited to the determination of C and O in samples of various origins.

[1] N. Ophoven et al., *Fast neutron induced gamma rays from (n,n'), (n,p) and (n, α) reactions on CaCO₃*, *J. Radioanal. Nucl. Chem.* 331, 5729 (2022)
DOI: 10.1007/s10967-022-08594-6

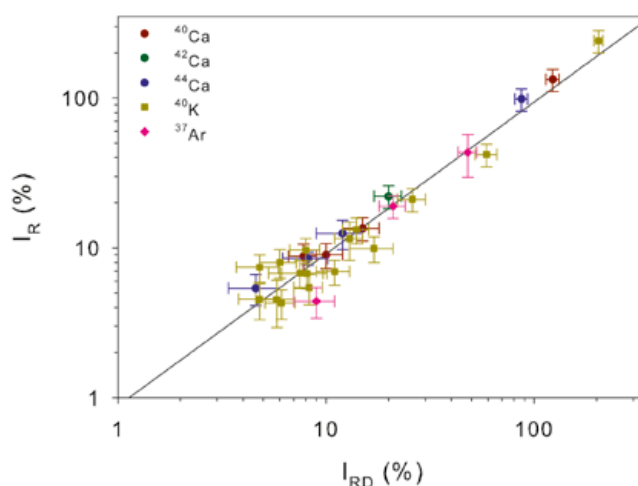


Figure 1: Relationship between relative intensities I_R of the prompt gamma rays induced by (n,n'), (n,p) or (n, α) reactions on calcium measured in this work and the relative intensities I_{RD} tabulated in the Demidov Atlas (Demidov et al., Atlas of Gamma-ray Spectra from the Inelastic Scattering of Reactor Fast Neutrons, Moscow, Atomizdat, 1978). The solid line represents the fit of the data with $I_R = a \times (I_{RD})^b$, $a = 0.88 \pm 0.13$ and $b = 1.01 \pm 0.05$.

Classical modeling of positronium cooling in silicon nanochannel plates

F. Guatieri^{1,2,3}, S. Mariuzzi^{1,2}, C. Hugenschmidt³, R. S. Brusa^{1,2}

¹Department of Physics, University of Trento, Trento, Italy; ²TIFPA/INFN, Trento, Italy; ³Heinz Maier-Leibnitz Zentrum (MLZ), Technical University of Munich, Garching, Germany

Silicon nanochannel plates (NCPs) are nanostructured devices capable of converting positrons (e^+) into cold positronium (Ps) and are employed in a variety of experiments. We were able to formulate the first Monte Carlo model of Ps cooling in NCPs capable of quantitatively estimating crucial characteristics of the NCP operation, such as cooling time, angular distribution of emitted Ps, and the fraction of Ps that annihilates into three gamma quanta.

Silicon NCPs are nanostructures obtained by electrochemically etching silicon single crystals to create a forest of hollow channels with lengths of 1 to 2 microns and diameters in the order of 10 nanometers. Positrons implanted into NCPs tend to form hot Ps in the channels and these are then forced by the structure to interact with the silicon before being emitted into vacuum. This interaction reduces the Ps temperature, allowing the production of cold Ps that can be used in spectroscopy experiments operated at NEPOMUC.

Although qualitative descriptions of Ps production and cooling had been presented in the past, a quantitative simulation of the process was still missing. We built upon the geometric model we had used in the past to simulate implantation of positrons into NCPs [1] and formulated an effective scattering model of the Ps atoms into the nanoscopic channels. We treated Ps atoms as classical point particles, which is an approximation that, given the size of the nanochannels, is expected to hold up until cryogenic temperatures are reached. The exact interaction dynamics of a Ps atom with the walls of a nanochannel are too complex to be derived *ab initio*; nonetheless our simulations showed that the Ps emission angle depends mostly on the angular cross section of such a process. Consequently, we were able to use emission angle measurements to formulate an effective angular cross section for the scattering of a Ps atom with the channel walls.

We have used our model to predict parameters that can be experimentally measured and validated against the literature. Predictions obtained from the model closely match the behavior of NCPs at room temperature, while they fail to correctly describe cryogenically cooled NCPs. This is an indication that, as the De Broglie wavelength of Ps atoms becomes comparable with the channel diameter, a transition to a cooling regime where quantum effects play a major role takes place, a fact that was predicted in 2010 by Mariuzzi but not yet observed experimentally.

[1] F. Guatieri et al., *Classical modeling of positronium cooling in silicon nanochannel plates*, *Phys. Rev. B* **106**, 035418 (2022)

DOI: [10.1103/PhysRevB.106.035418](https://doi.org/10.1103/PhysRevB.106.035418)

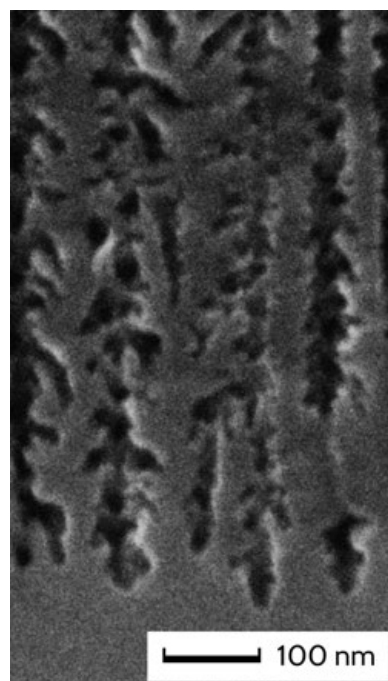


Figure 1: Section SEM imaging of an NCP converter section showing the irregular shape of the channel walls. This irregularity is one of the main factors contributing to the impossibility of formulating from theory alone a scattering model for Ps atoms against the channel walls.

New polarized neutron diffraction setup on POLI for precise high-field investigations up to 8 T

V. Hutanu^{1,2}, H. Thoma^{1,2}, H. Deng^{1,2}, J. Xu^{1,2}, G. Brandl², A. Weber², V. Rubanskyi², J. Peters³,
W. Luberstetter^{1,2}, T. Krist⁴, G. Roth¹, L. Peters¹, T. Brückel⁵, S. Mattauach²

¹Institute of Crystallography, RWTH Aachen University, Aachen, Germany; ²Jülich Centre for Neutron Science (JCNS) at MLZ, Forschungszentrum Jülich GmbH, Garching, Germany; ³Heinz Maier-Leibnitz Zentrum (MLZ), Technical University of Munich, Garching, Germany; ⁴NOB Nano Optics Berlin GmbH, Berlin, Germany; ⁵Jülich Centre for Neutron Science (JCNS) and Peter Grünberg Institut (PGI) (JCNS-2/PGI-4), Forschungszentrum Jülich GmbH, Jülich, Germany

Magnetic field is an important parameter for studying modern research topics. A new setup consisting of a strong superconducting magnet and a bender polarizer has been implemented on the hot neutron single crystal diffractometer POLI. It facilitates high-field measurements with polarized/unpolarized neutrons and features low stray fields, large vertical-horizontal access, and a wide sample space suitable for multiparameter studies.

Polarized neutron diffraction (PND) is a powerful tool for studying condensed matter physics and to probe the spin and orbital properties of unpaired electrons. It makes it possible to unambiguously determine complex magnetic correlations and small ordered moments, separate magnetic and nuclear contributions, and study spin-orbital entangled states by mapping out the magnetization density at the unit cell level. The single crystal diffractometer POLI, built on the hot source of the MLZ, is particularly dedicated to these polarized neutron measurements and can additionally host bulky sample environments.

New setup for high magnetic field investigations

We recently implemented a new actively shielded asymmetric split-coil superconducting magnet with a maximal field of 8 T. The magnet is designed to facilitate the single crystal diffraction with polarized/unpolarized neutrons and has very low stray fields (25 Oe at one meter away from

the magnet's center). A large opening ($-5-25^\circ$ vertical and 300° horizontal) and a large sample space allow one to use area detectors and complex sample environments, e.g., electric fields and pressure cells. Very recently, a dilution refrigerator insert has been successfully tested on the magnet, reaching the base temperature of 50 mK.

Although the new magnet is actively shielded, reducing the stray field by an order of magnitude compared to the classical design, its fringe field gradients are still too large to be used with the sensitive ^3He polarizer of the previous setup. To overcome this issue, a new large beam size cross section ($130 \times 42 \text{ mm}^2$) solid-state supermirror bender polarizer has been developed (Fig. 1). The bender polarizer consists of Si wafers coated with $m=3$ Fe/Si supermirrors and strong NdFeB-type permanent magnets. The bending radius is optimized for the short wavelengths used on POLI. A high neutron polarization above 99% could be confirmed for the magnet's complete field range. The optimized transmissions for the desired spin component are about 18.2% for 1.15 \AA and about 15.5% for 0.9 \AA .

[1] V. Hutanu et al., *New Polarized Neutron Diffraction Setup for Precise High-Field Investigations of Magnetic Structures up to 8 T at MLZ*, *IEEE Transactions on Magnetics*, 58(2), 1 (2022).

DOI: [10.1109/TMAG.2021.3082260](https://doi.org/10.1109/TMAG.2021.3082260)

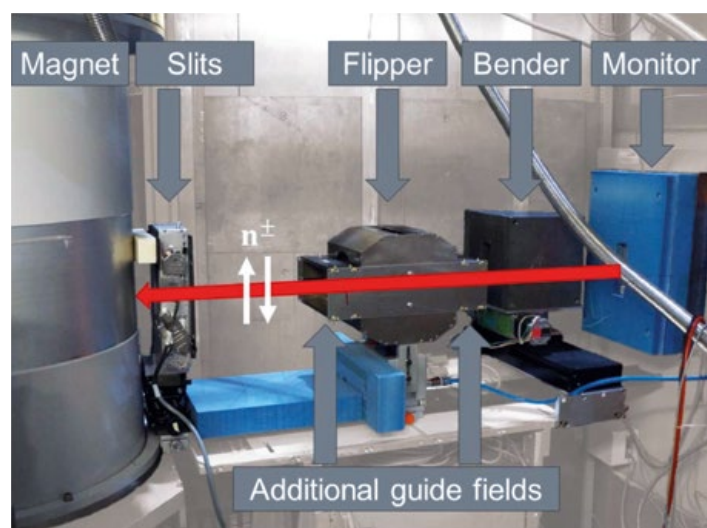


Figure 1: Components of the new PND setup on POLI along the incoming neutron path.

Extending MIEZE spectroscopy towards thermal wavelengths

J. K. Jochum^{1,2}, C. Franz³, T. Keller⁴, C. Pfeleiderer^{2,5}

¹Heinz Maier-Leibnitz Zentrum (MLZ), Technical University of Munich, Garching, Germany; ²Physics Department E51, Technical University of Munich, Garching, Germany; ³Jülich Centre for Neutron Science (JCNS), Forschungszentrum Jülich GmbH, Garching, Germany; ⁴Max Planck Institute for Solid State Research, Stuttgart, Germany; ⁵Centre for Quantum Engineering (ZQE), Technical University of Munich, Garching, Germany

MIEZE spectroscopy is a spin-echo technique ideally suited for the investigation of magnetic phenomena. Operating MIEZE with wavelengths down to 2 Å would extend the dynamic range to an energy resolution of 6.58 μeV at momentum transfers of 3 Å⁻¹ and energy transfers up to 20.5 meV which are required for the investigation of new unusual ground states without long-range order.

Recent advances in neutron instrumentation have been motivated by a need for the highest energy resolution over a wide range of momentum transfers to investigate new and exotic ground states without long-range order or well defined excitations, such as for example quantum spin liquids. One line of development has been towards multi-analyzer spectrometers, such as the CAMEA spectrometer, which has recently gone into user operation at the Paul Scherrer Institute.

Here, we suggest an extension of the MIEZE technique towards shorter wavelengths that will increase the accessible energy and momentum transfers at the spectrometer RESEDA, towards 20.5 meV and 3 Å⁻¹ respectively.

TIGER – Thermal mieze for GrEater Ranges

The implementation of TIGER at RESEDA will require the installation of an additional polarizer, analyzer and velocity selector as well as translation systems for automated

switching between the velocity selectors and polarizers for thermal and cold neutrons. The components of RESEDA that would be upgraded in TIGER are highlighted in light red in Fig. 1.

An additional thermal velocity selector with a transmission of 91%, a screw angle $\alpha = 15.5^\circ$, a blade height of 60 mm, 144 blades and a maximum rotation speed of 21 000 rev min⁻¹ will ensure operation down to $\lambda = 2$ Å.

Similarly to the current polarizer at RESEDA, a polarizing cavity consisting of two parallel channels, each with two V cavities in series and a total length of 2040 mm and a wavelength range from 1.8 to 7.9 Å would be used for neutron polarization. As a neutron polarization analyzer device, a Fe/Si $m = 5$ transmission bender with integrated 80' collimator would be best suited.

As RESEDA offers several modes of operation (NRSE, MIEZE, MIEZE-SANS), the integration of TIGER should be such that an easy change between the different instrumental configurations is guaranteed, including a system that permits switching automatically between the different selectors and different polarizing cavities.

[1] J.K. Jochum et al., *Extending MIEZE spectroscopy towards thermal wavelengths*, *J. Appl. Cryst.* 55, 1424 (2022)
DOI: 10.1107/S1600576722009505

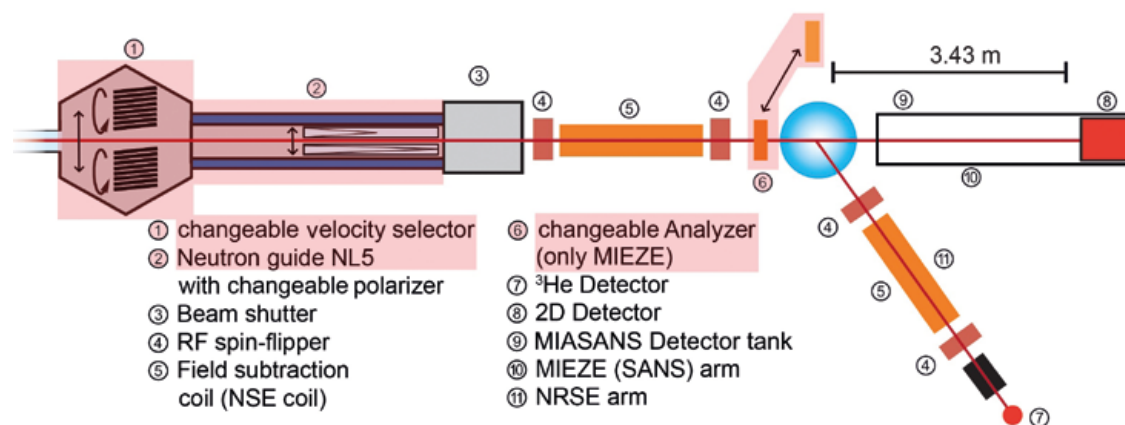


Figure 1: Schematic of the proposed setup for thermal neutrons (TIGER) at the beamline RESEDA. Components of RESEDA to be upgraded in TIGER are highlighted in light red.

Design of a neutron polarizing bender for a new cold triple-axis spectrometer

J. Xu¹, M. Atterving¹, M. Skoulatos¹, A. Ostermann¹, R. Georgii¹, T. Keller^{2,3}, P. Böni⁴

¹Heinz Maier-Leibnitz Zentrum (MLZ), Technical University of Munich, Garching, Germany; ²Max Planck Institute for Solid State Research, Stuttgart, Germany; ³Max Planck Society Outstation at MLZ, Garching, Germany; ⁴Physik-Department E21, Technical University of Munich, Garching, Germany

Now that the instrument FLEXX has been transferred from the HZB to the MLZ, it will be combined with the instrument MIRA to make up LaDiff, a cold triple-axis spectrometer with Larmor diffraction capabilities. To adapt LaDiff to its new beamport, we designed and optimized a solid-state reflection-type C-bender polarizer that can be placed after the monochromator inside the radiation shielding, using Monte Carlo ray tracing simulations.

Polarized neutron scattering is a powerful tool for studying the physics related to magnetism and superconductivity. Many neutron triple-axis spectrometers have the option of using polarized neutrons. The cold neutron triple-axis spectrometer FLEXX at HZB has been transferred to the MLZ where it will require a new neutron polarizer. We designed a solid-state polarizing bender with Monte Carlo ray tracing simulations.

A solid-state bender polarizer consists of stacks of thin Si wafers coated with polarizing supermirrors (SMs). The wafer stacks are bent into a C or S shape to avoid neutrons being transmitted without interactions with the SMs. A reflection-type bender [Fig. 1(a)] has wafers with SMs on both sides and absorbing layers on the top, allowing only spin-up neutrons to be reflected by the SMs and transported through the curved Si wafer. In a transmission-type bender [Fig. 1(b)], the absorbing layers are omitted, such that at

the exit both the reflected spin-up and the transmitted spin-down neutrons are present. The spin-up neutrons are deviated by the curvature and are absorbed in a subsequent collimator. In general, a reflection-type bender delivers better performance but has the disadvantage of deflecting the neutron beam and often increasing its divergence.

Our numerical exploration and optimization

We undertook a comprehensive study among several popular polarizer models using simulations and optimized the parameters (the wafer thickness, the SM reflection critical angle, the bending curvature, and the collimation) to achieve the most promising reflection- and transmission-type C-benders. We proposed an improved transmission-type C-bender [Fig. 1(c)] which shows a performance as good as the reflection type bender [Fig. 1(d)-(f)]. The new design can be realized by using two remanent polarizing collimators (reflecting only spin-down neutrons) in front of and behind a bender. However, for practical and technical reasons, we decided to use the optimized reflection-type C-bender.

[1] J. Xu et al., *Design of a Neutron Polarizing Bender for a Cold Triple-Axis Spectrometer, Nuclear Instruments and Methods in Physics Research Section A: Accelerators, Spectrometers, Detectors and Associated Equipment 1031, 166526 (2022)*

DOI: 10.1016/j.nima.2022.166526

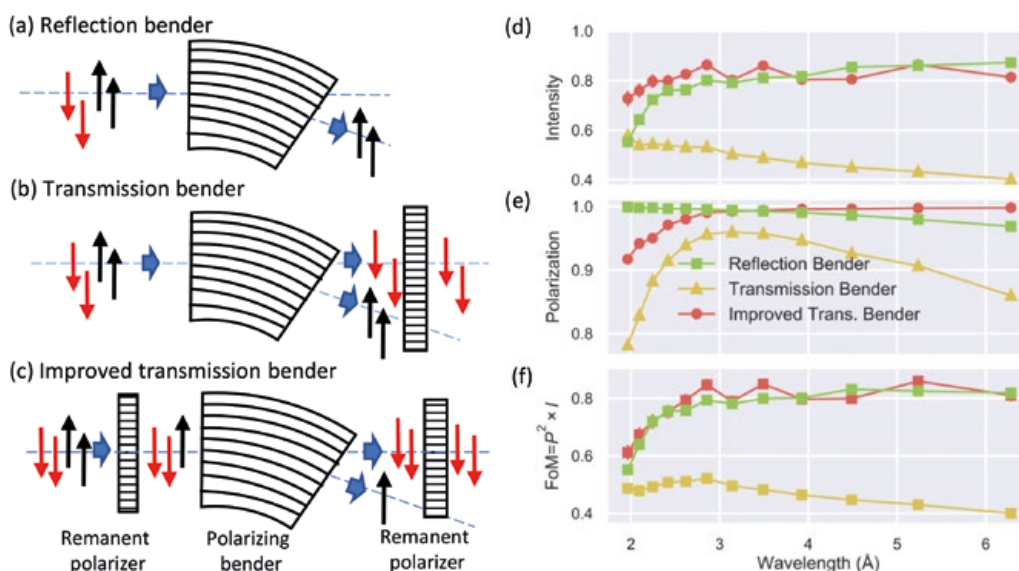


Figure 1: (a)-(c): Schematic plots for the reflection bender, the transmission bender, and the improved transmission bender. (d)-(f): Simulated intensity, polarization, and figure-of-merit (FoM) at the sample positions for three types of polarizers over the desired wavelength band.



9

News from the instruments



News from the instruments

W. Lohstroh¹, S. Mattauch², C. Hugenschmidt¹, T. Schrader², A. Ostermann¹, D. Gorkov^{1,3}, J. Jochum¹,
A. Schneidewind², Z. Revay¹, M. Hofmann¹, A. Radulescu², C. Hauf¹, M. Skoulatos¹, M. Schulz¹

¹Heinz Maier-Leibnitz Zentrum (MLZ), Technical University of Munich, Garching, Germany; ²Jülich Centre for Neutron Science (JCNS) at MLZ, Forschungszentrum Jülich GmbH, Garching, Germany; ³II. Physikalisches Institut, Universität zu Köln, Köln, Germany

During the time without neutrons, we have been busy upgrading and further improving the capabilities at the instruments in user service. Moreover, instrument assembly in the guide hall east is well underway and the two instruments that were transferred from Berlin arrived in Garching.

New options and higher efficiency at the instruments

Some of the instruments that are already in routine user operation underwent major upgrades. For RESEDA, 2022 was marked by the MIASANS project, which focused on the optimization of RESEDA for small angle MIEZE. At the beginning of the year, the new superconducting coils were installed, which provide fields up to 300 mT and can support spin flips with up to 8 MHz, thus pushing the maximum achievable Fourier time of RESEDA beyond 100 ns. We are looking forward to first tests with neutrons! In December, we also took a last look at the old flight tube of RESEDA, and disassembled it to make space for the new SANS tank that will arrive early in 2023. The new detector tank will offer increased flexibility in the available Q-ranges and an improved Q-resolution.

At BIODIFF, the former manual collimator positioning unit was replaced by a hexapod. This allows for quick and automated adjustment of the collimation unit using the direct neutron beam and, with that, increased efficiency during operation of the instrument. Switching between different

aperture setups is easy via a cassette insert. In addition, a new cryo-insert was designed and manufactured to fit into the detector chamber of BIODIFF. The new precise 1-circle goniometer in combination with a mini-kappa goniometer allows for efficient data collection in combination with an N₂-cryo-stream. The new installation makes it possible to go beyond the so-called step-scan measurements and to move the omega-axis pseudo-continuously (micro-stepping) while the shutter is open. With that, we expect to reach an enhanced resolution for measuring the integral intensity of the Bragg peaks.

The instrument KOMPASS is getting ready for hot commissioning of the analyzer. The first science in diffraction mode had already been successfully demonstrated and now the triple axis mode is also ready for operation with neutrons. In the secondary part of the spectrometer, either a horizontal V-cavity or a Heusler unit can be used for polarization analysis. The analyzer unit was further improved as regards the shielding and the reliability when being remounted. To guide the neutron polarization at the sample, a set of Helmholtz coils is presently operational and a CRYOPAD device is awaiting installation. The cold triple axis instrument PANDA received its multiplexed analyzer option BAMBUS which has been successfully constructed and installed in Garching and is now ready to be tested. As an alternative option to the traditional single analyzer setup, BAMBUS offers 20 channels of 2° each, so that a total of 40° angular coverage can be measured simultaneously for five final energies, respectively.

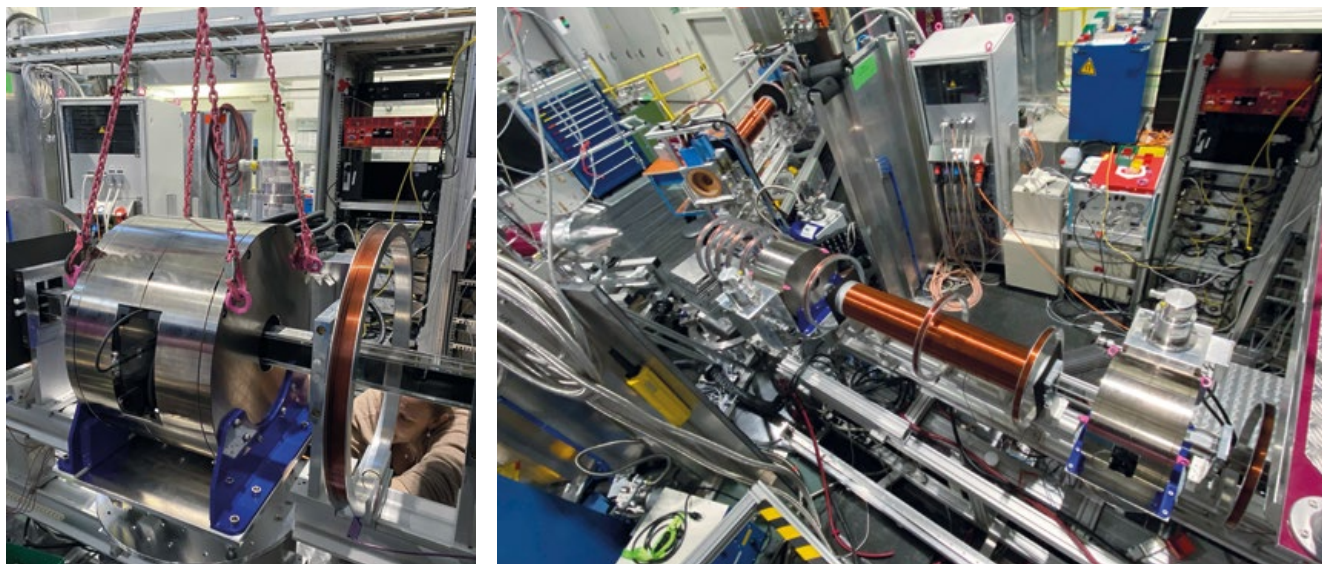


Figure 1: Installation of the new superconducting coils and the instrument RESEDA.

Switching between the two secondary spectrometer options will take less than one hour. A new ^3He laser pumped polarizer and analyzer has been developed for POLI. The goal is to produce two optimized, very compact devices incorporating a ^3He cell, furnace, AFP coil, the magnetic cavity, and a laser with a mirror system. The device is expected to be installed at the instrument at the beginning of 2023.

Upgrades at the small angle instruments include new measuring modes at KWS-3, which were developed to further improve the measurement data resolution achieved. The technical realization took place in 2022 and a second, optional sample position was installed at the instrument. With this upgrade, the available Q-range of the new second sample location is now $0.0006\dots 0.012 \text{ \AA}^{-1}$. MARIA will see a rebuild of its neutron guide, albeit involuntarily, due to an implosion caused by aging. To prevent similar scenarios in future, those parts of the neutron guide that have to hold the vacuum themselves, due to geometrical constraints, will be manufactured according to a new design out of an aluminum-glass-sandwich construction. At the flipper position, this solution is not possible, and therefore a vacuum housing around the neutron guide is going to be designed and will additionally lead to enhanced performance over the “original construction” of the flipper itself.

The PGAA instrument has been continuously modernized. The instrument is now equipped with four HPGe detectors and four scintillator annuli for Compton suppression. The standard arrangement of these detectors is the following: a large (60-%) detector and the planar low-energy (LEGe) detector are placed on the two sides of the sample to collect the prompt gamma radiation. A second, 30-% detector can be used for gamma-gamma coincidence measurements, or placed on the top of the detector shielding to serve as the decay counting station of the short-cyclic in-beam activation

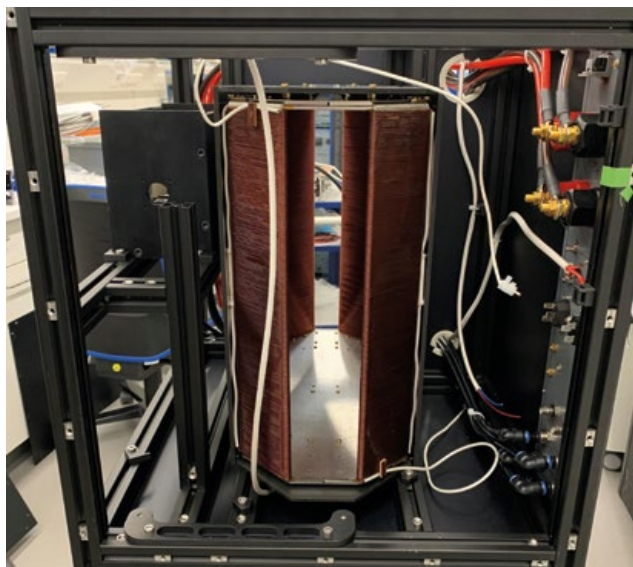


Figure 2: The new ^3He modules for polarization analysis at POLI.

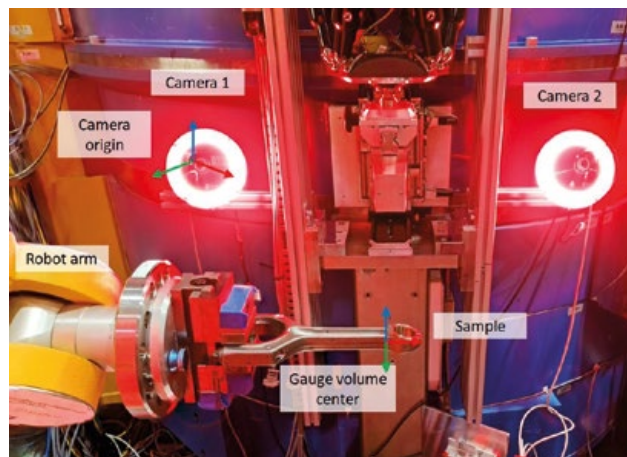


Figure 3: The new optical positioning system for the robot at STRESS-SPEC.

analysis setup. The fourth detector is located in the low-background counting chamber to measure the activated samples after irradiation. All digital spectrometers were upgraded to be the most up-to-date, based on 64k ADC-s, facilitating the acquisition of two 32k gamma-ray spectra. This feature allows for the parallel acquisition of Compton-suppressed and unsuppressed spectra simultaneously, without the need for any special-signal shaping and timing electronic units. The Neutron Depth Profiling setup has been developed within the framework of a BMBF project. The thin silicon detectors offer a uniquely low spectral background and permit the deepest possible profiling of lithium or boron atoms. The target chamber allows measurements of lithium-ion batteries operando using a potentiostat. A new 2-D detector under test facilitates mapping over a surface.

The neutron strain scanner STRESS-SPEC was one of the first neutron diffractometers at which an industrial robot for sample handling and positioning was used. However, industrial robots are still limited in their use due to insufficient absolute positioning accuracies of up to $\pm 0.5 \text{ mm}$ in some cases. Usually, an absolute positioning accuracy of 10% of the smallest gauge volume size – which in the case of modern neutron diffractometers is in the order of $1 \times 1 \times 1 \text{ mm}^3$ – is necessary to allow accurate strain tensor determination and correct centering of local texture measurements. In 2022, the original robot setup at the neutron diffractometer STRESS-SPEC has therefore been upgraded to a high accuracy positioning/metrology system. To achieve a spatial accuracy better than $50 \text{ }\mu\text{m}$ during measurement of the full strain tensor, the sample position is tracked continuously by an optical metrology system, and the position actively corrected. Together with two newly designed radial collimators that create more space in the sample environment area, the residual stress analysis capabilities for large complex parts is further enhanced. In addition, a newly designed laser furnace can be mounted at the robot flange to conduct, for example, texture measurements at elevated temperatures of up to 1300°C .

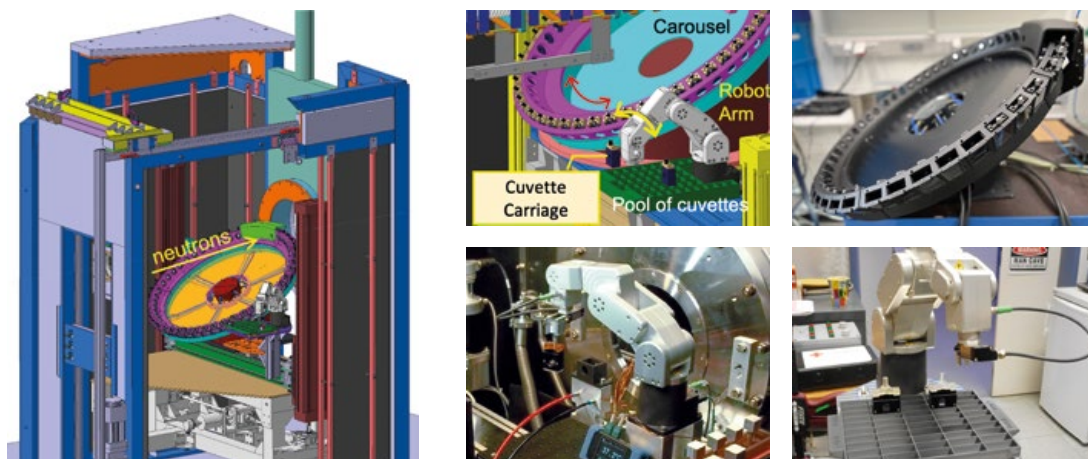


Figure 4: Schematic presentation of the new sample positioning system at KWS-2 for continuous supply of samples to the instrument (left and top middle), the cuvette carousel during the commissioning phase at JCNS (top, right), the robot arm during the tests at KWS-2 (bottom, middle) and with the pool of cuvettes (bottom, right).

New sample environment options

KWS-2 also goes 'robotics' with its new 48-fold sample changer. The instrument, with its high intensity and extended momentum transfer, is dedicated to the study of mesoscopic structures and structural changes during fast kinetic processes in soft condensed matter, chemistry and biology. Typically, a large number of samples are measured during short experiments at this high-throughput instrument. A new versatile in-beam sample positioning system, which includes a multi-position carousel (48 positions) with sample temperature control between 5°C and 85°C (allowing different temperatures for cuvette groups), robotic elements, and a pool of sample cuvettes (50 positions), is currently being installed at the sample position. This allows the instrument to be continuously supplied with samples while minimizing sources of error through fully automated sample changing and positioning, and the ability to pool experiments from different user teams when similar experimental conditions are required. The new compact setup is intended to remain installed at the sample position as the default option and to be in operation for all routine experiments, i.e. about 80% of the beam time at KWS-2. For the remaining experiments, that require more specialized sample environments such as rheometers, stop-flow or humidity chambers, easy removal and precise repositioning by a zero-point clamping system allows for a smooth change of options.

A couple of new sample environment possibilities have been introduced into the suite. For the JCNS small angle instruments (SANS/VSANS), a new high pressure stopped flow setup has been put into operation that makes it possible to follow the kinetics of a reaction after the fast mixture of two liquids under pressure. Current parameters of the new device are a pressure range below 600 bar, mixing time above 100 msec and mixing volume above 0.3 ml. Two additional options of the new sample environment will be proposed to users: (1) simple pressure cell an easy means of sample filling; (2) investigation of the fast temperature jump kinetics under pressure.

At TOFTOF, a fibre optic based Raman spectrometer (Horiba iHR 320, 784 nm @ 80 mW on sample) has been commissioned to permit secondary characterization of the samples. As a form of vibrational spectroscopy it is sensitive to chemical groups and their local environment, and can therefore be used to monitor chemical reactions and understand the packing of molecules, such as lipids in bilayers, and the folding of polymers such as proteins, and will yield complementary information on sample status during the neutron spectroscopy measurements. Any self or substrate supported sample may be measured. Additionally, a temperature controlled optical cell (quartz windows) allows Raman spectra from powders, liquid, solutions or gels in a temperature range of -20 to 100°C to be measured. This is being complemented by a cell which allows a sample to be subjected to a controlled composition vapor (e.g. D₂O, H₂O, D/H-ethanol etc.) and temperature.

New additions to the instrument suite – Arrival in Garching

Our two new additions to the instrument suite at the MLZ, namely the instruments FLEXX/LADIFF and FIREPOD, that had been dismantled at the Helmholtz-Zentrum Berlin (HZB), finally arrived in Garching in the autumn of 2022.



Figure 5: The instruments FLEXX/LADIFF and FIREPOD arrive in Garching after they had been dismantled in Berlin and packed into containers.

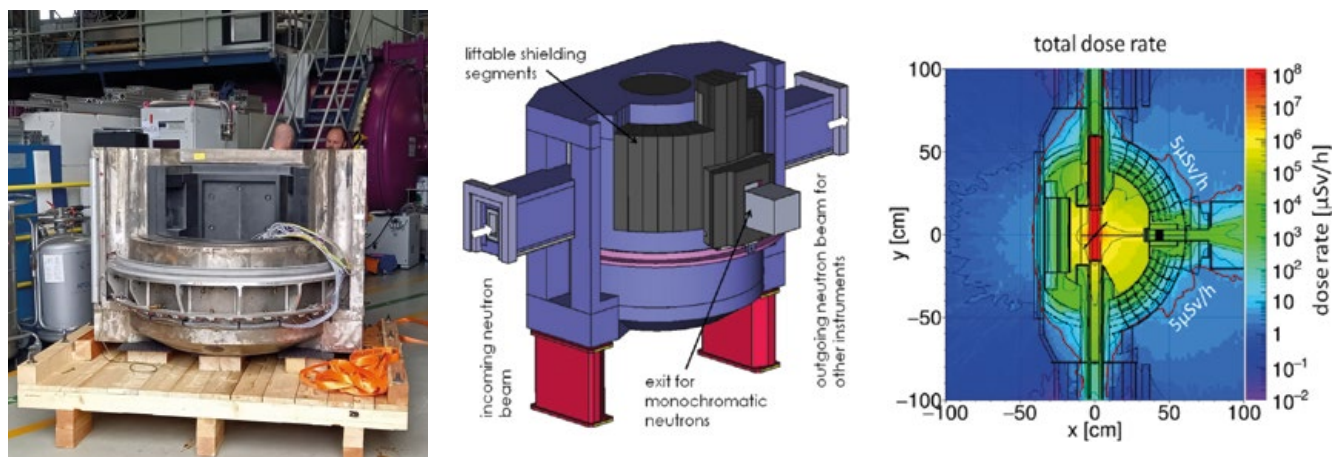


Figure 6: Left: FLEXX monochromator shielding as received from Berlin, middle: drawing of the FLEXX shielding, to be upgraded and used on LaDiff. Right: Total dose rate distribution (sum of neutron and γ -radiation) around the upgraded monochromator shielding of LaDiff, to be used at its new position at the FRM-II.

Now, we are busy unpacking the containers, and instrument assembly and the integration into the experimental hall (FIREPOD) and the neutron guide hall west (FLEXX/LADIFF), respectively, has started. In the meantime, we have also been busy preparing the concepts for the new biological shielding to adapt for the higher flux at the MLZ, and we will see the technical realization in 2023. This applies not only to the shielding of LADIFF, but also to the beam port SR8, which will see a complete rebuild to allow for the parallel operation of the powder diffraction suite consisting of SPODI, ERWIN/RESI and FIREPOD.

Moreover, the instrument assembly in the guide hall east is ongoing. For example, the steel structure for POWTEX, that will carry the neutron shielding housing, the detector chamber with the sample position and the chopper cascade have been placed and aligned to their final position. TOPAS has its chopper cascade positioned and the detector bench in the detector chamber structure installed. Similarly, detector integration at the instrument SAPHIR began, and the magnetic feedback structure for PERC began to emerge.

In addition, the first part of the positron instrument suite from NEPOMUC was transferred into the east hall, i.e. the

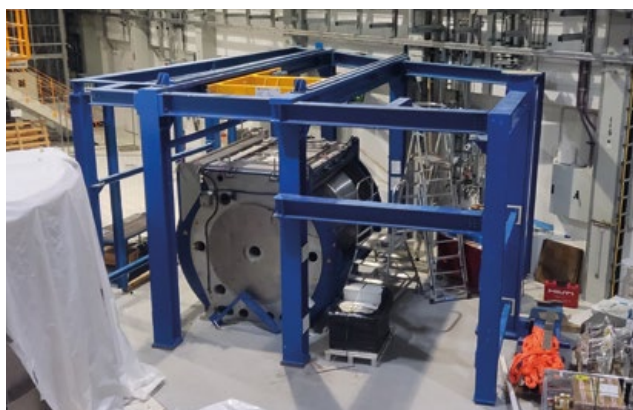


Figure 7: The sample chamber and the steel structure for the shielding house of POWTEX at its final position in the guide hall east.

positron annihilation induced Auger Electron Spectrometer (PAES), thus vacating the space in the experimental hall which is needed to install the neutron guides that will feed into the guide hall east. Design of the new positron beamline to eventually connect the positron instrumentation in the new, dedicated enclosed space in the guide hall east is well underway. In the meantime, even without neutrons, the Coincidence Doppler Broadening Spectrometer (CDBS) is routinely operated for bulk defect spectroscopy using small ^{22}Na sources and a new software package has been developed, allowing the read out of multiple detector pairs and averaging CDB spectra. The ^{22}Na beam has been upgraded for fully remote control and a new strong positron emitter has been installed. The efficiency of the conventional positron lifetime spectrometer has been improved considerably by digital read-out of four independent scintillation detectors.

And finally – in case there are no neutrons but you would like to learn more about neutron imaging – visit our ANTARES model. This 1:20 interactive model demonstrates the basic principle of the imaging technique, intended for the general public and students. Instrument parameters can be adjusted from a touchscreen, similar to performing a real experiment. The model used an LED lamp as a source to demonstrate the effect of collimation, sample detector distance, wavelength selection on the spatial resolution, or to illustrate the principles of a tomography.



Figure 8: Interactive model of ANTARES to demonstrate its working principle – and a real visitor's magnet at the open day exhibitions.



Reactor & Development



Drought – a neutron deficit relative to the average availability at a given location and season¹

A. Pichlmaier

Forschungs-Neutronenquelle Heinz Maier-Leibnitz (FRM II), Technical University of Munich, Garching

In 2022, no neutrons for the scientific community and other clients of the FRM II could be delivered. The reason for this was a micro-leakage of the central channel, a component essential for reactor operation. The reactor restart requires the problem to be fixed. This in turn can only be done by manufacturing and installing a new central channel. Therefore, the reactor crews were busy carrying out the usual in service inspections, dealing with the daily challenges of a complex machine and, especially, anticipating most of the “big” ten-year-inspections initially scheduled for 2024.

Take last year’s report, replace “cold source” (CNS) with “central channel” (Zentralkanal, JEC) and leave almost everything else untouched: this would have been an easy way to write this report and I was tempted to do so, yet it would not have done justice to the tremendous work done by the reactor crews during this year of neutron-drought.

Detecting the leak

In early 2022, when getting ready for the first reactor cycle of the year, the automated leak detection system JFT triggered an alarm. On investigating its cause, it became clear that the leak was really tiny – a drop every couple of minutes at the most – and only leaking into the JFT-system, designed to detect and contain leaks of this kind. However, operational procedures are also clear on this point: the leak needed to be fixed before another restart of the reactor. Further investigation revealed its exact position at the compensator of the central channel. This was bad news since nobody could imagine how to remedy this situation other than by replacing the central channel. Even such a tiny incident relating to the central channel is reportable according to the applicable legislation. It was reported to the state regulator in accordance with the procedures and on time.

Why is the central channel important?

The central channel serves several purposes:

- Enclosure of the cooling medium (H₂O)
- Separation of cooling and moderating media (H₂O/D₂O)
- Coolant guide for cooling the fuel element JKA

- Positioning of the fuel element
- Support of the control rod JDA (without drive)
- Ensuring coolant supply to the control rod
- Ensuring the mobility of the control rod
- Support of the solid absorber
- Ensuring free access to the fuel element for refueling after dismantling of internals

A formidable component indeed, yet replaceable by design and to be exchanged regularly – but this had never been done before and was initially foreseen for 2024. The fabrication had already been initiated some years ago but had never made it to the top of the task list. Therefore it had been only partly completed. At the time of writing, it will still be some months before the new component is ready and at the FRM II. As with the cold neutron source, nobody had seriously expected it to be replaced before 2024.

Fabrication is time consuming

What makes it so special and demanding to fabricate the central channel in general, and the compensator in particular? The compensator is made of the material EN AW-5754 (AlMg3). This is a common material in research reactors. In fact, it accounts for most of the Aluminum components in the neutron field of the FRM II. However, very few manufacturers have ever undertaken to use it as a compensator and FK1-component (this is the highest class of components relevant to safety at the FRM II). Without going into details: this means that a lot of effort goes into the qualification of material, of procedures and of the manufacturer, and that a great deal of involvement on the part of the regulator’s technical support organization, as well as a lot of time-consuming work overall, is required. Figures 1 and 2 give some impression of the setup. Note that the central channel is in total almost three meters long and, with the two compensators, forms one single component.

Other main activities in 2022

While the central channel undoubtedly grabbed the lion’s share of the attention, the other activities of the reactor crews were significant and passed smoothly, albeit mostly unrecognized by the outside world. Early in 2022, it was decided to move the 10-year 2024-inspections forward to 2022. These inspections concern primarily the bigger components in a high neutron field such as the moderator ves-

¹ adapted from <https://en.wikipedia.org/wiki/Drought>



Figure 1: Dummy Compensator

sel, the beam tubes and its plugs, the hot source. It takes more than half a year to complete them. They are often pressure tests and visual inspections that require significant preparatory work and are only possible when the reactor is shut down. Due to the unstinting commitment of the crews, all of these tests were accomplished successfully, thus fulfilling one of the requirements to allow for a further ten years of reactor operation. Besides, it will help to minimize the downtime when the FRM II is back in operation.

Permission for Mo-99 facility

In July, the FRM II got permission (first amendment to the reactor license) to build and operate the facility for production of the medically important radioisotope Molybdenum-99/Technetium-99m (Mo-99/Tc-99m). Already in October, the necessary heat exchangers were installed. They will transfer more than 400 kW of heat produced during the irradiation of the targets used for the production of Mo-99 to the secondary cooling loop of the reactor. This is an important milestone in making the FRM II fit for the future.

In 2022, another radioisotope became more and more important for medical applications: Lutetium-177 (Lu-177) is now licensed in North America and is likely to be in Europe soon. ITM Isotope Technologies Munich SE, based on the FRM II premises, is globally the key player in Lu-177 production for medical applications. Even when in full operation, FRM II would not be in a position to produce enough Lu-177 to cover the sharply rising demand. Given this situation, the FRM II successfully applied for an extension of its license and developed the necessary equipment to handle this isotope in one of its hot cells ("Ringlabor 3") thus becoming service provider for ITM. This is a classic

win-win-situation: ITM can serve more patients waiting for treatment, for the FRM II it generates some additional income and helps to maintain its capability to handle highly active radioactive material.

Furthermore, the gamma irradiation facility using radiation emanating from spent fuel saw significant use in this year of no neutron production: among other things, it was used to irradiate salt crystals from rock-formations that are candidates as final repositories for nuclear waste.

Transport of fresh and spent fuel remains a daunting task

The transport of fresh and spent fuel remains an open question. No transport was possible in 2022. Although the FRM II is prepared to transport spent fuel, the recipient is not entirely ready yet. Concerning the delivery of fresh fuel, some progress has been made towards resolving the situation with the delivery of fresh fuel to the FRM II.

Outlook

If all goes according to schedule, the central channel will be mounted and commissioned towards the end of 2023 and the FRM II will return to user operation in 2024. For us as operators, this is the noblest of all tasks for 2023.

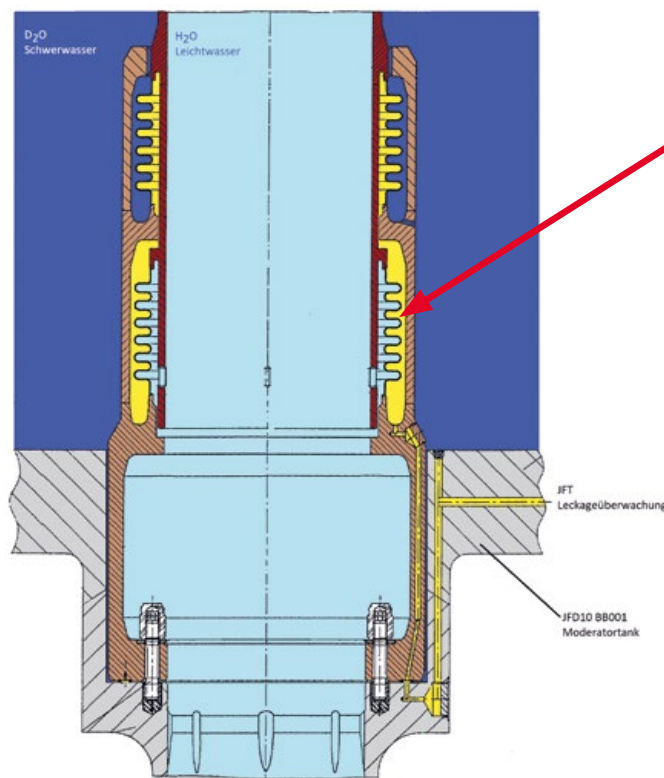


Figure 2: Bottom part of the central channel JEC in brown color. Light water light blue, heavy water dark blue, leak detection system JFT in yellow. Moderator vessel JFD in grey. The red arrow on the right marks the compensator with the approximate position of the leak.

A LEU solution for the conversion of FRM II

C. Reiter, T. Chemnitz, K. Shehu, J. Shi, W. Petry

TUM Center for Nuclear Safety and Innovation, Technical University of Munich, Garching, Germany

FRM II is Germany's most powerful research reactor and uses Highly Enriched Uranium (HEU) fuel containing 93% of the fissionable uranium-235. The Technical University of Munich (TUM) operates the reactor and has been mandated to convert the FRM II to a lower enrichment fuel. In 2022, the conversion project made good progress. The ion irradiation technique has again proven its capabilities and produced equivalent results to an in-pile irradiation. That allowed to study the growth of the amorphous interdiffusion layer that forms between Uranium Molybdenum fuel and the Aluminum matrix. In addition, the results of the parameter study to identify suitable core designs has indicated that conversion converting the FRM II to a fuel element with low-enriched fuel is scientifically possible assuming monolithic U-10Mo can be qualified for the FRM II.

Further insight into out-of-pile ion irradiation testing of high-density metallic Uranium fuel [1]

The U-Mo/Al dispersion fuel – Uranium Molybdenum (U-Mo) fuel particles embedded in an Aluminum (Al) matrix – is a promising candidate for the conversion. Under irradiation, an amorphous interdiffusion layer (IDL) forms between U-Mo fuel particles and the Al matrix, which has detrimental effects on the U-Mo fuel performance, such as reducing the thermal conductivity and mechanical stability of the fuel system. For a safe reactor operation these effects have to be suppressed. Previous irradiation tests have demonstrated

that using a Zirconium-Nitride (ZrN) coating as a diffusion barrier between U-Mo and Al is an advantageous option to limit the IDL formation.

Hence, a systematic evaluation of the effect of ZrN as a diffusion barrier in an U-Mo/Al fuel system utilizing out-of-pile ion irradiation technique was proposed, which allows for a significant reduction in the complexity of handling highly radioactive materials and experimental expenses. Furthermore, it enables flexible control of irradiation conditions. The samples were fabricated using the physical vapor deposition (PVD) method to achieve the coated fuel system which is beneficial for ion irradiation experiments.

In the first experiment, the samples were prepared with the irradiation geometry where the U-Mo is the substrate and the ions impinge on the Al top layer. Iodine ions with an energy of 80 MeV were used for irradiation to mimic the fission products generated during in-pile irradiation.

To investigate the effect of coating quality, cracks in ZrN coatings were prepared by microindentation, to provide potential paths for the interdiffusion of U and Mo. Fig. 1 reveals the comparability of in-pile and ion irradiation – all types of IDL formation found in in-pile irradiated fuel were successfully reproduced by ion. These results have proven that ion irradiation is an adequate however much more convenient tool for the development of novel high-density metallic Uranium fuels for research reactors.

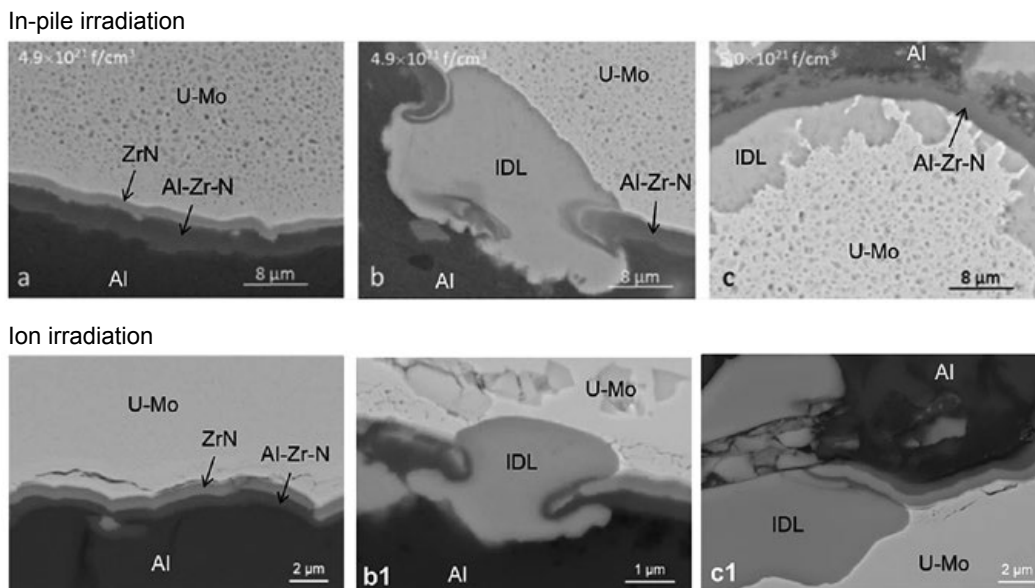


Figure 1: A comparison of the Al-ZrN-UMo system under in-pile irradiation and ion irradiation

A second experiment is designed to use U-Mo-ZrN-Al layered samples, in which the Al is the substrate and the U-Mo top coating will encounter ions first, replicating the actual path of fission products released in the fuel during in-pile irradiation. The indents in the ZrN coatings are distributed far enough from each other to avoid the overlapping of the generated dislocation in the material. The designed samples will be irradiated with high-energy Xe ions at the Argonne Tandem Linac Accelerator System (ATLAS) at Argonne National Laboratory (ANL) in the next beam time scheduled in 2023.

A LEU solution for the conversion of FRM II [2]

In 2022, a major breakthrough has been achieved as the extensive parameter study to identify feasible conversion scenarios for the FRM II, indicates that a fuel element with low enriched uranium (19.75%) is possible.

The simulations by the TUM researchers have been independently confirmed by the ANL in the USA using different computer codes. They are based on the most recent technical drawings and thus ensure state-of-the-art calculations.

For the proposed LEU core design, it is assumed that the monolithic U-10Mo fuel system is suitable and can be qualified for conversion. Besides the novel high-density U-Mo fuel, longer fuel plates and other changes, the proposed core design also relies on a so called flow restrictor.

The flow restrictor is basically a venturi Nozzle at the end of the fuel plates (see Fig. 2). Adjusting the coolant flow in a nuclear reactor is a known concept and is used e.g. in nuclear power plants. The flow restriction introduces a localized area reduction and thus a flow resistance down-stream of the fuel plates. This area change provides an additional pressure drop along the flow path. The flow restrictor geometry ensures satisfying the pressure drop requirement in the nominal flow direction while achieving the same mass flow rate as the current HEU design. Due to the location of the restrictor, the pressure at the exit of the coolant channel for the LEU design is greater than the pressure of the HEU design. The saturation temperature increases due to higher coolant pressure improving the thermal safety margins.

In the study, it could be demonstrated that the proposed LEU reactor design would not violate the agreed criteria for conversion: 1. Satisfy all safety requirements, 2. Compatible with the current reactor design (see Fig. 3), 3. Achieve a cycle length identical to the current core, which is 60 days, 4. Marginal loss of max. 10% in average neutron flux in the beam tube nozzles.

According to the fuel fabricator, the proposed changes to the fuel element can be manufactured. In addition, the irra-

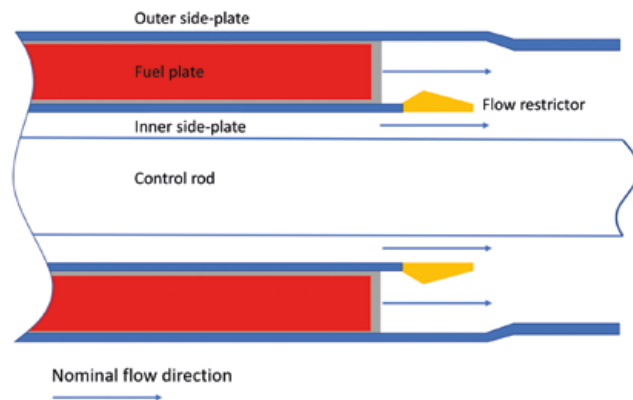


Figure 2: Schematic of the proposed flow restrictor

diation tests performed previously with monolithic U-10Mo fuel suggest that this fuel is suitable for use in the FRM II reactor. Thus, a conversion to LEU of the FRM II is scientifically possible assuming monolithic U-10Mo can be qualified for the FRM II.

Acknowledgement

This work was supported by a combined grant (FRM2023) from the Bundesministerium für Bildung und Forschung (BMBF) and the Bayerisches Staatsministerium für Wissenschaft und Kunst (StMWK).

[1] J. Shi, B. Ye, D. Salvato, A. Leenaers, T. Chemnitz, W. Petry, *Design and out-of-pile ion irradiation testing of ZrN coated UMo/Al fuel system*, In *Proceedings: Nuclear Materials Conference proceedings*. Ghent (Belgium): Elsevier (2022)

[2] C. Reiter, A. Bergeron, D. Bonete-Wiese, M. Kirst, J. Mercz, R. Schönecker, K. Shehu, B. Ozar, F. Puig, J. Licht, W. Petry, P. Müller-Buschbaum, *A Low-Enriched Uranium (LEU) option for the conversion of FRM II*, *Annals of Nuclear Energy*, 183, 109599 (2023)

DOI: 10.1016/j.anucene.2022.109599

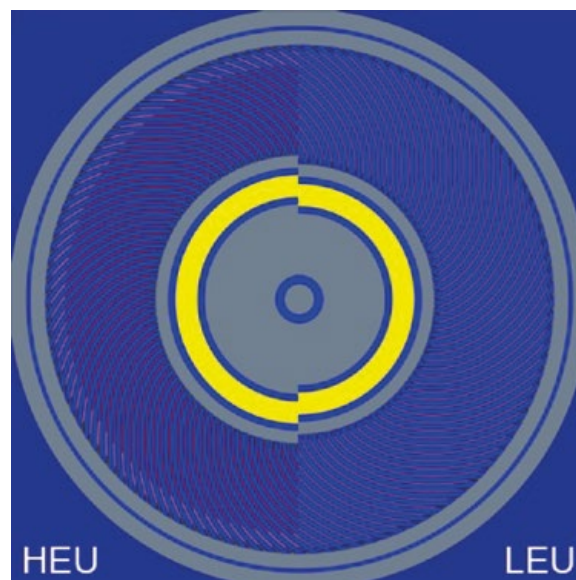


Figure 3: x-y cut through the current HEU core (left) and proposed LEU design (right)



Facts & Figures



The year in pictures



January 24th

Staff members control the millimeter-precise positioning of the central mast directly from the reactor pool. Removing the defective cold neutron source was one of the main tasks for the FRM II operation team in early 2022.

March 2nd

How do neutrons help to diagnose and treat cancer? Dr. Tobias Chemnitz explains the use of radioisotopes and tumor irradiation at the FRM II during his talk at the "Science for everyone" lecture series at the Deutsches Museum in Munich. A livestream also enables viewers at home to take part despite the pandemic.



April 4th

Welcome to new colleagues: The three directors (back row from left) Prof. Dr. Peter Müller-Buschbaum, Dr. Axel Pichlmaier and Robert Rieck took 6 new employees aboard on a day dedicated to the newbies.



April 29th

Face-to-face and at eye level: Prof. Dr. Karen Mossman, Vice President Research at McMaster University in Canada (2nd from right), and her colleague Soren Habel, Strategic Advisor for Internationalization (r.), visit Dr. Christian Reiter, Head of the TUM Center for Nuclear Safety and Innovation (CSNI; 2nd from left), Dr. Tobias Chemnitz (l.) and the technical director of the FRM II, Dr. Axel Pichlmaier (middle). The cooperation between McMaster and FRM II will enable an exchange of staff and students.



April 28th

What do you need neutrons for? The MLZ participates in the nationwide event "Girls'-Day", welcoming 18 interested girls. They get a first impression of the answers by making their own atoms out of colored beads, experimenting with liquid nitrogen and during a tour led by Dr. Johanna Jochum (r.).

May 9th

Beer and science: At the public event "Pint of Science", Dr. Nicolas Walte, instrument scientist at the MLZ, talks about "Pallasites: Origin of the jewels from the sky". The pub in the city center of Munich attracted several dozen visitors.

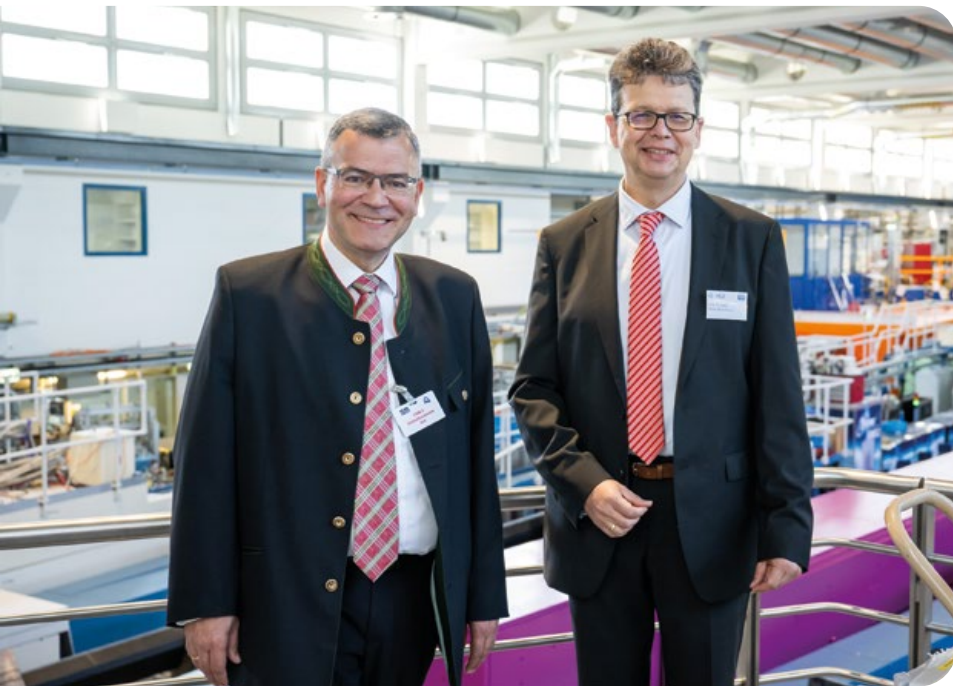


May 19th

A free neutron lives for 887 seconds in the FRM II. Dr. Johanna Jochum (l.) and Dr. Sebastian Mühlbauer take on the exciting journey of Nobby, the neutron, at the first Science Slam of the Mechanical Engineering Student Council at the Technical University of Munich. The film can be watched on FRM II's YouTube channel.

May 23rd

Why are neutrons so important for science? Prof. Dr. Astrid Lambrecht (5th from left), member of the Board of Directors at the Forschungszentrum Jülich (FZJ), and Prof. Dr. Thomas F. Hofmann (3rd from left), president of the Technical University of Munich (TUM), get answers from the FRM II und MLZ directors, when touring the FRM II.

**June 3rd**

A very interested State Minister (l.) visits the Research Neutron Source. On the gallery of the neutron guide hall, scientific director Prof. Dr. Peter Müller-Buschbaum (r.) shows Dr. Florian Herrmann the wide range of applications of neutrons.

June 27th

The FRM II and MLZ presented themselves as employers with a booth for the first time at the IKOM – Career Fair for Students in Garching.





June 29th

How do you become a Technical Director of a research reactor? And what exactly does he do? Dr. Axel Pichlmaier (l.) of the FRM II answers these questions at a podcast of the Technical University of Munich, produced by the journalist Fabian Dilger.

July 6th

Inaugural visit of the new vice president for communication and public engagement at the Technical University of Munich (TUM), Dr. Jeanne Rubner (m.) with the FRM II directors and communication team.



July 7th

FRM II offers open positions at the recruiting day of the Association of German Engineers (VDI) in Munich.

July 8th

FRM II goes Deutsches Museum: The Deutsches Museum reopens for the first time after reconstruction presenting, among other things, a station for the research neutron source Heinz Maier-Leibnitz (FRM II) in the permanent exhibition “Atomic Physics”.

**July 25th**

Joint research and development activities between MLZ and ILL: Prof. Dr. Andreas Meyer, Associate Director at the Institut Laue – Langevin (ILL) (4th from right), visits the MLZ scientific and technical directors as well as the heads of the instrument services to strengthen their cooperation.

August 2nd

Their mission is to discover the neutron source, and the twelve motivated school-girls pursue this goal with a plan. As part of the “TUM Entdeckerinnen” program, the 13–15 year olds come to visit during their summer vacation and look behind the scenes at the research neutron source.





September 5th

Three Post-Docs are the first out of 15 selected Global Neutron Scientists (GNeuS), welcomed by Dr. Henrich Frielinghaus (l.) and Dr. Flavio Carsughi (r.). Their fellowships are funded via the Marie Skłodowska-Curie Actions of the European Union.

October 20th

It was an evening of interested questions and open discussions: Prof. Dr. Peter Müller-Buschbaum, Scientific Director of the FRM II and at the MLZ, and gallery owner Peter Litvai opened the exhibition “Neutron Source. A photo documentation of the research work of the Heinz Maier-Leibnitz Zentrum” at the Litvai Photo Gallery in the heart of Landshut’s old town.



October 24th

Exchange and Bavarian hospitality for our Swiss partners: The laboratory for neutron and muon instrumentation of the Paul Scherrer Institut with its head Prof. Dr. Marc Janoschek (3rd from the right) toured the MLZ.



October 3rd

More than 800 children and adults visit the talks, exhibition, hands-on-booths and the tours at the FRM II. This year, the Open Day was organized by the FRM II together with other research institutes and clusters on the Garching campus.

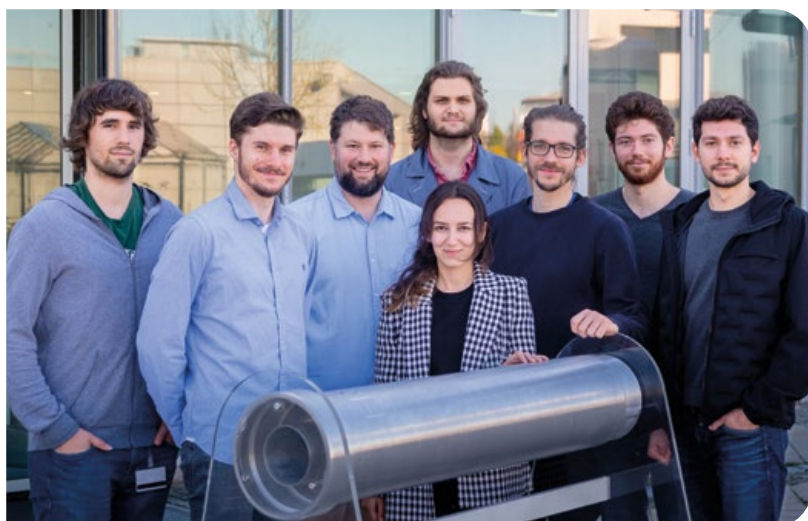


November 3rd

IAEA experts met at the invitation of FRM II head of irradiation and sources, Dr. Vladimir Hutanu (front, 2nd from left), and FRM II Technical Director, Dr. Axel Pichlmaier (2nd row, 2nd from right), to discuss and develop “Design aspects in the utilisation of research reactors”.

November 21st

Guides to Jülich’s instruments: Prof. Dr. Frauke Melchior, Member of the Board of Directors for Scientific Division at the Forschungszentrum Jülich, enjoys lectures by MLZ scientists as well as guided tours through the MLZ laboratories and to the scientific instruments operated by the Forschungszentrum Jülich.



November 25th

Scientifically speaking it is possible to convert the Research Neutron Source FRM II to a fuel element with Low Enriched Uranium (LEU). This conclusion is the result of Dr. Christian Reiter (3rd from left) and his team’s calculations, which have been independently confirmed by experts in the USA.

Awards

June 30th

Proactive and extra-mandatory commitment: Elisabeth Jörg-Müller (2nd from right) is awarded the Karl Max von Bauernfeind Medal. With this prize, the president of the Technical University of Munich, Prof. Dr. Thomas F. Hofmann (l.), honors the long-time assistant to the scientific directors at the FRM II.



August 23rd

Ground-breaking research in superconductivity and magnetism: Prof. Dr. Peter Böni of the Technical University of Munich receives the Walter Hälgl Prize, presented by the European Neutron Scattering Association at the International Conference on Neutron Scattering in Buenos Aires.

September 27th

Early and great commitment to the material science diffractometer STRESS-SPEC: Prof. Dr. Heinz-Günter Brokmeier from Technical University of Clausthal receives this year's prize of the Heinz Maier-Leibnitz Zentrum for instrumentation and scientific use from FRM II and MLZ scientific directors, Prof. Dr. Peter Müller-Buschbaum (l.) and Prof. Dr. Martin Müller (r.).

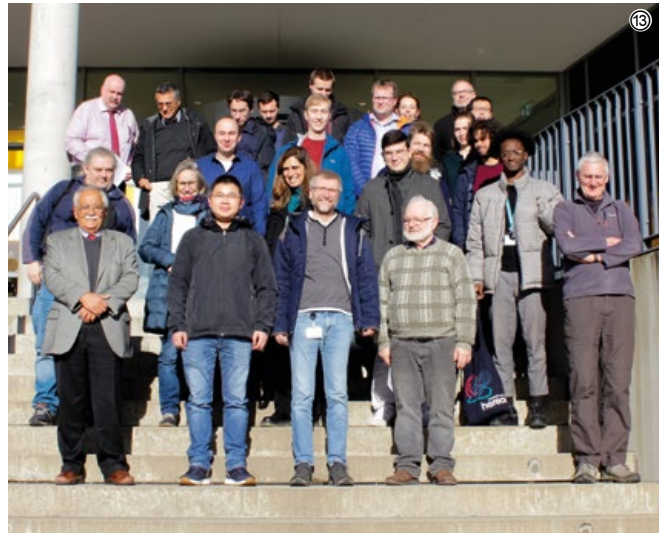
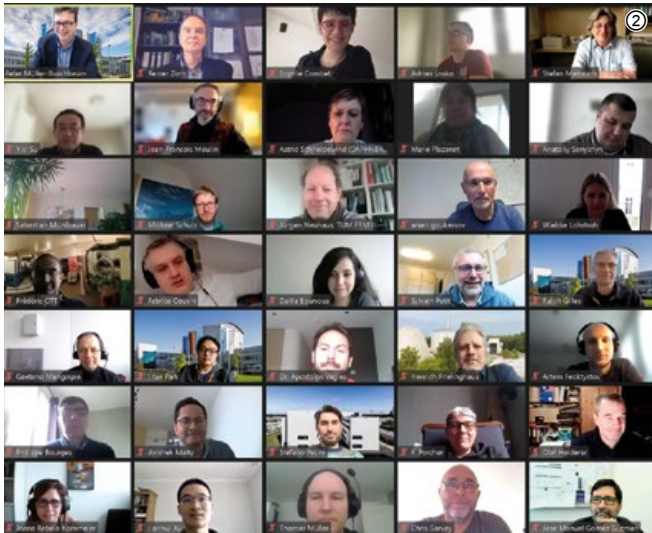


Workshops, Conferences and Schools

①	10 January – 19 December	Seminar: Neutrons for Science and Industry, Garching, hybrid	TUM / MLZ
②	7 – 8 February	German-French workshop launching GeFR@NS (Germany and France at Neutron Sources), online	MLZ / LLB
③	7 – 11 February	F-Praktikum, Hands-on training for TUM physics students, Garching	TUM / MLZ
④	31 May – 3 June	MLZ Conference 2022: Neutrons for mobility, Lenggries	Hereon / MLZ
⑤	27 June – 1 July	F-Praktikum, Hands-on training for TUM physics students, Garching	TUM / MLZ
⑥	5 – 8 July	WE-Heraeus-Seminar: “Antimatter: Positrons in Fundamental Research and Materials Physics”, Neustift, Austria	TUM / MLZ
⑦	29 August – 1 September	11 th International Serpent User Group Meeting, Garching	TUM / MLZ
⑧	5 – 16 September	24 th JCNS Laboratory Course – Neutron Scattering 2022, Jülich and Garching	JCNS / MLZ
⑨	8 September	8 th TUM Expert Forum, Garching	TUM / MLZ
⑩	4 – 5 October	3 rd JANA Workshop, Garching	MLZ
⑪	11 – 14 October	JCNS Workshop 2022 – Trends and Perspectives in Neutron Scattering: Experiments and data analysis in the digital age, Tutzing	JCNS / MLZ
⑫	19 – 27 October	Czech-Bavarian mini-school 2022 on large scale facilities and open data, Garching/Prague	TUM / MLZ
⑬	23 November	NeT Meeting: Workshop on the Assessment of Residual Stresses in Welds, Garching	TUM / MLZ
⑭	8 – 9 December	MLZ User Meeting 2022, Munich	MLZ



④



No neutrons, no research results? Far from it!

A. Voit, A. Görg

Heinz Maier-Leibnitz Zentrum (MLZ), Technical University of Munich, Garching, Germany

Even without neutrons, the number of 152 scientific media reports on research with neutrons at the MLZ and FRM II is gratifying. In order to facilitate access to science for the interested public, there are many innovations at the FRM II and MLZ this year: the FRM II can now also be found in the Deutsches Museum, Munich, there are new exhibits for FRM II visitors to touch, and the press team is striving for increased transparent communication via social media. This year alone, more than 800 adults and children eager for knowledge visited us on Open Day and Mouse Day. During 2022, 2142 visitors had a great experience on guided tours through the reactor.

349 media articles were published on the Research Neutron Source (FRM II) and the Heinz Maier-Leibnitz Zentrum (MLZ) in 2022, both in print and online media, as well as on TV and radio. This confirms the consistent media interest that we have been experiencing for years. So far this year, we have recorded over 35 press enquiries and 3 press visits plus the press conference in November on the subject of conversion – “Operation of FRM II with low-enriched uranium possible”. The number of 152 scientific media articles on research with neutrons at the MLZ and FRM II is again gratifying, mainly due to 13 press releases sent by the Technical University of Munich and the FRM II (see Fig. 1).

Science topics accounted for 44 percent of all contributions relating to the MLZ and FRM II in 2022. Neutron source topics include areas such as the planned transport of spent fuel elements to Ahaus, conversion and the reportable event on the central channel. Risk topics account for more than half of all articles, for example our press conference in November on the subject of conversion.

Number of scientific media articles

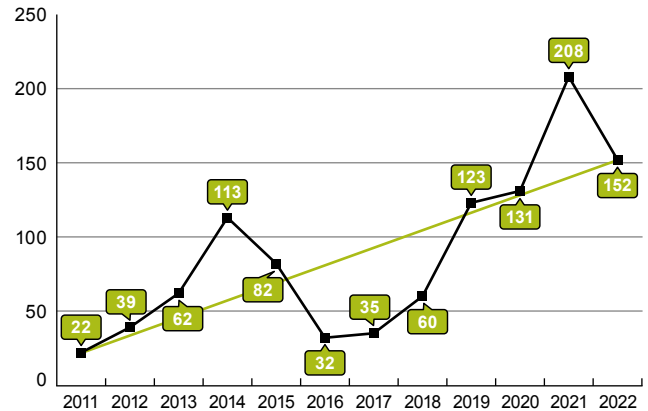


Figure 1: The trend line shows the continuous increase in scientific articles in the media about the FRM II and the MLZ (2011–2022).

Media coverage 2022

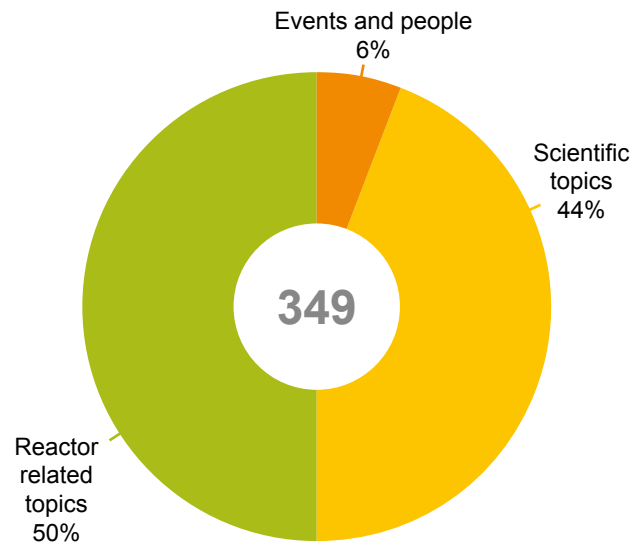


Figure 2: Science topics accounted for 44 percent of all contributions relating to the MLZ and FRM II in 2022. Neutron source topics include areas such as the planned transport of spent fuel elements, conversion and the reportable event on the central channel.



Figure 3: Press conference at the FRM II in Garching with TUM president Prof. Dr. Thomas F. Hofmann (front 2nd from left), FRM II scientific director Prof. Dr. Peter Müller-Buschbaum (left), reactor physicist Dr. Christian Reiter (2nd from right) and TUM spokesman Ulrich Meyer reporting on groundbreaking scientific findings on the research neutron source.

A new concept for guided tours

Over the past two years, only a few visitor tours took place at the FRM II due to the pandemic. In 2022, 2142 visitors had a great experience during the tours of the reactor. To ensure the very high quality of the tours, we have developed a new concept for guided tours. This includes new training material on how the FRM II works and on the scientific instruments, including examples of current research. As a supporting measure, we installed exhibits on the topics of radioi-

sotopes, silicon doping, elemental analysis and the structure determination of large biological molecules (proteins) at the respective stages of the visitor guide route. Other exhibits on scientific achievements and methods are planned.

Shortly before this year's open day, the visitor guides were able to take part in a trial tour and then discuss their experiences and they frequently asked questions.



Figure 4: New exhibits for elemental analysis (PGAA) and diffraction (BIODIFF) are located for visitors in the gallery of the Neutron Guide Hall.

Social media booming

In 2022, we significantly expanded the social media presence of the FRM II and MLZ.



227 Followers
since February 2016



219 Followers
since September 2021



354 Followers
since November 2021



570 Followers
since February 2019



55 Followers
since September 2021

Twitter community continues to grow

We continued to use the English-language Twitter account of the MLZ @mlz_garching very successfully in 2022. With 570 followers, we were once again able to increase our Twitter community in 2022 – for comparison: in 2021, there were 379, in 2020 236 followers. By the time of writing, we had tweeted 362 times. That means we, once again, increased the content on Twitter compared to last year (2021: 246 tweets in the entire year).

LinkedIn for employees and job seekers

Currently, the most booming channel on social media is the FRM II LinkedIn channel with 354 followers to date, which is a tripling compared to the numbers in 2021. We only opened the channel in 2021 (84 followers in 2021), and it has since developed into a reliable source of information for job seekers, colleagues from other research institutions, and our own employees. We regularly post news, events and job advertisements there. Independent contributions by employees are still rare, but the interaction rates on our own contributions are very high.

Live communication and other events

This year, many events again took place face-to-face, including the series “*Wissenschaft für Jedermann*” at the Deutsches Museum with 80 spectators and the *Pint Of Science Festival 2022*, where the FRM II and the MLZ each held its own lectures for the public together with TUM scientists. A new addition in 2022 was the *IKOM – Career Fair for Students*, where the FRM II was represented as an employer with a booth for the first time. Proven formats for schoolgirls also attracted numerous girls to the MLZ again: the *Girls’Day*, the *TUM-Discoverers*.

Science Slam with Nobby

A free neutron lives in the FRM II for 887 seconds – and that is quite long! Dr. Johanna Jochum and Dr. Sebastian Mühlbauer will take you on the exciting journey of Nobby, the neutron, at the first Science Slam of the Mechanical Engineering Student Council at the Technical University of Munich (TUM)! From nuclear fission to the path in the neutron guide to his abrupt end of life in a sample. Of course, a good dose of humor is not to be missed.



You will find the event on our YouTube channel:
@frmii-forschungs-neutronen5405

Mouse Door Opener Day & Open Day extended

The largest and most important event in terms of visitor numbers was the Open Day and the parallel Mouse Door Opener Day on October 3. There were numerous advertising ploys for the open day, including distribution via the TUM-wide newsletter, advertising banners in social media and on the screens distributed across all TUM locations and on the subway.

The organization this year was a bit more complex than in previous years, as we were able to gain a number of new partners such as the Max Planck Institute of Quantum Optics, the Munich Institute of Biomedical Engineering, the Institute of Medical Microbiology, Immunology and Hygiene and the four Munich Clusters of Excellence as well as the company ITM Isotope Technologies Munich SE. All this had to be coordinated.

This paid off: More than 800 children and adults visited the varied program at the various venues that we had coordinated together. 287 adults and 64 children attended the guided tours at the FRM II. We managed this successfully thanks to enthusiastic support from the circle of colleagues.



Figure 5: The organizing team of this year’s Mouse Open House and Door Opener Day in Garching.

FRM II goes Deutsches Museum

In July 2022, the Deutsches Museum reopened after a first reconstruction and now shows, among other things, in the permanent exhibition “Atomic Physics” a stage in the Research Heinz Maier-Leibnitz neutron source (FRM II).

On a scale of 1:10 a true-to-life model of the FRM II reactor pool. Those who want to know more can inform themselves at a media point in German and English about the functioning of the neutron source, safety aspects, research examples and current information on the conversion to lower enriched uranium.

PARI IV – Bringing society inside the walls of scientific facilities

The Public Awareness of Research Infrastructures (PARI) three-day conference held in July 2022 at the SKA Observatory’s Global Headquarters (U.K.) discussed the science communication issues that practitioners face at research infrastructures, like community building, science diplomacy and equity, diversity and inclusion in STEM. We concluded that we need to bring society within the walls of the scientific facilities as much as we need to help scientists engage with society.

With 142 participants (of which 60 in-person), 24 nationalities from almost every continent and 53 talks in three days, this PARI conference was a focused and highly engaged gathering of science communication practitioners at research infrastructures around the world. A record-breaking heatwave and equally rare travel difficulties did not stop them from traveling to Jodrell Bank in the U. K., where the headquarters of the SKA Observatory (SKAO) hosted the event.

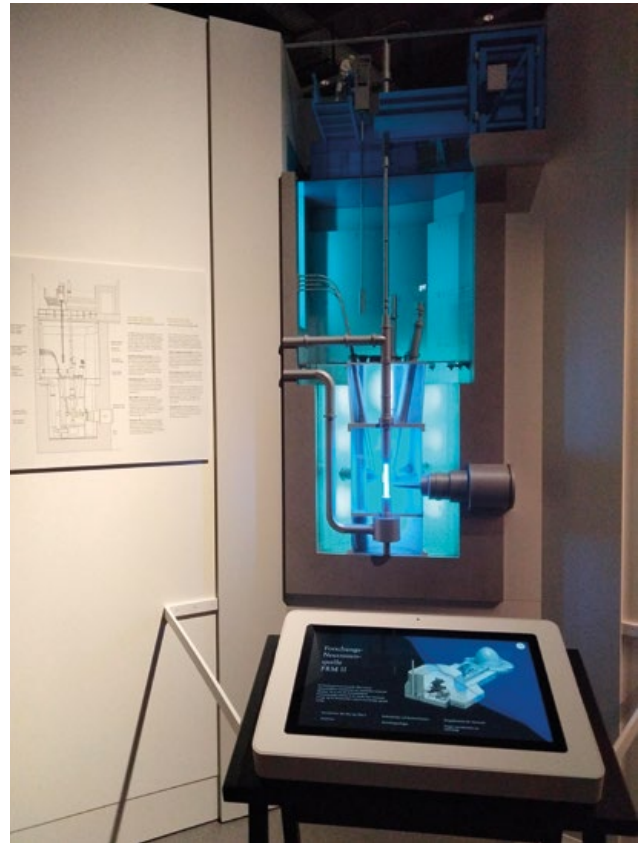


Figure 6: Model of the FRM II reactor pool at the “Atomic Physics” exhibition of the Deutsches Museum in Munich.



Figure 7: Science is for everyone with press officer Andrea Voit & Figure 8: Science communication is... with press officer Anke Görg.

Back to reality!

F. Erdem¹, I. Lommatzsch², R. Schurek²

¹Heinz Maier-Leibnitz Zentrum (MLZ), Technical University of Munich, Garching, Germany;

²Jülich Centre for Neutron Science (JCNS-4) at MLZ, Forschungszentrum Jülich GmbH, Garching, Germany

The year began once more under the cloud of the pandemic. We had prepared everything for a restart under these circumstances but, unfortunately, had to rethink. After a virtual visit at the ICNS in Buenos Aires, the User Office was present at the SNI 2022 in Berlin and was able to close the year with a warm welcome to the participants of the annual MLZ Users 2022!



Figure 1: GhOST on tour.

In addition to a number of smaller tasks like the MLZ newsletter and the start of preparations for the ECN2023 which will be hosted in Garching by the MLZ in March, the User Office visited the ICNS at Buenos Aires – but only virtually. We were able to present a new short movie about the user service at the MLZ!

Two weeks later, it was time to travel again after a long lean period! The destination was the SNI 2022 (German Conference for Research with Synchrotron Radiation, Neutrons and Ion Beams at Large Facilities) in Berlin.

The MLZ hosted the successful event in Garching in 2018, and this time HZB invited all researchers using synchrotron,



Figure 2: Dr. Ralph Gilles (MLZ) at the end of his talk at the SNI 2022 – reminding everybody to submit an abstract to the ECNS 2023.



Figure 3: The interactive poster of MLZ at the SNI 2022. Just grab an info card and a pen!

neutron and/or ion beams to Germany's beautiful capital. The User Office presented an interactive poster (see Fig. 3!) and was delighted to meet users again!

The year ended with the traditional MLZ User Meeting. After two years of virtual meetings, it was wonderful to extend invitations to an in-person event again! We returned to the venue where the last real meeting had also taken place in 2019 and everybody enjoyed the diversified program of the Science Groups' workshops on the first day, the interesting plenary talks by Dr. Henry Fischer (ILL) and PD Dr. Frank Weber (KIT) on the second day, and last but not least the lively breaks with coffee and snacks as well as the Bavarian dinner with a lot of beer! There were plenty of topics for discussion: the most exciting one for sure being the planned upgrade program MORIS which had been introduced by the MLZ director and spokesman Prof. Dr. Martin Müller.



Figure 4: Finally: A real poster session!



Figure 5: Full house during the update by MLZ Director Prof. Dr. Peter Müller-Buschbaum.

Organization

FRM II and MLZ

The Forschungs-Neutronenquelle Heinz Maier-Leibnitz (FRM II) provides neutrons for research, industry and medicine and is operated as a Corporate Research Center by the Technical University of Munich (TUM). Scientific use of the FRM II, with around 1000 user visits per year, is organized within the Heinz Maier-Leibnitz Zentrum (MLZ).

The chart below shows the overall network comprising the Neutron Source FRM II and the MLZ, as well as the funding bodies and the scientific users that perform experiments at the MLZ, addressing the major challenges facing present-day society.

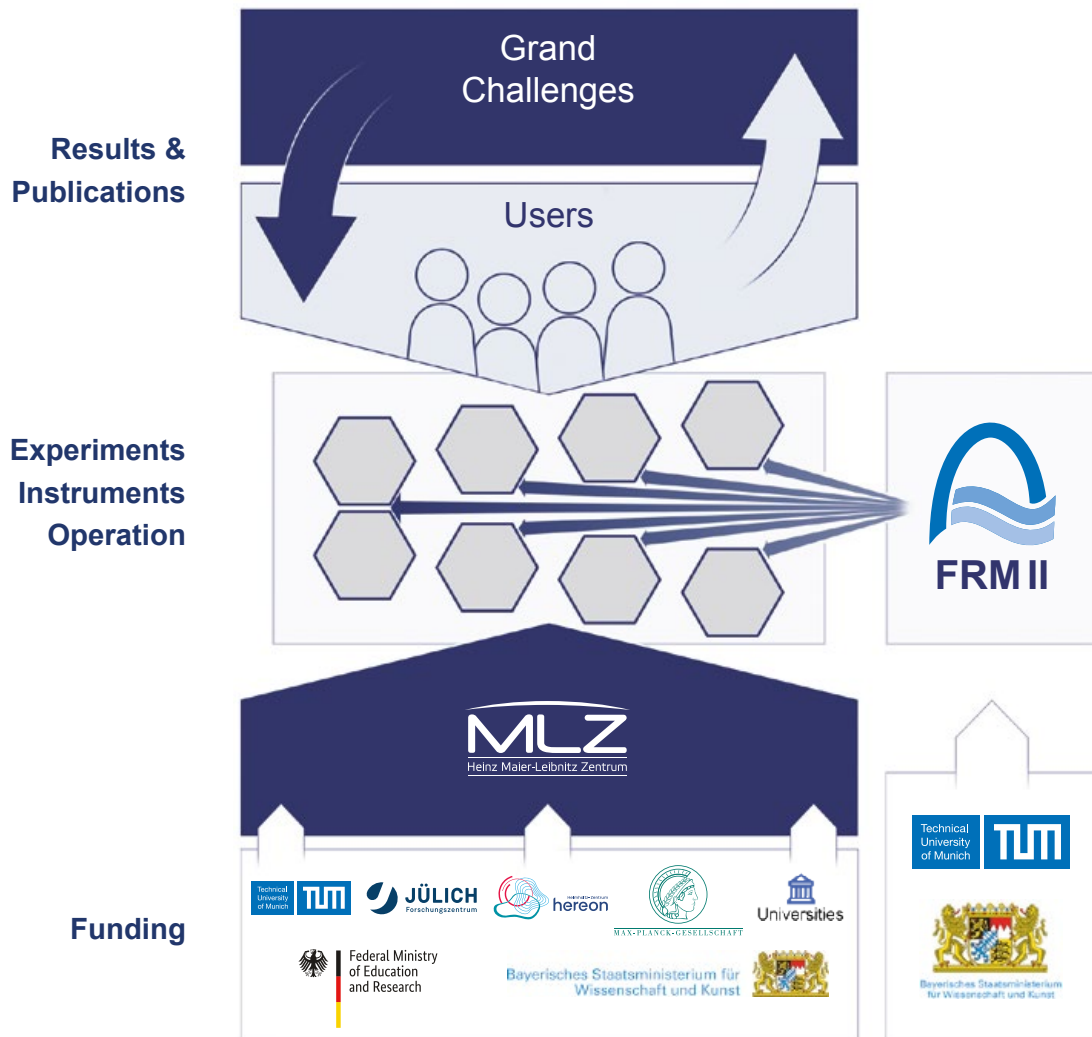


Figure 1: The neutron source FRM II and the user facility MLZ.

Scientific Director MLZ, HGF

Prof. Dr. Martin Müller

Technical Director FRM II

Dr. Axel Pichlmaier

Scientific Director MLZ, FRM II

Prof. Dr. Peter Müller-Buschbaum

Administrative Director FRM II

Robert Rieck

Scientific Cooperation at the Heinz Maier-Leibnitz Zentrum (MLZ)

The Heinz Maier-Leibnitz Zentrum with its cooperating partners, the Technical University of Munich (TUM), Forschungszentrum Jülich GmbH (FZJ) and Helmholtz-Zentrum hereon GmbH is rooted in a network of strong partners including the Max Planck Society (MPG) and numerous university groups that benefit from scientific use of the Forschungs-Neutronenquelle Heinz Maier-Leibnitz. The organizational chart of the MLZ is shown below.

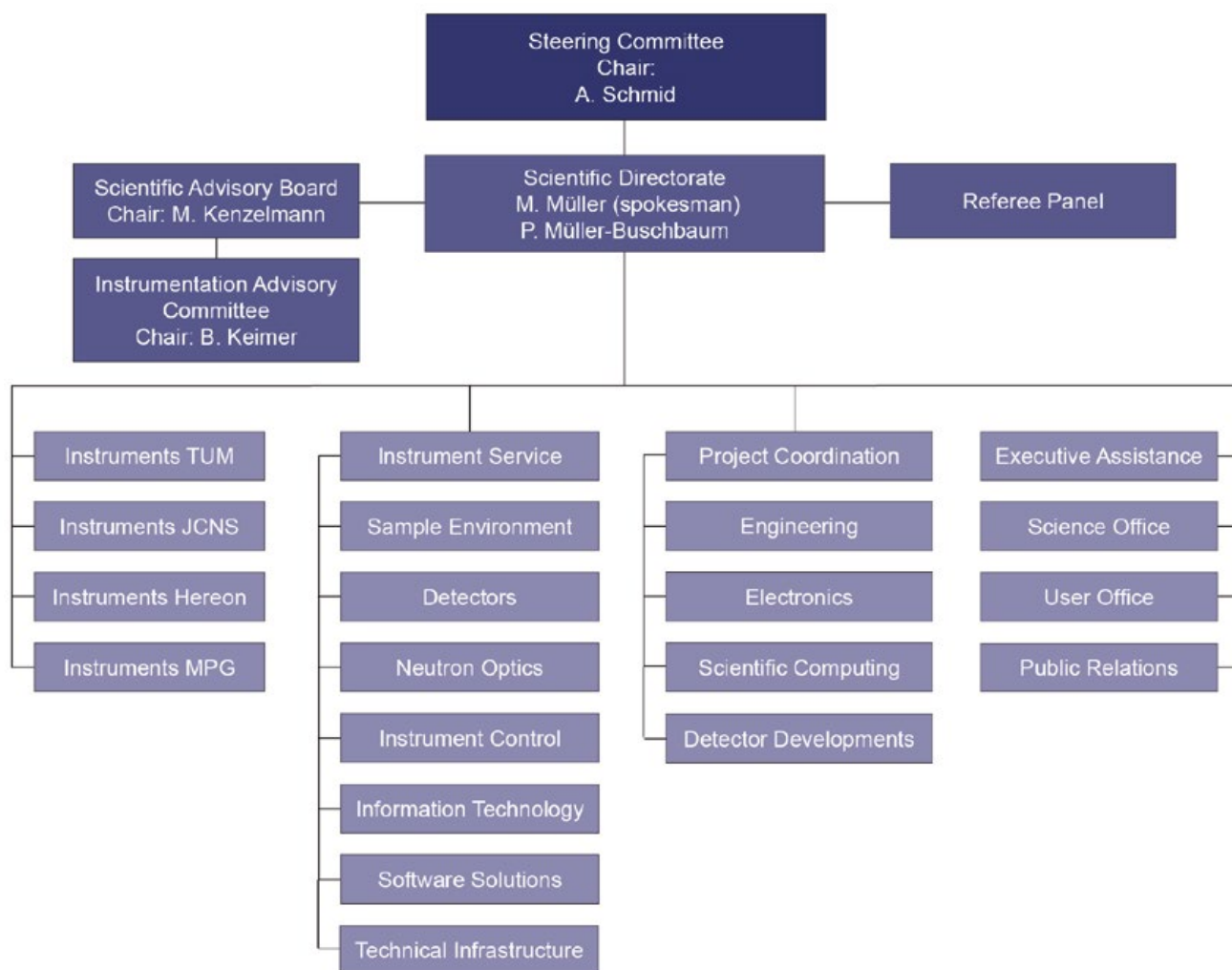
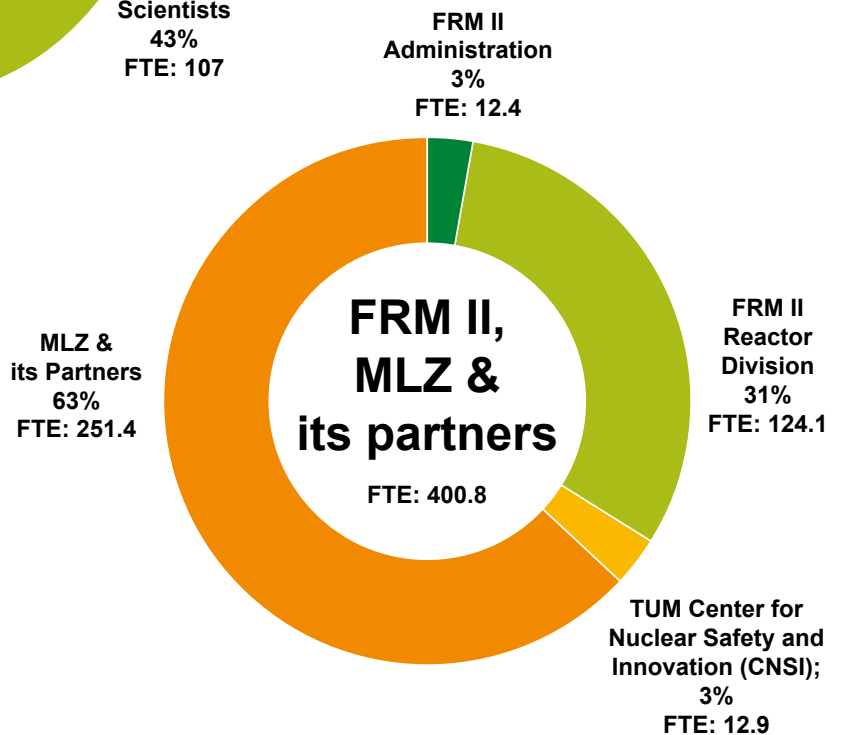
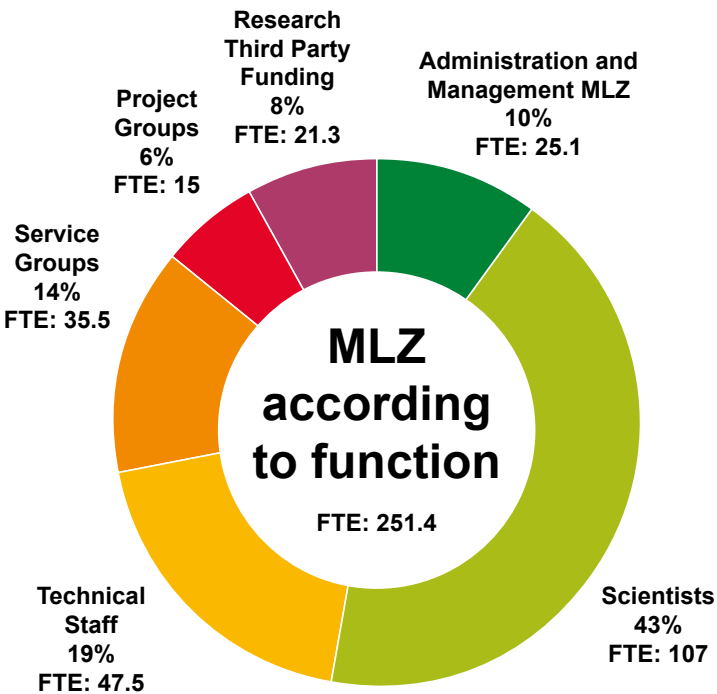
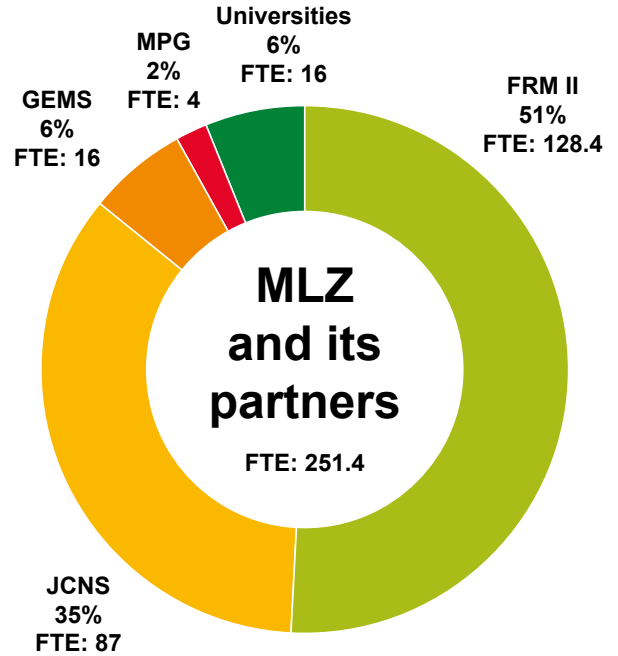


Figure 2: Organizational chart MLZ.

Staff

The charts below show the staff of MLZ and FRM II. The staff of MLZ, as per their share among the partners with a detailed break-down of their function within the MLZ is also depicted.



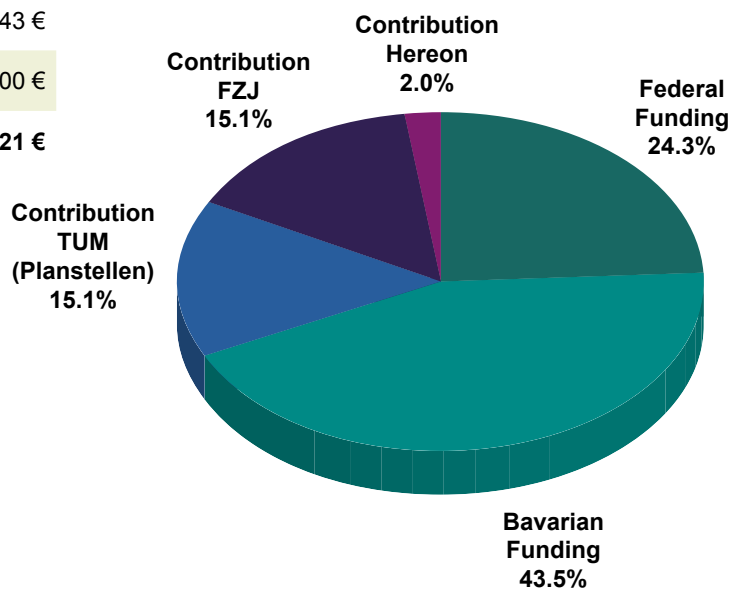
FTE = Full Time Equivalent

Budget

The tables and charts below show the revenue and expenses for 2022.

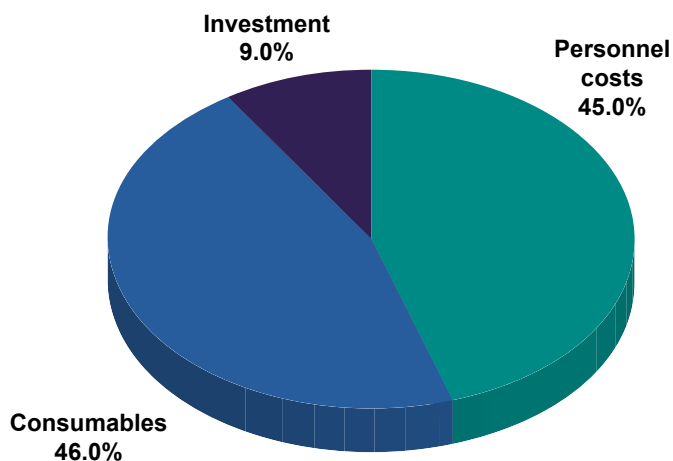
Revenue 2022

Federal Funding	16.700.000 €
Bavarian Funding	29.821.270 €
Contribution TUM (Planstellen)	10.387.608 €
Contribution FZJ	10.379.643 €
Contribution Hereon	1.320.000 €
Total	68.608.521 €



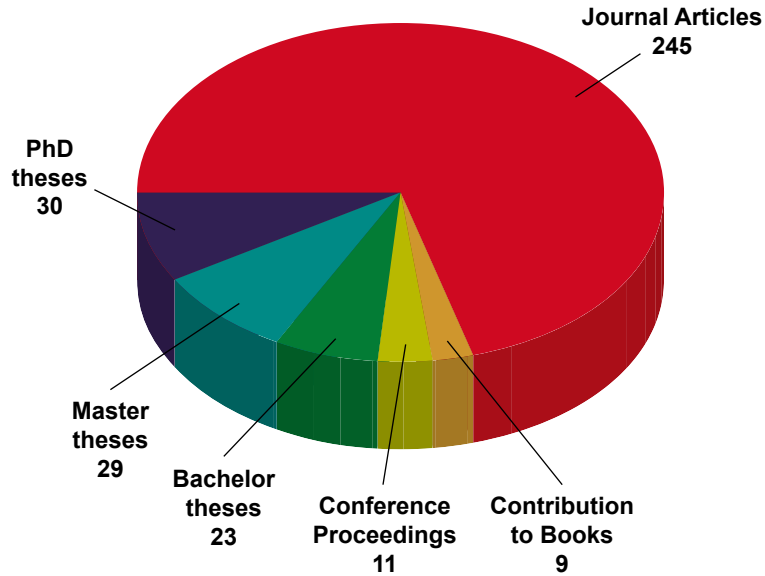
Expenses 2022

	TUM	FZJ	Hereon	Total
Personnel costs	19.327.681 €	10.237.789 €	1.399.000 €	30.964.471 €
Consumables	28.746.807 €	2.696.456 €	296.000 €	31.739.263 €
Investment	2.864.473 €	3.152.353 €	214.000 €	6.230.826 €
Total	50.938.961 €	16.086.598 €	1.909.000 €	68.934.560 €



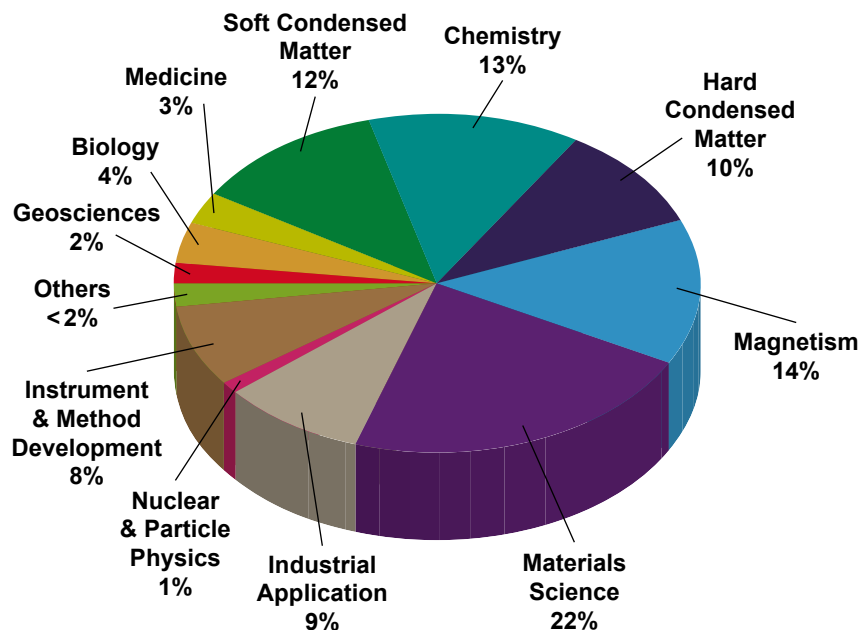
Publications & Theses

In 2022, we received notice of a total of 265 scientific publications, including journal articles, contributions to books and conference proceedings (<https://impulse.mlz-garching.de/> and figure below). Furthermore, in total 82 theses supervised by staff of the MLZ and its partner institutions were completed in 2022.

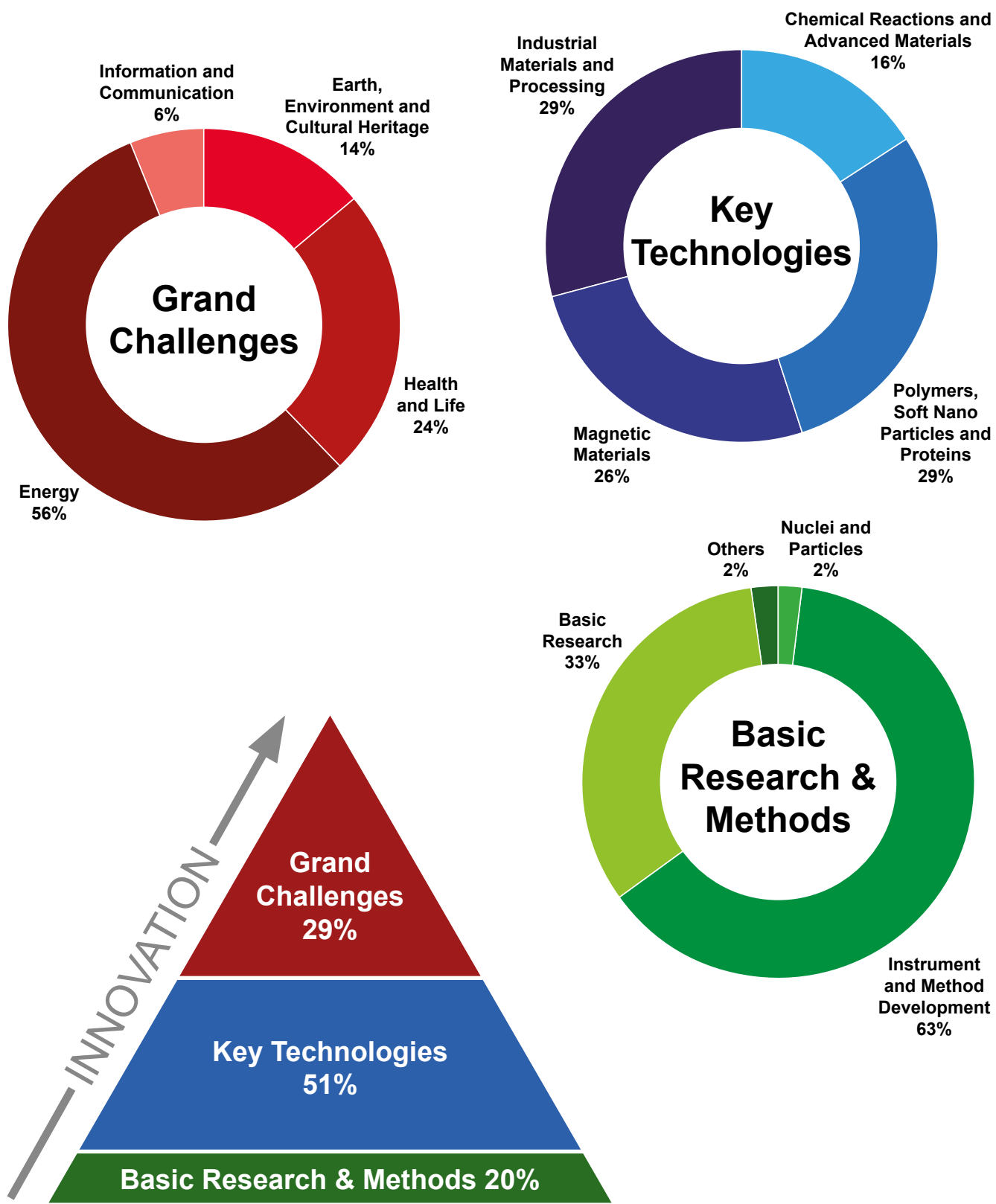


In 2022, 165 PhD theses, based on experiments at the MLZ or method and instrument developments for the MLZ, were either ongoing or completed. Of these, 135 are under the direct supervision of staff at the MLZ and its collaboration partners while the others involve external users. In total, 32 of the 165 PhD theses have been completed in 2022, including external users. Of all the doctoral students, around 90% come from German universities, around 9% from other universities in Europe and less than 1% from the rest of the world.

The next figure shows the classification of the journal articles by Scientific Area (several tags per journal article are possible):

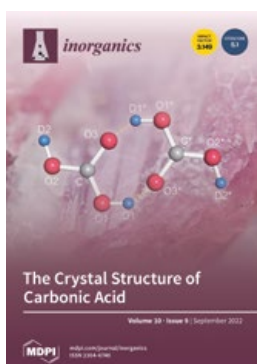


The journal articles at the MLZ can be pictured as a pyramid: Basic Research & Methods (20%) required to tackle the Key Technologies (51%) and articles that address directly the Grand Challenges of our society today (29%). The circular charts represent the individual subjects being dealt with within these three categories.



Cover pages

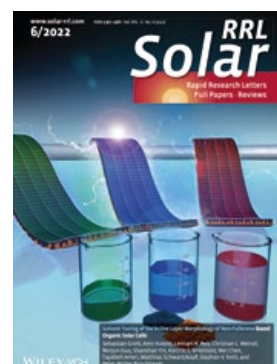
Research by MLZ scientists and at the FRM II made it to the cover pages of several journals in 2022 (see selection below).



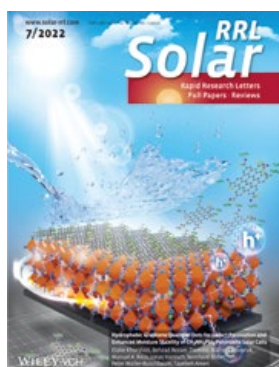
S. Benz, D. Chen, A. Möller, M. Hofmann, D. Schnieders, R. Dronskowski:
The Crystal Structure of Carbonic Acid. *Inorganics* 10(9), 132 (2022)



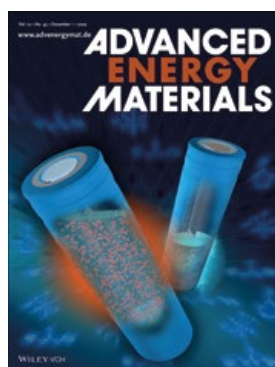
D. R. Sørensen, A. Ø. Drejer, M. Heere, A. Senyshyn, M. Frontzek, T. Hansen, C. Didier, V. K. Peterson, D. B. Ravnsbæk, M. R. V. Jørgensen:
An Easy-to-Use Custom-Built Cell for Neutron Powder Diffraction Studies of Rechargeable Batteries. *Chemistry-Methods* 2, e20220004 (2022)



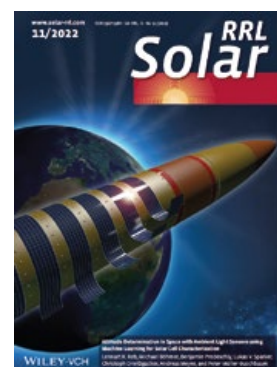
S. Grott, A. Kotobi, L. K. Reb, C. L. Weindl, R. Guo, S. Yin, K. S. Wienhold, W. Chen, T. Ameri, M. Schwartzkopf, S. V. Roth, P. Müller-Buschbaum:
Solvent Tuning of the Active Layer Morphology of Non-Fullerene Based Organic Solar Cells. *Solar RRL* 6(6), 2101084 (2022)



E. Khorshidi, B. Rezaei, D. Blätte, A. Buyruk, M. A. Reus, J. Hanisch, B. Böller, P. Müller-Buschbaum, T. Ameri:
Hydrophobic Graphene Quantum Dots for Defect Passivation and Enhanced Moisture Stability of $\text{CH}_3\text{NH}_3\text{PbI}_3$ Perovskite Solar Cells. *Solar RRL* 6(7), 2200023 (2022)



D. Petz, V. Baran, C. Peschel, M. Winter, S. Nowak, M. Hofmann, R. Kostecki, R. Niewa, M. Bauer, P. Müller-Buschbaum, A. Senyshyn:
Aging-Driven Composition and Distribution Changes of Electrolyte and Graphite Anode in 18650-Type Li-Ion Batteries. *Advanced Energy Materials* 12, 45 (2022)



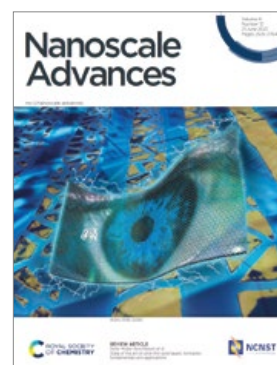
L. K. Reb, M. Böhmer, B. Predeschly, L. V. Spanier, C. Dreißigacker, A. Meyer, P. Müller-Buschbaum:
Attitude Determination in Space with Ambient Light Sensors using Machine Learning for Solar Cell Characterization. *Solar RRL* 6(11), 2200537 (2022)



P. Duchstein, P. I. Schodder, S. Leupold, T. Q. N. Dao, S. Kababya, M. R. Cicconi, D. de Ligny, V. Pipich, D. Eike, A. Schmidt, D. Zahn, S. E. Wolf:
Small-Molecular-Weight Additives Modulate Calcification by Interacting with Prenucleation Clusters on the Molecular Level. *Angewandte Chemie International Edition* 61 (40), e202208475 (2022)



N. Walte, G. J. Golabek:
Olivine aggregates reveal a complex collisional history of the main group pallasite parent body. *Meteoritics & planetary science* 57(5), 1098 (2022)



S. Liang, M. Schwartzkopf, S. V. Roth, P. Müller-Buschbaum:
State of the art of ultra-thin gold layers: formation fundamentals and applications. *Nanoscale advances* 4(12), 2533 (2022)

Committees

Steering Committee

Chair

Dr. Albert Schmid
Bavarian State Ministry of Science and the Arts

Members

Albert Berger
Technical University of Munich

Prof. Dr. sc. techn. Gerhard Kramer
Technical University of Munich

Dr. Jürgen Kroseberg
Federal Ministry for Education and Research

Prof. Dr. Astrid Lambrecht
Forschungszentrum Jülich GmbH

Prof. Dr. Matthias Rehahn
Helmholtz-Zentrum hereon GmbH

Guests

Prof. Dr. Martin Müller
Helmholtz-Zentrum hereon GmbH

Prof. Dr. Peter Müller-Buschbaum
FRM II, Technical University of Munich

Prof. Dr. Stephan Förster
Forschungszentrum Jülich GmbH

Dr. Axel Pichlmaier
FRM II, Technical University of Munich

Robert Rieck
FRM II, Technical University of Munich

Dirk Schlotmann
Forschungszentrum Jülich GmbH



Figure 1: Steering Committee meeting in May 2022 with D. Schlotmann, G. Kramer, R. Rieck, J. Kroseberg, A. Lambrecht, M. Rehahn, P. Müller-Buschbaum, A. Berger, A. Schmid, A. Pichlmaier, S. Förster, and M. Müller (from left to right).

Scientific Advisory Board

Chair

Prof. Dr. Michel Kenzelmann
Paul Scherrer Institute, Villigen

Members

Prof. Dr. Lise Arleth
University of Copenhagen

Alejandro Javier Guirao Blank
Volkswagen AG, Wolfsburg

Dr. Jens Gibmeier
Karlsruhe Institute of Technology (KIT)

Prof. Dr. Martin Fertl
Johannes Gutenberg University, Mainz

Prof. Dr. Thomas Hellweg
Bielefeld University

Prof. Dr. Bernhard Keimer
Max Planck Institute for Solid State Research, Stuttgart

Prof. Dr. Rainer Niewa
University of Stuttgart

Prof. Dr. Julian Oberdisse
Université de Montpellier

Dr. Victoria Garcia Sakai
ISIS Neutron and Muon Source, Didcot

Prof. Dr. Helmut Schober
European Spallation Source, Lund

Prof. Dr. Regine v. Klitzing
Technical University of Darmstadt



Figure 2: Meeting of the Scientific Advisory Board in May 2022 with A. Guirao Blank, J. Gibmeier, M. Müller, J. Oberdisse, M. Fertl, T. Hellweg, M. Kenzelmann, P. Müller-Buschbaum, L. Arleth, and B. Keimer (from left to right).



Figure 3: Virtual Instrumentation Advisory Committee meeting in February 2022 with H. Rønnow, M. Braden, B. Keimer, J. Neuhaus, U. Köster, F. Ott, S. Mattauch, M. Fernández-Díaz, C. Niedermayer, W. Lohstroh, P. Müller-Buschbaum, C. Pappas, R. Woracek, M. Müller, and S. Busch (from left to right and top to bottom).

Instrumentation Advisory Committee

Chair

Prof. Dr. Bernhard Keimer
Max Planck Institute for Solid State Research, Stuttgart

Members

Dr. Maria Teresa Fernández-Díaz
Institut Laue-Langevin, Grenoble

Prof. Dr. Ulli Köster
Institut Laue-Langevin, Grenoble

Prof. Dr. Christof Niedermayer
Paul Scherrer Institute, Villigen

Dr. Frédéric Ott
Laboratoire Léon Brillouin, Saclay

Prof. Dr. Catherine Pappas
Delft University of Technology

Prof. Dr. Henrik Rønnow
Ecole Polytechnique Fédérale de Lausanne

Dr. Robin Woracek
European Spallation Source, Lund

MLZ User Committee

Chair

Prof. Dr. Tommy Nylander
Lund University

Members

Dr. Andrea Scotti
RWTH Aachen University

Dr. Jens Gibmeier
Karlsruhe Institute of Technology

Dr. Ana Brás Würschig
University of Cologne

Dr. Sandra Cabeza
Institut Laue-Langevin, Grenoble

Prof. Dr. Holger Kohlmann (Observer on behalf of the KFN)
Leipzig University

Evaluation of Beam Time Proposals: Members of the Review Panels

Dr. Markus Appel
Institut Laue-Langevin, Grenoble

Prof. Dr. Lise Arleth
Niels Bohr Institute
University of Copenhagen

Dr. Mikhail Avdeev
Frank Laboratory of Neutron Physics
Joint Institute for Nuclear Research, Dubna

Prof. Dr. Piero Baglioni
University of Florence

Dr. Luis Fernández Barquín
University of Cantabria, Santander

Prof. Dr. Peter Battle
University of Oxford

Dr. Matthew Blakeley
Institut Laue-Langevin, Grenoble

Dr. Johann Bouchet
Commissariat à l'énergie atomique et
aux énergies alternatives, Arpajon

Dr. Philippe Bourges
Laboratoire Léon Brillouin, Saclay

Prof. Dr. William Brant
Uppsala University

Prof. Dr. Richard Campell
University of Manchester

Dr. Petr Čermák
Charles University, Prague

Dr. Robert Cubitt
Institut Laue-Langevin, Grenoble

Dr. Sabrina Disch
University of Cologne

Dr. Stephan Eijt
Delft University of Technology

Prof. Dr. Ulli Englert
RWTH Aachen University

Prof. Dr. Björn Fåk
Institut Laue-Langevin, Grenoble

Dr. Bela Farago
Institut Laue-Langevin, Grenoble

Prof. Dr. Rafael Omar Ferragut
L-NESS, Como

Dr. Anne-Caroline Genix
Laboratoire Charles Coulomb
Université Montpellier

Dr. Francesco Grazzi
National Research Council of Italy,
Florence Research Area

Dr. Christian Grünzweig
Paul Scherrer Institute, Villigen

Dr. Klaus Habicht
Helmholtz-Zentrum Berlin für
Materialien und Energie

Prof. Dr. Thomas Hellweg
Bielefeld University

Prof. Dr. Paul Henry
ISIS Neutron and Muon Source, Didcot

Dr. Ingo Hoffmann
Institut Laue-Langevin, Grenoble

Dr. Dirk Honecker
ISIS Neutron and Muon Source, Didcot

Dr. Christy Kinane
ISIS Neutron and Muon Source, Didcot

Dr. Joachim Kohlbrecher
Paul Scherrer Institute, Villigen

Dr. Reinhard Kremer
Max Planck Institute for
Solid State Research, Stuttgart

Prof. Dr. Christian Krempaszky
Technical University of Munich, Garching

Prof. Dr. Jeremy Lakey
University of Newcastle

Dr. Reidar Lund
Oslo University

Dr. Sandrine Lyonnard
Commissariat à l'énergie atomique et
aux énergies alternatives, Grenoble

Dr. Nicolas Martin
Laboratoire Léon Brillouin, Saclay

Dr. Gwilherm Nénert
PANalytical B.V., Almelo

Dr. Thomas Nitschke-Pagel
TU Braunschweig

Dr. Esko Oksanen
European Spallation Source, Lund

Prof. Dr. Andrea Orecchini
Università degli Studi di Perugia

Dr. Alessandro Paciaroni
Università degli Studi di Perugia

Prof. Dr. Christine Papadakis
Technical University of Munich, Garching

Dr. Oleg Petrenko
University of Warwick

Dr. Thilo Pirling
Institut Laue-Langevin, Grenoble

Prof. Dr. Radosław Przeniosło
University of Warsaw

Prof. Dr. Diana Lucia Quintero Castro
University of Stavanger

Dr. Navid Qureshi
Institut Laue-Langevin, Grenoble

Dr. Florin Radu
Helmholtz-Zentrum Berlin für
Materialien und Energie

Dr. Sarah Rogers
ISIS Neutron and Muon Source, Didcot

Dr. Emmanuel Schneck
Max Planck Institute of
Colloids and Interfaces, Potsdam

Prof. Dr. Roland Schwab
University of Tübingen

Dr. Romain Sibille
Paul Scherrer Institute, Villigen

Dr. Thorsten Soldner
Institut Laue-Langevin, Grenoble

Prof. Dr. Thomas Sottmann
University of Stuttgart

Dr. Andreas Stark
Helmholtz-Zentrum hereon GmbH

Dr. Johannes Sterba
Atominstytut Wien, TU Wien

Dr. Christopher Stock
University of Edinburgh

Dr. Pavel Strunz
Nuclear Physics Institute, Řez near Prague

Dr. Anne Stunault
Institut Laue-Langevin, Grenoble

Dr. László Szentmiklósi
Hungarian Academy of Sciences, Budapest

Dr. Kristiaan Temst
KU Leuven

Dr. Alexander Tsirlin
Augsburg University

Prof. Dr. Regine von Klitzing
Technical University of Darmstadt

Dr. Oksana Zaharko
Paul Scherer Institut, Villigen

Prof. Dr. Hongbin Zhang
Technical University of Darmstadt

Partner institutions



Bavarian Research Institute of
Experimental Geochemistry and Geophysics
University of Bayreuth
www.bgi.uni-bayreuth.de



Georg-August-Universität Göttingen
• Geowissenschaftliches Zentrum
www.uni-goettingen.de/de/125309.html



German Engineering Materials Science Centre GEMS
Helmholtz-Zentrum hereon GmbH
www.hereon.de/central_units/gems/index.php.de



Jülich Centre for Neutron Science JCNS
Forschungszentrum Jülich GmbH
www.jcns.info



Karlsruhe Institute of Technology

- Institute for Applied Materials – Energy Storage Systems (IAM-ESS)
www.iam.kit.edu/ess/



Ludwig-Maximilians-University

- Section Crystallography
www.lmu.de/kristallographie
- Faculty of Physics
www.softmatter.physik.uni-muenchen.de



Max Planck Institute for Solid State Research
Stuttgart

www.fkf.mpg.de



RWTH Aachen University

- Institute of Crystallography
www.ifk.rwth-aachen.de
- Institute of Inorganic Chemistry
www.iac.rwth-aachen.de/go/id/plnz/



**TECHNISCHE
UNIVERSITÄT
DRESDEN**

Technische Universität Dresden

- Institute of Solid State and Materials Physics
www.tu-dresden.de/mn/physik/ifp



Technical University of Munich

TUM School of Natural Sciences

- E13 – Chair for Functional Materials
www.functmat.ph.tum.de
- E18 – Institute for Hadronic Structure and Fundamental Symmetries
www.e18.ph.tum.de
- E51 – Chair for the Topology of Correlated Systems
www.sces.ph.tum.de

Central Scientific Institution

- RCM – Radiochemie München
www.rcm.tum.de



Klinikum rechts der Isar

Technical University of Munich

- MRI – Klinikum rechts der Isar
www.mri.tum.de



Technical University of Munich

- Excellence Cluster ORIGINS
www.origins-cluster.de/



TECHNISCHE
UNIVERSITÄT
WIEN
Vienna University of Technology

Vienna University of Technology

- Neutron- and Quantum Physics
Research area at the Atominstitut Vienna
Abele Group
<https://ati.tuwien.ac.at/forschungsgruppen/nqp/home/>



Universität der Bundeswehr München

- Institute of Applied Physics and Measurement
Technology
www.unibw.de/lrt2

Universität zu Köln



University of Cologne
Faculty of Mathematics and
Natural Sciences

- Institute for Nuclear Physics
www.ikp.uni-koeln.de
- Institute of Physics II
www.ph2.uni-koeln.de

PHYSIKALISCHES
INSTITUT



UNIVERSITÄT
HEIDELBERG
ZUKUNFT
SEIT 1386

Universität Heidelberg

- Physikalisches Institut
www.physi.uni-heidelberg.de/

Imprint

Publisher

Technische Universität München
Forschungs-Neutronenquelle
Heinz Maier-Leibnitz (FRM II)
Lichtenbergstr. 1
85747 Garching
Germany

Phone: +49.89.289.14965
Fax: +49.89.289.14995
Internet: www.mlz-garching.de
www.frm2.tum.de
E-Mail: jahresbericht@frm2.tum.de

Editorial Office, Design and typesetting

Diana Fleischer
Anke Görg
Connie Hesse
Michael Hörmannsdorfer
Christoph Kreileder
Sarah Metz
Reiner Müller
Björn Pedersen
Robert Schulze (getyourdesign, Berlin)
Andrea Voit

Editors

Henrich Frielinghaus
Robert Georgii
Markus Hölzel
Michael Hofmann
Olaf Holderer
Johanna Jochum
Peter Link
Martin Meven
Andreas Ostermann
Zsolt Revay
Anatolij Senyshyn
Christian Stieghorst
Apostolos Vagias
Marcell Wolf

Photographic credits

Front cover
and p.17
p. 6
Chris Hohmann (MCQST)
top: Drohnenaufnahme/FRM II
bottom left: Andreas Heddergott (TUM)
bottom 2nd left:
Christian Schmid (hereon)
bottom 2nd right:
Alessandra Schellnegger
bottom right: Astrid Eckert (TUM)

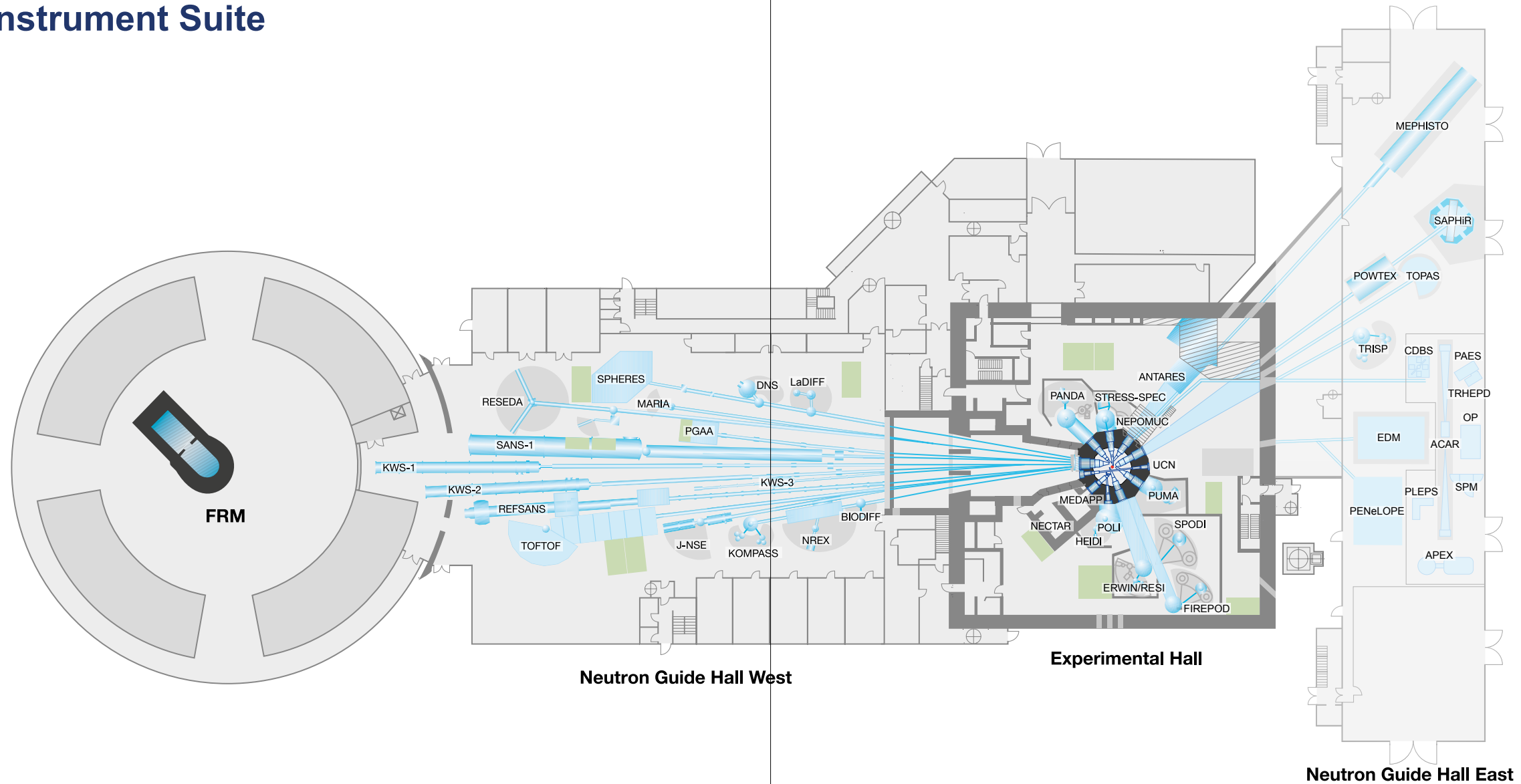
p. 8/9
p. 18
p. 19
Jan Greune (MCQST)
graphic elements by Nobu Tamura
graphic elements by ESA, NASA,
M. Kornmesser

p. 20/21
p. 22
p. 23
p. 24
Bernhard Ludewig (FRM II/TUM)
Nat Commun ISSN 2041-1723
BMW
Andreas Heddergott (TUM)

p. 30/31
p. 82/83
p. 87
p. 92
p. 93
p. 93
p. 99
Wenzel Schürmann (FRM II/TUM)
Wenzel Schürmann (FRM II/TUM)
middle: Bayerische Staatskanzlei
bottom: Andreas Heddergott (TUM)
top: Andreas Heddergott (TUM)
middle: Wenzel Schürmann (FRM II/TUM)
bottom (2): Paul Warpole (SKAO)

Editors, authors or FRM II/TUM:
other images

MLZ Instrument Suite



Instrument	Description	Neutrons	Operated by	Funding	Instrument group at MLZ
ANTARES	Radiography and tomography	cold	TUM, GEMS	TUM, Hereon	FRM II, GEMS
BIODIFF	Diffractometer for large unit cells	cold	TUM, JCNS	TUM, FZJ	FRM II, JCNS
DNS	Diffuse scattering spectrometer	cold	JCNS	FZJ	JCNS
ERWIN/RESI**	Powder diffractometer	thermal	LMU, KIT	TUM, ErUM	FRM II
FIREPOD*	Powder diffractometer	thermal	TUM	TUM	FRM II
HEIDI	Single crystal diffractometer	hot	RWTH Aachen	FZJ	JCNS
J-NSE	Spin-echo spectrometer	cold	JCNS	FZJ	JCNS
KOMPASS	Three axes spectrometer	cold	Uni Köln, TUM	ErUM, TUM	FRM II
KWS-1	Small angle scattering	cold	JCNS	FZJ	JCNS
KWS-2	Small angle scattering	cold	JCNS	FZJ	JCNS
KWS-3	Very small angle scattering	cold	JCNS	FZJ	JCNS
LaDIFF*	High resolution larmor diffraction and inelastic scattering	cold	TUM	TUM	FRM II
MARIA	Magnetic reflectometer	cold	JCNS	FZJ	JCNS
MEPHISTO**	Instrument for particle physics, PERC	cold	TUM	TUM, DFG	FRM II
MEDAPP	Medical irradiation treatment	fast	TUM	TUM	FRM II
NECTAR	Radiography and tomography	fast	TUM, GEMS	TUM, Hereon	FRM II, GEMS
NEPOMUC	Positron source, CDBS, PAES, PLEPS, SPM, TRHEPD, OP, ACAR, APEX	-	TUM, UniBw München	TUM	FRM II

*construction
 **reconstruction
 ErUM: instrument construction funded by ErUM-Pro (BMBF)

Instrument	Description	Neutrons	Operated by	Funding	Instrument group at MLZ
NREX	Reflectometer with X-ray option	cold	MPI Stuttgart	MPG	MPI Stuttgart
PANDA	Three axes spectrometer	cold	JCNS	FZJ	JCNS
PGAA	Prompt gamma activation analysis, Neutron activation analysis (NAA), Neutron depth profiling (NDP)	cold	Uni Köln	TUM	FRM II
PUMA	Three axes spectrometer	thermal	KIT	TUM	FRM II
POLI	Single-crystal diffractometer polarized neutrons	hot	RWTH Aachen	FZJ	JCNS
POWTEX*	Time-of-flight diffractometer	thermal	RWTH Aachen, Uni Göttingen, JCNS	ErUM, FZJ	JCNS
REFSANS	Reflectometer	cold	GEMS	Hereon	GEMS
RESEDA	Resonance spin-echo spectrometer	cold	TUM	TUM	FRM II
SANS-1	Small angle scattering	cold	TUM, GEMS	TUM, Hereon	FRM II, GEMS
SAPHIR*	Six anvil press for radiography and diffraction	thermal	Uni Bayreuth	ErUM, TUM	FRM II
SPHERES	Backscattering spectrometer	cold	JCNS	FZJ	JCNS
SPODI	Powder diffractometer	thermal	KIT	TUM	FRM II
STRESS-SPEC	Materials science diffractometer	thermal	TUM, GEMS	TUM, Hereon	FRM II, GEMS
TOFTOF	Time-of-flight spectrometer	cold	TUM	TUM	FRM II
TOPAS*	Time-of-flight spectrometer	thermal	JCNS	FZJ	JCNS
TRISP	Three axes spin-echo spectrometer	thermal	MPI Stuttgart	MPG	MPI Stuttgart
UCN*	Ultra cold neutron source, EDM, PENeLOPE	ultra-cold	TUM	TUM, DFG	FRM II

Front page:

The propagation of spin waves perpendicular to skyrmions displays a quantization of the circular orbits. In addition, the circular orbit is topologically non-trivial: it carries a subtle twist, researchers have found out using neutrons at the instrument RESEDA (see p. 17).

Back page:

View of the FRM II reactor building in the evening.



Heinz Maier-Leibnitz Zentrum (MLZ)

www.mlz-garching.de

DOI: 10.14459/2022md1689570